

OPTICAL SHOP APPLICATIONS FOR LASER TRACKER
METROLOGY SYSTEMS

By

Benjamin B. Gallagher

A Thesis Submitted to the Faculty of the
DEPARTMENT OF OPTICAL SCIENCES
In Partial Fulfillment of the Requirements
For the Degree of
MASTER OF SCIENCE
In the Graduate College
THE UNIVERSITY OF ARIZONA

2003

STATEMENT BY AUTHOR

This thesis has been submitted in partial fulfillment of requirements for an advanced degree at The University of Arizona and is deposited in the University Library to be made available to borrowers under the rules of the Library.

Brief quotations from this thesis are allowable without written special permission, provided that accurate acknowledgement of the source is made. Requests for permission for extended quotation from or reproduction of this manuscript in whole or in part may be granted by the head of the major department or the Dean of the Graduate College when in his or her judgment the proposed use of the materials is in the interest of scholarship. In all other instances, however, permission must be obtained from the author.

APPROVAL BY THESIS DIRECTOR

This thesis has been approved on the date shown below:

James H. Burge
Associate Professor of
Optical Sciences and Astronomy

Date

ACKNOWLEDGEMENTS

I would like to thank Joan and Steve Ihlenfeldt at ATT Metrology Inc. for their donation of time and access to a Laser Tracker Metrology System. This donation made possible the research presented in this thesis.

I would also like to thank my advisor Jim Burge for his patience, guidance, and for giving me an opportunity to succeed at the Optical Sciences Center.

Finally, I would like to thank my wife, Michelle, and son, Trey, for their incredible support that has allowed me to reach my personal goals.

TABLE OF CONTENTS

List of Figures	6
List of Tables	9
Abstract	10
Chapter 1. Introduction.....	12
Chapter 2. Background.....	18
2.1. Laser Tracker Theory.....	18
2.1.1. Theory of Operation.....	19
2.1.2. Error Sources for Laser Tracker	22
2.1.3. Specification for Laser Tracking Systems	28
2.2. Laser Tracker Applications.....	31
2.2.1. Dynamic Applications	31
2.2.2. Static Applications.....	33
2.2.3. Combining Dynamic and Static Measurements.....	37
2.2.4. Combination of Laser Tracker Data with Other Measurement Data.....	38
2.3. Displacement Interferometry	39
2.3.1. The Basic Displacement Interferometer	41
2.3.2. Homodyne Distance Measuring Interferometer	42
2.3.3. Heterodyne Distance Measuring Interferometer.....	43
2.3.4. Error Sources for Displacement Interferometers	44
2.3.4.1. Environmental Errors.....	45
2.3.4.2. Installation Errors.....	47
2.3.5. Specifications and Applications.....	51
2.4. Position Sensing Detectors	52
2.4.1. PSD Applications.....	54
2.4.2. PSD Operation Principles	55
2.4.3. Specifications and Selection of the PSD.....	57
2.5. Optical System Alignment.....	58
2.5.1. Geometry of Optical Alignment	58
2.5.2. Impacts of System Misalignment	62
2.5.3. Error Budget for Optical System Alignment	65
2.5.4. Optical Alignment Tools	70
Chapter 3. Evaluation of tracker as an Optical Tool	77
3.1. Gauge Block Investigation.....	78
3.2. Radius of Curvature Investigation	80
3.2.1. Location of Tracker with Respect to Surface Being Measured	82
3.2.2. Effects of Number of Data Points used to Generate a Surface	85

TABLE OF CONTENTS (CONT.)

3.2.3.	Effects of Reducing the Area Scanned to Produce Profile	87
3.2.4.	Radius of Curvature Summary	93
3.3.	Optical Alignment.....	96
3.3.1.	Effects of Tracer Location on the Repeatability of the Tracker	97
3.3.2.	Effects of Number of Data Points used to Generate a Surface.....	98
3.3.3.	Effects of Reducing the Area Scanned to Produce a Profile	99
3.3.4.	Active Alignment.....	102
3.3.4.1.	Active Alignment by Creating a Reference Sphere.....	103
3.3.4.2.	Active Alignment with Fiducials	104
3.3.5.	Alignment Summary.....	107
3.4.	Image Tracking	113
3.4.1.	PSD Characterization.....	115
3.4.1.1.	Setup and Software Interface	115
3.4.1.2.	Stabilization Investigation	118
3.4.1.3.	Incident Power on the Detector Characterization	120
3.4.1.4.	Calibration Coefficients	121
3.4.1.5.	Other PSD considerations	125
3.4.1.6.	PSD Characterization Summary	127
3.4.2.	Relating the PSD data and the Laser Tracker data	128
3.4.2.1.	PSD/Tracker Ball Bracket Design	128
3.4.2.2.	Relating the PSD to the Axis of Rotation	132
3.4.2.3.	Relating the Tracker Ball to the Axis of Rotation	134
3.4.2.4.	Combining Tracker Data with PSD Data.....	135
3.4.3.	Simulation of Image Tracking	137
3.4.3.1.	Calibration of PSD and Tracker Ball	138
3.4.3.2.	Simulation Procedure and Results	140
3.4.3.3.	Error Sources for Image Tracking Simulation.....	142
3.4.4.	Image Tracking Summary	143
3.5.	Miscellaneous	145
3.5.1.	Diffraction Grating Investigation.....	145
3.5.2.	Fold Mirror Investigation.....	147
3.6.	Summary of Laser Tracker Evaluation	148
Chapter 4.	Other testing and alignment techniques.....	150
4.1.	Power spectral density analysis of image jitter.....	150
4.1.1.	Measurement Techniques and Impacts of Line-of-Sight Jitter.....	151
4.1.2.	Power Spectral Density.....	153
4.1.3.	Software	155

TABLE OF CONTENTS (CONT.)

4.1.4.	Line-of-Sight Jitter Measurements with Software.....	159
4.2.	Adding Auxiliary Lenses to Alignment Telescopes	163
4.2.1.	First Order Optical Analysis.....	164
4.2.2.	Alignment of Compensating Lens to Telescope.....	167
4.2.3.	Hardware.....	169
4.3.	Expediting Alignments with an Adjustment Matrix.....	171
4.3.1.	Technique to Expedite Complex Alignments.....	172
4.3.2.	Fold Mirror Alignment Using Adjustment Matrix	174
Chapter 5.	Conclusion	179
5.1.	Summary	179
5.1.1.	Evaluation of Laser Tracker as a tool for the Optical Shop.....	180
5.1.2.	Other Testing and Alignment Techniques	182
5.2.	Future Work.....	184
APPENDIX A:	PSD Interface User Guide and Software Code	186
APPENDIX B:	Hardware Drawings.....	198
REFERENCES	202

LIST OF FIGURES

Figure 1.1. Laser Tracker Applications [20].....	16
Figure 2.1. Laser Tracker Components from US Patent Number 4,714,339 [10].....	20
Figure 2.2. Point in space in Cartesian and Spherical Coordinates	21
Figure 2.3. Spherical Coordinate System with True Vertical Axis.	25
Figure 2.4. Horizontal Error and Vertical Error as a function of θ	25
Figure 2.5. Error due to beam misalignment to the tracking mirror	27
Figure 2.6. Laser Tracking System [20]	28
Figure 2.7. Radius Sweep and Out of Plane Deviation.....	33
Figure 2.8. Zeiss Coordinate Measuring Machine [30]	34
Figure 2.9. Surface Map from Composite Optics Incorporated.....	37
Figure 2.10. Combining a Laser Tracker with Coordinate Measuring Arms. [35]	38
Figure 2.11. Twyman-Green Interferometer.....	40
Figure 2.12. Homodyne interferometer schematic [37].....	43
Figure 2.13. Heterodyne Interferometer schematic [37].....	44
Figure 2.14. Measurement Drift vs. Interferometer Temperature [39].....	47
Figure 2.15. Cosine Error in Displacement Interferometers.....	48
Figure 2.16. Abbé Error	49
Figure 2.17. Dead Path Error in a Displacement Interferometer	50
Figure 2.18. 45 x 45 mm PSD from On-Trak [40]	52
Figure 2.19. Response curve for single pixel PSD. [40].....	53
Figure 2.20. Triangulation Probe from SiTek [41].....	54
Figure 2.21. Dual Axis PSD Schematic [40]	56
Figure 2.22. Optical Axis and Center of Curvature of an optical system.	59
Figure 2.23. Clocking of off-axis spheres and aspheres.	60
Figure 2.24. Segmented mirror with 1.5 mrad tilt between segments [44]	62
Figure 2.25. Cassegrain Telescope	63
Figure 2.26. Three Mirror Offner Relay System	67
Figure 2.27. Top Level Error Budget for 3 mirror Offner Relay System.....	67
Figure 2.28. Alignment error budget for Offner Relay system.....	68
Figure 2.29. Perturbation to Wavefront error relationships.....	70
Figure 2.30. Taylor Hobson Alignment Telescope [49].....	71
Figure 2.31. Alignment telescope setup [49].....	72
Figure 2.32. Interferometer used to align segmented primary mirrors.	73
Figure 2.33. Photograph of alignment fiducial produced by CGH.....	75
Figure 3.1. Setup for gauge block test	79
Figure 3.2. Results of Gauge Block Measurement at different ranges.	80
Figure 3.3. Tracker Locations with Respect to the Mirror Under Test.....	83
Figure 3.4. Radius Measurement Error as a Function of Tracker Location	84
Figure 3.5. Standard Deviation of Radius Report as a Function of Tracker Location. ...	85
Figure 3.6. Scanning patterns for different measurement techniques.....	86
Figure 3.7. Radius Measurement Error as a Function of Points to Generate Surface	86

List of Figures (Cont.)

Figure 3.8. Radius Measurement Error as a Function of % of sphere profiled	89
Figure 3.9. Change in Sag Error as a function of % of sphere profiled.....	90
Figure 3.10. Radius Measurement Error as a Function of R/#	92
Figure 3.11. Photograph with tape.....	94
Figure 3.12. Center of Curvature Location vs. Tracker Location.....	97
Figure 3.13. Center of Curvature Location vs. Number of Points to Generate Surface ..	99
Figure 3.14. Center of Curvature Location vs. Mirror R/#.....	100
Figure 3.15. Corrected Radius Measurement Error as a Function of R/#.....	102
Figure 3.16. Mirror with alignment fiducials.....	104
Figure 3.17. Offner relay system using 16.7” primary mirror.	109
Figure 3.18. Optical Layout of the LSST telescope.....	110
Figure 3.19. Conceptual diagram of image tracking.....	114
Figure 3.20. PSD Characterization Schematic.....	115
Figure 3.21. PSD Interface Developed in Lab View.	117
Figure 3.22. Standard Deviation of Data Set as Setup Evolved	119
Figure 3.23. Final Stabilization Test Data	120
Figure 3.24. Standard Deviation vs. Laser Intensity.....	121
Figure 3.25. X and Y axis Voltage vs. Position.....	122
Figure 3.26. X and Y Calibration Coefficients across center of detector.	123
Figure 3.27. System warm up time	126
Figure 3.28. PSD Tilt Characterization, without room lights and filter	126
Figure 3.29. Photograph of Newport Rotation Stage.....	129
Figure 3.30. Exploded view of PSD/Tracker Ball mount.....	130
Figure 3.31. Bracket design for use when tracker is located to the side of the adapter.	131
Figure 3.32. Geometry of the Axis of Rotation	133
Figure 3.33. Origin of Measurement when PSD and Tracker ball are combined.....	136
Figure 3.34. Setup for image Tracking Simulation.....	138
Figure 3.35. PSD/Tracker Ball Assembly mounted on Rail.....	139
Figure 3.36. Diffraction Grating when used in Double Pass.	147
Figure 3.37. Fold Mirror Test Setup.	147
Figure 4.1. Effects of jitter on an imaging system [52]	152
Figure 4.2. Power Spectral Density Computational Block Diagram	156
Figure 4.3. Power Spectral Density Software verification.	158
Figure 4.4. LOS Jitter Test Setup.....	159
Figure 4.5. Time domain line of sight jitter signal.	160
Figure 4.6. LOS Jitter Report for simple pointing system.....	161
Figure 4.7. Simple optical system to be aligned on an optical table (side view).....	165
Figure 4.8. Image locations of reticles through an optical system.....	166
Figure 4.9. Decentering a lens compensates for wedge in a lens.	169
Figure 4.10. Exploded view of adapter assembly.	170

List of Figures (Cont.)

Figure 4.11. Fold mirror must be positioned to send bore sight through two reticles... 174	174
Figure 4.12. Fold Mirror Cell. 175	175
Figure 4.13. Images of R1 and R2 in alignment telescope 176	176

LIST OF TABLES

Table 2.1. Leica LTD500 System Specifications	29
Table 2.2. Specifications for the SMX 4500 Laser Tracking System.	30
Table 2.3. Hewlett Packard Displacement Interferometer Specifications	51
Table 2.4. PSD Measurement System Components	58
Table 2.5. Conic Constants	61
Table 3.1. Specifications for SMX 4500 laser tracker.....	77
Table 3.2. Radius of Curvature Measurements with traditional techniques.	82
Table 3.3. Average and Standard Delta Sag on 16.7 inch mirror	91
Table 3.4. Comparison of Sag Error for Different Axes of Laser Tracker.....	101
Table 3.5. Results of Active Alignment Simulation.....	106
Table 3.6. Error Budget for LSST mirror alignment.	110
Table 3.7. Expected Radius Error from Tracker Measuring LSST Mirrors	111
Table 3.8. Predicted Error using Active Alignment Features of Laser Tracker	113
Table 3.9. Key Components used in PSD Characterization.	116
Table 3.10. Calibration Coefficients across the detector	124
Table 3.11. PSD Offsets.....	139
Table 3.12. Results of Image Tracking Simulation	141
Table 3.13. Summary of Error sources for image tracking simulation.....	142
Table 4.1. Mean and Standard Deviation of Image Jitter	160
Table 4.2. Comparison of Standard Deviation Calculations.....	162

ABSTRACT

A laser tracking system, or a laser tracker, is an interdisciplinary system that combines many engineering disciplines to make an extremely accurate and versatile three dimensional coordinate measuring instrument. These disciplines include optics, precision mechanics, servo systems, numerical computation, and computer control techniques. Although trackers are optical based systems relying on heterodyne laser interferometry to perform measurements, there have not been many optical shop applications that have been developed utilizing this powerful tool.

This thesis evaluates the laser tracker as a tool for the optical shop. Included in this thesis is an extensive background chapter that investigates the theory of the laser tracker, error sources, and current applications. An extensive list of references was built that describes the work that is currently being done with laser trackers and what improvements the different groups around the world are doing to improve its performance. This thesis builds upon this work by documenting a series of experiments that were designed to evaluate the tracker's ability to make optical measurements.

The tracker's ability to measure the radius of curvature of a spherical optical element, the tracker's ability to align an optical system, and the tracker's ability to track an image was

evaluated. Many variables were considered to test the tracker's ability to measure radius of curvature and the variable that impacted the tracker's performance the most was the R/# of the optic being measured. Slow optics do not have much sag in their surface and the tracker's performance was limited by its ability to measure sag. To evaluate the tracker as an alignment tool, the repeatability of the reported location of the center of curvature was investigated. As with the radius of curvature evaluation, the tracker's performance was limited by the R/# of the optic under measurement. A relationship between expected measurement error and R/# was developed and the expected error in inches was found to be equal to $3.6E-4*(R/\#)^2$. For measurement errors less than 40 microns, optics R/2 and faster should be measured by the tracker.

The tracker's ability to track an image was also evaluated. An image is not a physical thing that the tracker can touch but it can locate a camera or detector that can detect an image. To track an image the data from the tracker and the data from the detector must be combined to locate the image. Image tracking is described and simulated in this thesis.

The laser tracker is shown to be a powerful tool that can have many applications in the optical shop. Its ability to make accurate large scale measurements would be very useful for a variety of applications. This thesis also suggests future studies that should be performed that would better define the tracker's role in the optical shop.

CHAPTER 1. INTRODUCTION

A laser tracking system, or laser tracker, is an interdisciplinary system that combines many engineering disciplines to make an extremely accurate and versatile measuring instrument. These disciplines include optics, precision mechanics, servo systems, numerical computation, and computer control techniques. A laser tracker is an optical measuring device that is capable of making highly accurate three-dimensional static and dynamic measurements. Although trackers are optical based systems relying on heterodyne laser interferometry to perform measurements, there have not been many optical shop applications developed that utilize this powerful tool.

There are many different tools that are capable of making 3-D measurements. Theodolites and coordinate measuring machines are traditional tools that can make these types of measurements. Since the advent of the laser in the 1960's many tools that utilize the laser have been developed to make 3-D measurements. These tools include laser tracking systems, "time of flight" systems, laser scanning systems, Moiré systems, laser speckle pattern sectioning, interferometry, and photogrammetry systems [1, 2, 3]. Different systems have been developed for different needs. Some systems make measurements with ranges over one mile and some systems are capable of making sub-

micron measurements, but they may only have a range of a few millimeters. The laser tracker was chosen as the topic of this thesis because of its versatility. The tracker is the only system capable of making dynamic measurements as well as static measurements and it is capable of making measurements with accuracy of 25 microns. The tracker has a range of less than a meter to more than 35 meters making large-scale projects an ideal application for the laser tracker.

Laser trackers have been existence since the late 1960's when research facilities such as Sandia National Labs developed these tools to track projectiles in space such as missiles or airplanes [4, 5]. Laser trackers were used for other military applications as well. They allowed targeting systems on airplanes to "lock on" to a target while both the airplane and the target were moving. These early trackers used azimuth and elevation gimbals with encoders to find the angular information and used "time of flight" methods to determine the distance between the tracker and the target. To make "time of flight measurements" the tracker must know when the laser was fired and have a detector that tells the system when the reflected laser makes it back to the tracker. The tracker can then take into account the speed of light and calculate the distance between the tracker and the target. To track a target or "lock on" to a target, an operator views output from an image forming detector, and using a joystick, tells the system what feature in the scene to track. Then software in the tracker follows the prescribed feature and moves a tracking mirror to keep the target illuminated by the laser. These early trackers were good for long range

measurements of over 10,000 feet, but for short ranges the range finders are not fast enough to make accurate "time of flight" measurements

In 1980 Allen Greenleaf with Itek Optical Systems proposed to use four distance measuring interferometers in combination with a tracking system to make a surface profiling machine. [6, 7] This profilometer is now known by its trade name "Surfitek" and is still being utilized on some large scale astronomical mirror fabrication such as the SOAR telescope. [8] In 1986 Kam Lau wrote a paper and filed US Patent number 4,714,339 that built upon Greenleaf's system and used a distance measuring interferometer in combination with azimuth and elevation encoders to make highly accurate dynamic measurements [9, 10]. The incorporation of the encoders on the azimuth and elevation gimbals of the tracking system enabled this laser tracker to be housed in one compact and portable unit. The distance measuring interferometer tracks the distance between the tracker and a retroreflective target. The retroreflective target then reflects the beam back onto itself allowing a photo detector on the tracker to record the return beam location. As the target moves the return beam on the photo-detector moves and sends information to a servo system. The servo system then adjusts a tracking mirror to keep the return beam at a nominal position on the photo detector. The laser tracker that Kam Lau proposed was developed to measure robotic performance. Factories were beginning to use robots to automate welding, cutting, and assembly processes. These automated processes required a new level of precision from the robots, and the measuring instruments of the time were incapable of measuring the dynamic

positioning performance of the robots. Lau's patent was granted in 1987 and soon after the first prototypes were completed. Many upgrades to Lau's tracker have since been built and proposed. In 1995 J.P. Prenninger proposed employing a CCD camera so the tracker could measure orientation as well as position. [11] In 1998 J.H. Gilby proposed using two trackers tracking the same point to improve the accuracy of the trackers [12]. In 1998 using three trackers to provide measurements based on the concept of trilateration was proposed and tested [13]. NPL in the United Kingdom is building a CMM that utilizes 4 laser trackers to measure distance and is reporting accuracies of 1ppm [14]. Also other upgrades have been proposed including modifying the tracker mirror to improve accuracy, using the trilateration concept to determine orientation, adding a fourth tracker for calibration using the trilateration measurement technique and others [15, 16, 17, 18, 19]

Many universities and labs have built their own laser trackers for internal and experimental use. The three main suppliers that build and sell laser trackers are Leica Geosystems, FARO inc. (formerly SMX), and Automated Precision Incorporated. Many other companies offer metrology services and will rent these units or send a crew to perform measurements on site.

The Laser tracker was initially developed to measure the dynamic performance of robots. Since 1985 many new applications have been developed for the tracker because of its extreme flexibility and high performance. The tracker is still the best option to make

dynamic measurements, and its ability to measure a point in space very accurately has allowed the tracker to replace coordinate measuring machines, theodolite metrology systems, and videometric systems. Figure 1.1 shows some of the applications that have been developed using laser trackers.



Figure 1.1. Laser Tracker Applications [20]

The laser tracker can perform robot calibration, perform large-scale measurements on aircraft, boats, or other large assemblies, perform surface inspections, and provide an invaluable assembly aid. In the Laser Tracker Applications Section of the background chapter, current static and dynamic applications will be investigated in detail.

This thesis investigates the Laser Tracking System in detail and investigates potential optical applications for this powerful tool. An extensive background chapter is included in this thesis that investigates laser tracker theory, error sources, and current applications. Many experiments are presented in this thesis and they show the versatility of the laser tracker and the usefulness of this tool in the optical shop. Potential optical shop applications for this tool include radius of curvature measurement, optical system alignment, image tracking, and optical system performance testing. Each one of these applications is investigated and presented in this thesis. This thesis also makes suggestions on future uses of Laser Tracking Systems and what improvements to the tracking systems would make the Laser Tracking Systems even more useful in the optical shop.

CHAPTER 2. BACKGROUND

This chapter investigates the theory behind all of the major aspects of the research presented in this thesis. A discussion of the test equipment used in this research will be found in this section. Included in this discussion will be theory of operation, current applications, and specifications for the equipment used to complete this research. This section includes the following discussions:

- Laser Tracker Theory
- Laser Tracker Applications
- Displacement Interferometry Theory and Applications
- Position Sensing Detector Theory and Applications
- Optical System Alignment

2.1. Laser Tracker Theory

The laser tracker is basically a portable Coordinate Measuring Machine (CMM) that can make both dynamic and static measurements while a traditional CMM can only make static measurements. The laser tracker utilizes a laser interferometer and angle encoders to track the location of a reference target as it moves through space. The tracker's CPU

combines the distance information from the laser interferometer with the angle information from the encoders to calculate the X,Y,Z coordinate of the reference target.

2.1.1. Theory of Operation

The laser tracker used and evaluated in this research is a tracker very similar to the tracker Kam Lau first proposed in 1985. The following components make up the Laser Tracker System:

- Distance measuring heterodyne interferometer that uses a laser, an interferometer, and a fringe counter.
- Beam splitters to split both the outgoing and the incoming beams.
- Azimuth and elevation motors with encoders to steer the beam to the target and provide angular information to the CPU.
- A retroreflector or corner cube that reflects the beam back onto itself.
- A Position Sensing Detector or a CCD to analyze the return beam's location.
- A CPU to control the servo system and calculate the position of the target.

Figure 2.1 from US Patent 4,714,339 shows the basic concepts of the laser tracker.

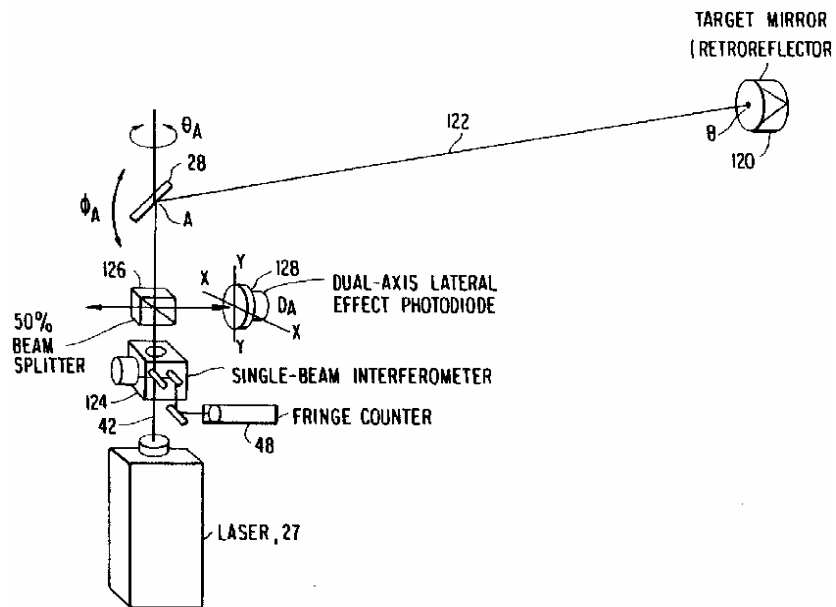


Figure 2.1. Laser Tracker Components from US Patent Number 4,714,339 [10]

The distance measuring interferometer is of the heterodyne configuration consisting of a dual frequency source similar to the HP5501 laser, in combination with a modified Twyman Green interferometer. The theory behind this interferometer and displacement interferometry will be discussed in section 2.3, the displacement interferometry section of this chapter. To calculate the X, Y, Z coordinate of the retroreflector the CPU combines the distance information from the interferometer with the angle information from the encoders to calculate the position of the target. The data from the interferometer and encoders gives the position of the target in spherical coordinates and the CPU simply converts the data from spherical coordinates to Cartesian coordinates to give the location of the target. Figure 2.2 shows a point in space in both Cartesian in spherical coordinates.

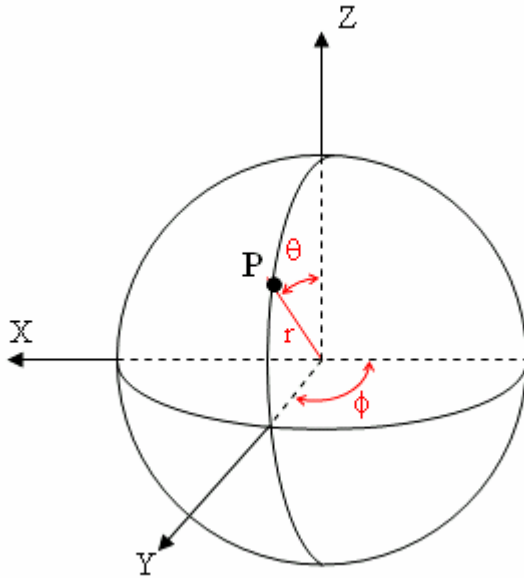


Figure 2.2. Point in space in Cartesian and Spherical Coordinates

The relationship between spherical and Cartesian coordinates can be described with the following equations:

$$X = r \sin(\theta) \cos(\phi) \quad (2.1)$$

$$Y = r \sin(\theta) \sin(\phi) \quad (2.2)$$

$$Z = r \cos(\theta) \quad (2.3)$$

To track the retroreflector the beam splitter not associated with the interferometer takes a small portion of the return beam and sends it to a position sensing or CCD detector (see Figure 2.1). As the target moves, the return spot on the detector moves and this movement is sent as an error signal back to the servo control system. The servo system then moves the tracking mirror to keep the return laser spot at a nominal position and keep the error signal to a minimum.

Because the tracker uses displacement interferometry to determine distance, the tracker must be calibrated before making any measurements. Most trackers have a location on the tracking unit itself where the target can be placed and the tracker can be calibrated. The location of this calibration point has been precisely measured at the factory that built the tracker and also serves as the origin for the system or the default coordinate system. One of the most powerful features of laser trackers is their ability to change the reference coordinate system. This feature gives the user the ability to make relative measurements from features of the part or system that is being measured. For example in an optical system, the reference coordinate system could be set at the center of curvature of the primary mirror and all subsequent measurements can be made from that point in space.

2.1.2. Error Sources for Laser Tracker

The laser trackers available on the market today claim that they can give the position of a target to within .001" or 25 μ m of its actual position. Some of the systems mentioned in the introduction claim better performance but these systems are still in the prototype stage and are not available from manufacturers. Many factors can contribute to potential errors in the readings from the laser tracker [9]. These error sources include:

- Angular Encoding Errors.
- Tracking Errors.
- Orthogonality (height of standards) errors.

- Distance measuring errors.
- Errors from Beam misalignment.

Angular Encoding Errors Encoding errors and pointing accuracy errors present the biggest obstacle in the laser tracker's performance. To have a system accuracy of $25\mu\text{m}$ or better the angular pointing accuracy must be better than $2.5\mu\text{rad}$ [9]. To minimize this error, the best available motors and encoders are used. Also, air bearings are used for both the azimuth and elevation axes to ensure that the encoders provide the needed precision.

Tracking Errors Air turbulence and temperature gradients cause the refractive index of air to vary [21]. This variance in the refractive index can cause the laser beam to bend as it travels through space and this bending causes a tracking error. A 1°C temperature gradient causes 0.3 arc second error [9]. Temperature gradient can be minimized by rigorously controlling the temperature of an area where a measurement is being made or by dissipating heat sources by creating a laminar flow with fans. Many laser trackers are equipped with a weather station that measures the ambient temperature, humidity, and air pressure and uses these measurements to compensate the reported measurement for these error sources. Boeing has published a study that investigates how this compensation affects the overall calibration of the laser tracker [22]. This source of error is more thoroughly investigated in the displacement interferometry section of this chapter.

Orthogonality Errors These errors are also known as height of standards errors and come from the fact that the true vertical axis is not orthogonal to the horizontal axis. The amount of difference between the actual vertical axis and the nominal vertical axis is denoted with δ_v . Orthogonality errors have caused errors in surveying for years and are caused by the measurement staff not being held vertical. [23, 24] This surveying error must be considered with the laser trackers performance because the radius of the earth causes vertical to change slightly over the laser tracker's operating range. To calculate the maximum δ_v the radius of the earth and the range of the tracker must be considered. The range of most trackers is 35 meters and can track approximately over a 135° range in azimuth. This range over the earth's 6371 km radius translates into a maximum δ_v of approximately $10\mu\text{rad}$. Variations in true vertical from nominal vertical cause errors on both the horizontal and vertical axis and can be expressed with the following equations [9]:

$$\theta_h = r\delta_v \frac{\sin(\phi)}{\tan(\theta)r} \quad (2.4)$$

$$\theta_v = \frac{r}{2}\delta_v^2 \cos(\theta) \quad (2.5)$$

Where θ_h is horizontal error, θ_v is the vertical error, and θ , ϕ , and r are from the standard spherical coordinate notation and can be seen in Figure 2.3. Figure 2.3 also describes δ_v .

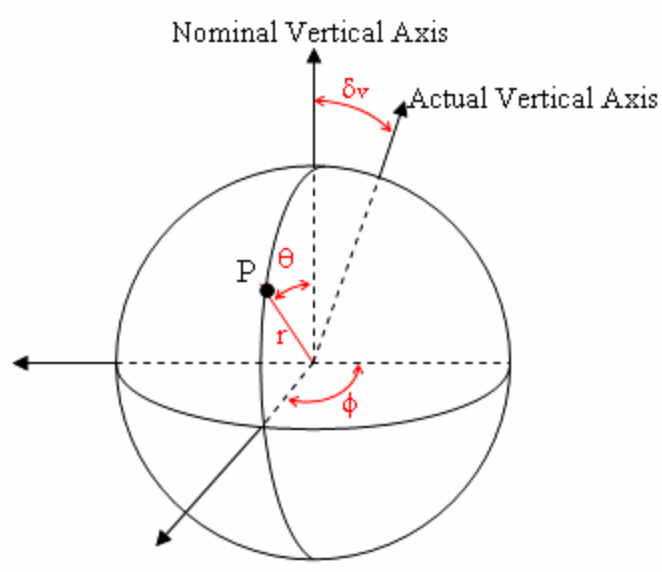


Figure 2.3. Spherical Coordinate System with True Vertical Axis.

Inspecting equation 2.4 and 2.5, it is clear that if the measurement range of the laser tracking system is kept close to horizontal, orthogonality errors can be minimized. Figure 2.5 plots the horizontal and vertical errors as a function of θ .

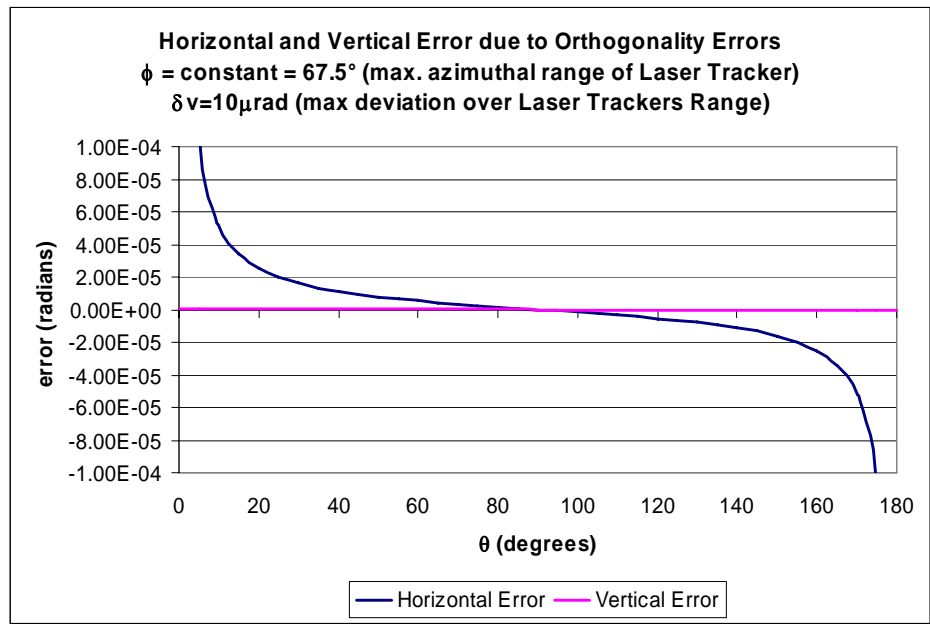


Figure 2.4. Horizontal Error and Vertical Error as a function of θ .

Figure 2.4 shows that the horizontal error rises to infinity when θ_a approaches vertical. Figure 2.4 also shows that if the measurement range is kept between 60 and 120 degrees or +/- 30 degrees from horizontal, these errors can be minimized.

Distance Measuring Error The laser interferometer can measure relative distances very accurately but the laser tracker gives an absolute coordinate of a point in space. To do this the tracker must be calibrated to a reference location. This calibration will have inherent errors and these errors will propagate and can even be magnified in subsequent measurements. The geometry of the spherical coordinate system causes the calibration errors to be magnified at extreme measurement angles from horizontal. If the measurement range is kept between +/- 30 degrees from horizontal the maximum error due to Calibration will be $1.323 \times$ calibration error. This error can be minimized by careful calibration to keep the calibration error low and also operating the tracker close to horizontal so that the multiplication factor applied to the actual calibration error can be minimized.

Beam Alignment The final error that will be discussed will be the error due to the laser beam not being aligned to the rotation axes of the pointing mirror. This is a similar to the collimation error inherent in surveying instruments [23]. The maximum error caused by this misalignment is shown in equation 2.6 and δ_{off} and β are defined in Figure 2.5.

$$\theta_{\max} = \frac{\delta_{off}}{\cos(\beta)} \quad (2.6)$$

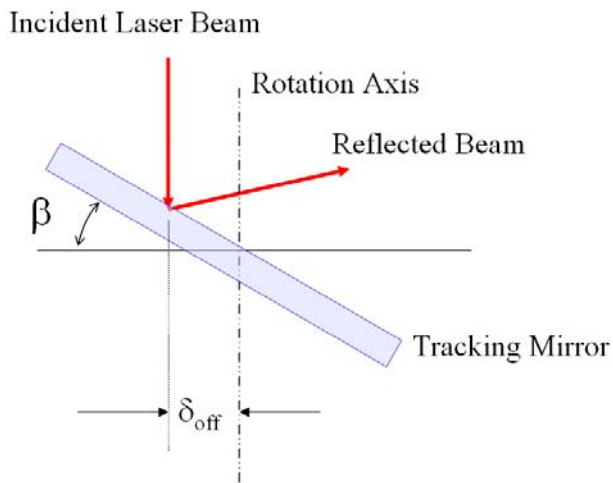


Figure 2.5. Error due to beam misalignment to the tracking mirror

Having an efficient servo system that keeps the return beam close to the nominal position can minimize beam alignment errors. Also, use of a hemispherical mirror has been proposed by Hong Jiang to minimize the error caused by laser beam misalignment [25]. Using the hemispherical mirror and a large δ_{off} of 0.5mm, Jiang shows that this technique reduced the beam alignment error from .57 mm to .06 μm .

As in any measuring machine there are many sources of error that contribute to the overall uncertainty of the device. These errors must be managed in an error budget to ensure that the errors do not combine to be greater than the overall uncertainty goal for the system. The mechanics of the error budget are discussed in detail in the optical alignment section of this chapter.

2.1.3. Specification for Laser Tracking Systems

Three main suppliers build and sell laser trackers including Leica Geosystems, FARO Inc. (formerly SMX), and Automated Precision Incorporated. Both the SMX and Leica Geosystems tracker were used in this research. The Leica Geosystems LTD500 3D Laser Tracking System is shown in Figure 2.6. The research presented in this thesis does not compare the different manufacturer's trackers but rather investigates the tracker's viability as a tool for the optical shop.

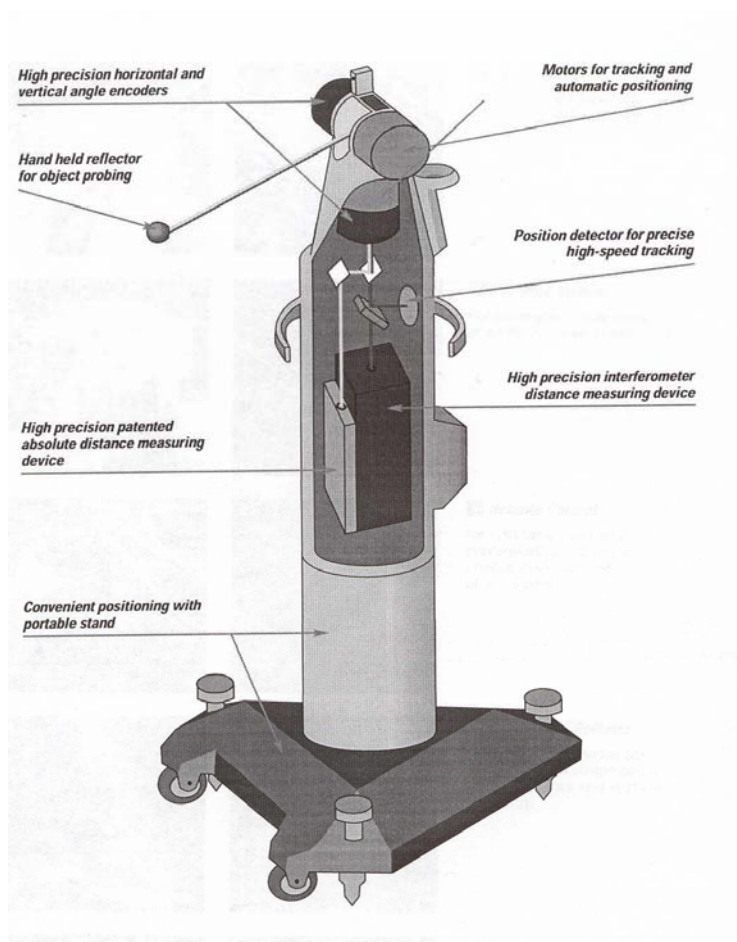


Figure 2.6. Laser Tracking System [20]

The LTD500 from Leica is a Portable Coordinate Measuring Machine complete with a controlling CPU, software, and the tracking unit itself. The tracking unit utilizes a heterodyne interferometer and angle encoders to make dynamic measurements. The tracker is also equipped with an absolute distance measuring device that will allow the tracker to move to prescribed target locations without having to follow a retroreflective target. Table 2.1 displays the performance specifications published by Leica for the LTD500 system.

Table 2.1. Leica LTD500 System Specifications

Tracking		Laser Interferometer	
Maximum Target speed	6.0 m/s	Principle of Operation	Heterodyne
Maximum Acceleration	2 g	Power	< 0.3 mW/CW
Range of Measurement		Wavelength	633 nm
horizontal	± 235°	Beam Diameter	
vertical	± 45°	1/e2	4.5 mm
distance	0-35 m		
Accuracy		Absolute Distance Meter	
Angle Resolution	0.14"	Principle of Operation	Light Polarization
Distance Resolution	1.26 μm	Power	<.5 mW/Pulsed
Repeatability *	± 2.5 ppm (μm/m)	Wavelength	780 nm
Absolute Accuracy of a Target		Beam Diameter	
Static *	± 5 ppm (μm/m)	1/e2	10 mm
Dynamic *	± 10-20 ppm (μm/m)	Accuracy	± 25 μm
* 1 σ value		Misc	
		Temperature Range	41°F - 104°F
		Relative Humidity	10% - 90%
		Elevation	0 - 10,000 ft

The SMX 4500 tracker is a comparable unit to the Leica LTD500. The SMX unit is also equipped with both a heterodyne laser interferometer as well as an absolute distance meter that can be used to help the tracker relocate the target if the beam is broken. Table 2.2 presents some of the specifications for the SMX laser tracker.

Both the Leica and the SMX laser tracker systems include a powerful software package that gives the user capability to take advantage of the trackers many features. These features include making static or dynamic measurements, creating a surface map of a surface, fitting data sets into standard shapes such as spheres or lines, and creating new coordinate systems based on features of the part that is being measured. The sampling rate of each laser tracker is approximately 1000 Hz and the software allows the user many different ways to log data. Position information can be logged continuously but the high data rate will make an extremely large data file quickly. To manage data file sizes, the software gives the user the capability to log the average position of a target location, make measurements only after the reference target has moved more than a prescribed distance, and other data logging schemes are available.

Table 2.2. Specifications for the SMX 4500 Laser Tracking System.

	Radial Interferometer	Radial ADM	Transverse Encoders
Performance			
Resolution	0.16 μm	0.5 μm	0.25 μm
Repeatability	1 μm + 1 $\mu\text{m}/\text{m}$	7 μm + 1 $\mu\text{m}/\text{m}$	3 μm + 1 $\mu\text{m}/\text{m}$
Accuracy	10 μm + 0.8 $\mu\text{m}/\text{m}$	20 μm + 1.1 $\mu\text{m}/\text{m}$	18 μm + 3.0 $\mu\text{m}/\text{m}$
Tracking			
Speed	4.0 m/s	N/A	180°/s
Acceleration	Unlimited	N/A	180°/s ²
Error	0	N/A	5 arc-seconds
Range	35 m	35 m	280° Vertical 115° Horizontal
Misc.			
Temperature	40° F - 110° F	40° F - 110° F	40° F - 110° F
Altitude	0 - 10,000 ft	0 - 10,000 ft	0 - 10,000 ft
Humidity	0 - 95%	0 - 95%	0 - 95%
Laser	0.5 mW HeNe	0.7 mW IR	N/A

2.2. Laser Tracker Applications

Many applications have been developed for the laser tracker since its inception. Because of their capabilities and their versatility, industries from aerospace to automotive have developed uses for this powerful tool. Applications are continuing to grow as laser trackers become more accurate and easier to use. Laser trackers can be used in four different classes of applications, including: dynamic measurements, static measurements, combination of static and dynamic measurements, and combination of tracker measurements with measurements from other devices.

2.2.1. Dynamic Applications

The laser tracking system was originally developed to make dynamic measurements that could calibrate a robot's positioning performance. To make a dynamic measurement a tracking ball or retroreflector is simply attached to the structure that is to be measured. Usually the tracker ball is seated into a nest on the structure. This nest locates the ball at a precise offset from the structure and this offset can be backed out of the laser tracker's measurements. After the ball is seated on the structure it can be set into motion and the tracker will follow the target and record the dynamic position of the target. Depending on the type of software that is included with the tracking system, many different data recording options are available. Typically for dynamic measurements the tracker is set to only record data after the target has moved more than a prescribed amount such as .25". This logging feature helps reduce the size of the computer file generated with each measurement set.

Currently a collaborative effort between the University of Washington and Boeing is taking place to develop industrial robot applications. By using laser trackers in more sophisticated ways, the collaboration hopes to improve the accuracy of the industrial robot [26,27]. In addition to robot performance calibration, laser tracker dynamic applications include calibration of coordinate measuring machines, calibration of precision milling machines, measurement of bearing run-out performance, as well as others. Caterpillar Inc. has even used the tracker to measure the performance of the track on their construction vehicles [28]. Their engineers attached a retroreflector to the end of one of the track pieces or shoes and recorded the movement of the ball as the tractor went through uneven terrain. Caterpillar engineers have tried to make this kind of measurement for years but were unsuccessful until they employed a laser tracking system.

A simple test was performed at the University of Arizona that shows the power of the dynamic tracking ability of the laser tracker. A retroreflector target was glued to the end of a rod approximately 35 inches in length and the rod was hinged near the other end. A Leica laser tracking system was used to track the retroreflector as the target was swung through a radius. The software recorded the dataset and was configured to only record data points if the target was moved more than 0.25 inch. After the dataset was recorded, the tracker's software was instructed to fit the data to an arc. The software generated a report that computed the radius of the arc to be 34.4053 inches and displayed the deviation from the arc and the out of plane variation for each data point. Using the data

contained in this report the radius deviations and out of plane deviations were plotted.

Figure 2.7 shows a plot of the radius sweep and a plot of the out of plane variation.

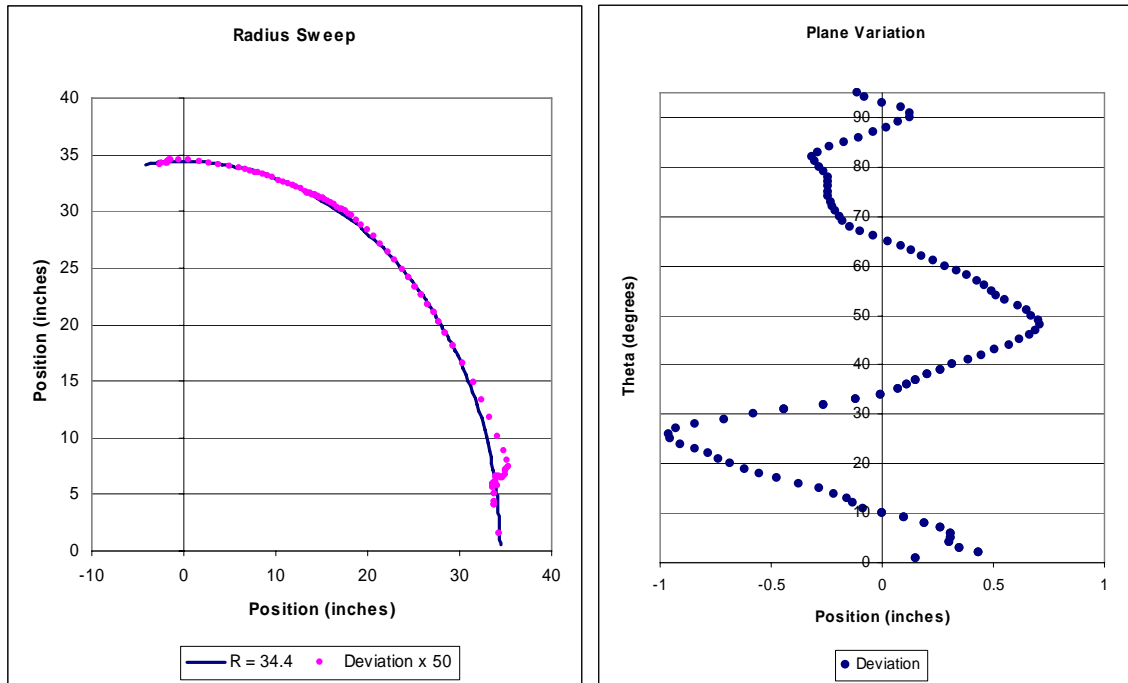


Figure 2.7. Radius Sweep and Out of Plane Deviation

This simple test gave an indication of how well the hinge was performing and how accurately this system was able to move the retroreflector in a true line. Figure 2.7 shows significant errors, but these errors were expected. The rod was held by hand and the hinge was simply two fingers holding one end of the rod while the other hand was used to sweep the rod through its motion.

2.2.2. Static Applications

Although the laser tracker was initially developed for dynamic measurements, the laser tracking systems that are available today have developed many static measurement

applications. When a laser tracker is used to make static measurements it has similar capabilities of a traditional CMM machine. A traditional CMM is typically a very large machine that utilizes a probe that is mounted on a motorized X, Y, Z stage. This probe touches an item under inspection at various locations. Encoders mounted on the X, Y, Z stage give the location of the probe and provide the 3-D measurement of the item that is being measured. To make a measurement, the item under inspection is laid on a table under the probe. Because of this the CMM must be bigger than the part that is being measured. The table that holds the item under inspection is extremely heavy and rugged to help offset the effects of environmental vibrations that can affect the measurement performance of the CMM. CMM have been used in the optical shop and can do a good job of profiling optics [29]. Pictured in Figure 2.8 is a CMM manufactured by Zeiss.



Figure 2.8. Zeiss Coordinate Measuring Machine [30]

A laser tracker measures an item in a similar way as a CMM. It uses azimuth and elevation encoders along with the distance information from the interferometer to create a spherical coordinate of the location of the tracker ball. This spherical coordinate is converted into an X, Y, Z coordinate to give the user more meaningful measurements. The power of the tracker to make static measurements comes from its long range and portability. The range of most commercially available laser tracking systems is at least 100, feet and this range can be carried out over 100 degrees in azimuth and 45 degrees in elevation. This allows the tracker to make CMM type measurements over an incredibly large volume. To further increase the measurement volume, a tracker can be moved to a new location to make more measurements on an item. This feature makes the laser tracker a portable coordinate measuring machine. To continue making measurements on a part of an assembly after moving the tracker a minimum of three reference points must be established. These reference points must be viewable from each measurement location position of the tracker. After the tracker is moved to a new measurement location the reference points must be reestablished. The portability and size of the tracker also allows the instrument to be stored in a small space when not in use.

Most trackers that are available today will provide a measurement with an accuracy of approximately .001". Although this accuracy is not as good as traditional CMMs, the tracker's range and portability still make the laser tracking system an attractive choice. New advances in tracker design continue to improve the accuracy of these instruments, and some groups are reporting accuracy of better than 0.0001" [14, 15, 25]. Because this

is better performance than most traditional CMMs, these advanced laser trackers could potentially be used to calibrate CMMs.

The large range and portability of the tracker has increased this tools versatility. Industries such as aerospace have found countless uses for the tracker to make large-scale measurements. Before the advent of the tracker, accurate large-scale measurements were difficult if not impossible to make. Boeing utilizes laser trackers to assist in the alignment of fuselage sections [20]. The laser tracker can quickly measure the pose of large sections to be assembled by making accurate measurements of alignment features that have been built into the sections. The laser tracker software can then tell the operator exactly how much misalignment is present in the sections, and the operator can make a precise adjustment to the location of one of the sections for proper alignment. Lockheed Martin is aligning tooling, such as drilling jigs, to aircraft bodies with laser trackers in the Joint Strike Fighter assembly [31]. Daimler Chrysler utilizes trackers to assist with assembly tooling [20]. NASA is currently investigating using a modified laser tracking system to install on the space shuttle. This system would replace its current videometric system that is used to measure the pose of satellites and would assist in the assembly of the international space station [32,33,34]. The Keck telescope in Hawaii has used laser trackers to assist with some of the large-scale metrology required with the construction of large observatories.

2.2.3. Combining Dynamic and Static Measurements

A third way to utilize the tracker is to combine the static and dynamic capabilities of laser tracking systems. A typical application that utilizes this technique would be to attach the retroreflector to a bearing race and spin the bearing. The tracker can dynamically track the reflector as it spins and can define an axis of rotation for the bearing. This axis can be used as a datum axis that static measurements can be made from.

A tracker can also be used as a surface profiler. To make a surface map the retroreflective ball can be mounted on the end of a rod and the ball can be manually slid across the surface. The tracker dynamically tracks the ball as it is slid across a surface and builds a dataset that can be reduced into a surface map. Figure 2.9 is a surface map of a radar dish that Composite Optics Incorporated built using a laser tracker.

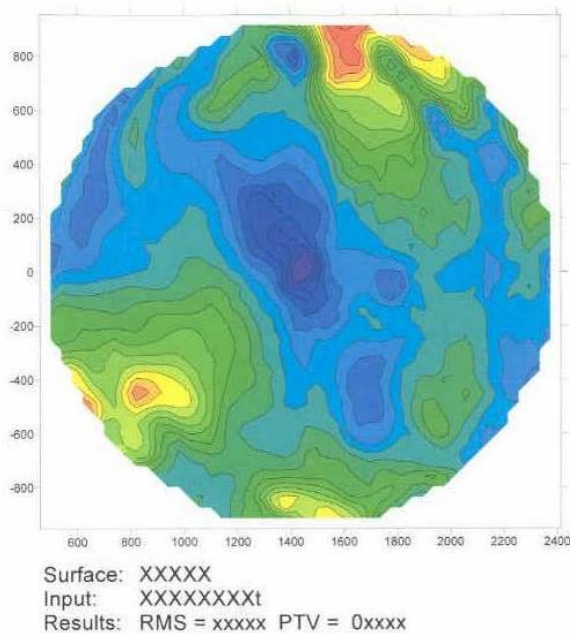


Figure 2.9. Surface Map from Composite Optics Incorporated

2.2.4. Combination of Laser Tracker Data with Other Measurement Data

The final application that will be discussed is the technique of combining the laser tracker data with data from other measurement instruments. Axila Incorporated has developed a scheme that uses an API laser tracker to measure the location of mounting pucks for their portable coordinate measuring arms. Axila's coordinate measuring arm is capable of making highly accurate and automated measurements, but the range of the arm is limited. The laser tracker is used to locate the measuring arm with respect to other measuring arms or to features on the assembly that is being measured. Figure 2.10 shows the API laser tracker measuring the location of a coordinate measuring arm.



Figure 2.10. Combining a Laser Tracker with Coordinate Measuring Arms. [35]

A triangular calibration fixture is mounted on the coordinate measuring arm's mounting platform, and the API laser tracker measures three points on this fixture. The coordinate measuring arm is then mounted to the platform to make local measurements. When the coordinate measuring arm measurements are combined with the laser tracker measurements, these local measurements can be related to a global coordinate system outside the measuring arm's range of motion.

Many different measuring techniques have been presented. These techniques show the versatility of this powerful tool. As understanding of the capabilities of these instruments continues to increase, new applications continue to be developed. Laser tracker systems are allowing engineers to creatively solve measurement and alignment tasks that were once extremely difficult if not impossible to complete.

2.3. Displacement Interferometry

A critical part of any laser tracking system is the displacement interferometer that is used to calculate the range portion of the measurement. Of the three pieces of information needed to calculate the X, Y, Z coordinate of the retroreflective target, the range information obtained from the interferometer is the most accurate. Some labs have demonstrated ways to increase the accuracy of the laser tracking system by using at least three laser trackers tracking the same point [13, 14, 15]. This scheme allows the system to calculate the X, Y, Z coordinate only using range information from the interferometers and eliminating the need for the encoders that diminish the laser tracker's accuracy.

Soon after the HeNe laser was invented in 1960, Airborne Instruments Labs introduced the first commercial displacement interferometer in 1964 [36]. This interferometer was configured in the Twyman-Green construction. This interferometer consists of a monochromatic light source, a beam splitter, a reference mirror, a measurement mirror, and an observation plane where interference fringes can be viewed. The Twyman-Green interferometer is a modified Michelson interferometer that was invented by A.A. Michelson in 1880. The only difference between the Twyman-Green interferometer and the Michelson interferometer is that the Michelson uses an extended source while the Twyman-Green uses a collimated monochromatic source. A block diagram of the Twyman-Green interferometer is pictured in Figure 2.11.

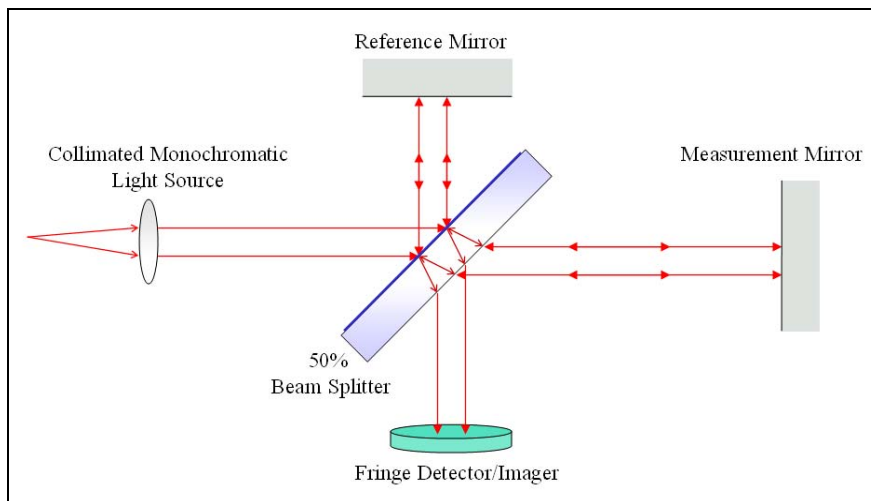


Figure 2.11. Twyman-Green Interferometer

2.3.1. The Basic Displacement Interferometer

The most common application for the Twyman-Green interferometer is to measure the surface figure of the mirror that is being measured, but displacement interferometry uses it to measure the location of the moveable measurement mirror. For most displacement interferometry applications, the moveable measurement mirror is a corner cube or some other type of retroreflector that reflects light parallel to the incident beam. The displacement interferometer uses the wavelength (λ) of light from the source as the length standard. Changes in optical path difference, or OPD, between the reference arm and the measurement arm can be measured by the interferometer. Each time the retroreflector is moved $\lambda/2$, the total OPD between the reference mirror and the measurement mirror is changed by one λ and each time the OPD changes by one λ , interference fringes are generated. While the moveable mirror is in motion, the displacement interferometer keeps track of how many times fringes have been created with a fringe counter. The fringe counter simply multiplies the number of times it has recorded a fringe by $\lambda/2$ to compute a distance. The displacement interferometer does not measure absolute distance. It measures relative distances because it can only sense changes in OPD between the reference and measurement mirrors. This is why laser tracking systems that utilize displacement interferometry must first be calibrated to a reference location before any meaningful measurements can be made.

The basic displacement interferometer described above has two primary limitations. It is incapable of sensing the direction of motion of the target mirror and the measurement

resolution is only $\lambda/2$. To overcome these problems two types of displacement interferometers have been developed. These types are Homodyne (DC) and Heterodyne (AC).

2.3.2. Homodyne Distance Measuring Interferometer

The Homodyne interferometer shown schematically in Figure 2.12 utilizes a monochromatic laser source, and adds a polarizing beam splitter, two quarter wave plates, and two linear polarizers to the basic Twyman-Green interferometer [37]. The homodyne interferometer analyzes the fringe intensity to determine distances below $\lambda/2$ and splits the return beam onto two detectors to determine the target's direction of motion. The return beam that is recombined at the polarizing beam splitter will be circularly polarized and then split again onto two detectors A and B. After the final split, the two beams will pass through linear polarizers that have their axis perpendicular to each other. Depending on whether the target is moving away from the interferometer or closer to the interferometer these linear polarizers cause the phase of the signal on A to lag or lead the signal on B by 90° . Homodyne interferometers are limited because any fluctuation of source intensity can be interpreted as target motion causing the power of the laser to rigorously be monitored and controlled.

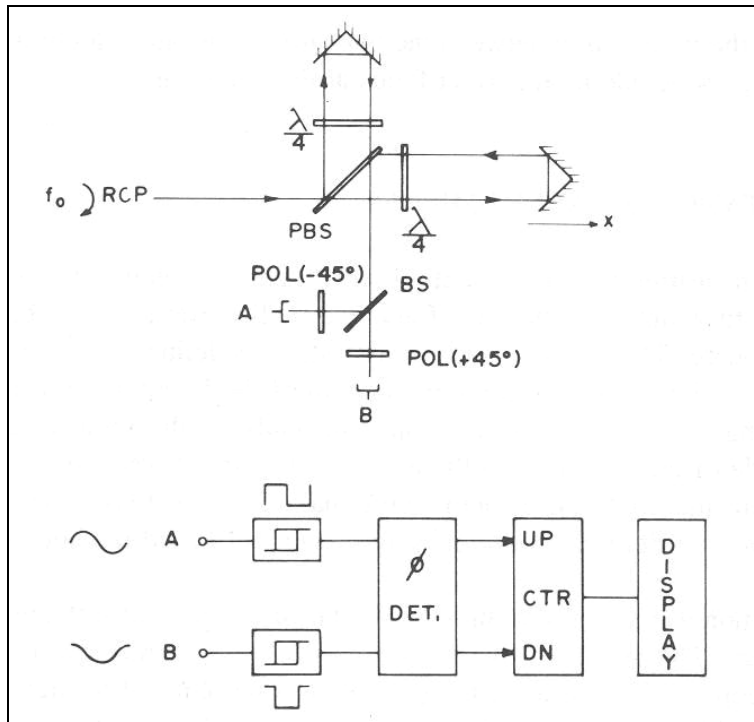


Figure 2.12. Homodyne interferometer schematic [37]

2.3.3. Heterodyne Distance Measuring Interferometer

Heterodyne interferometers improve on the homodyne interferometers by employing a dual frequency laser source to improve the resolution of the displacement interferometer. Many techniques are utilized to make a multiple wavelength source. One of the more common techniques is to use a single frequency source and applying a magnetic field to Zeeman split the beam into two frequencies of opposite circular polarizations. The heterodyne interferometer shown schematically in Figure 2.13 again employs two detectors, one to measure the frequency difference of the beam as it leaves the laser and the other to measure the frequency difference of the recombined beam. When the target

mirror is moving, the frequency of the light on this mirror will be Doppler shifted. The heterodyne interferometer then compares the information from the detectors to determine the direction of travel of the mirror and increase the systems resolution beyond $\lambda/2$ [37]. This method is advantageous because it uses the processing of electric signals to determine the distance and direction and these signals are not subject to drift.

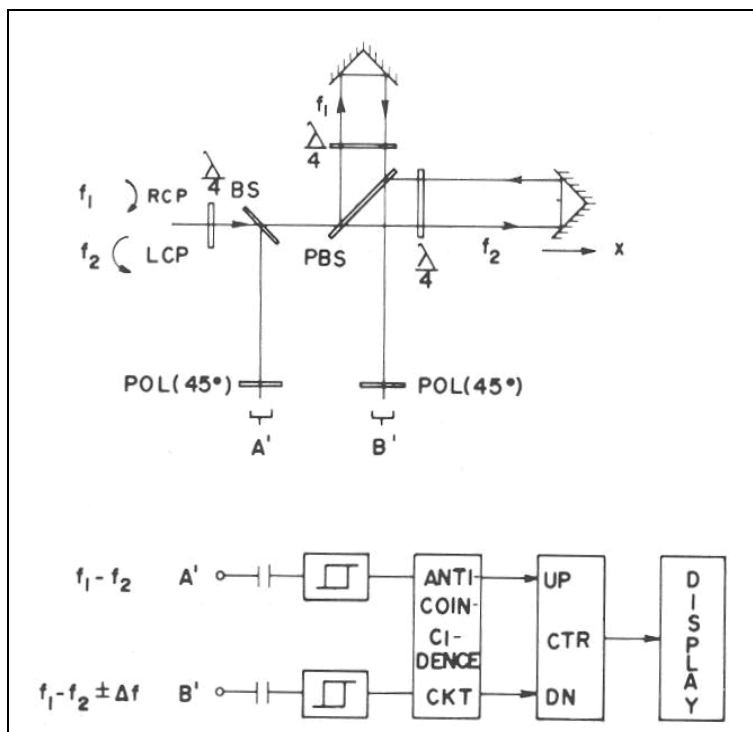


Figure 2.13. Heterodyne Interferometer schematic [37]

2.3.4. Error Sources for Displacement Interferometers

Intrinsic errors, environmental errors, and installation errors all affect the accuracy of the displacement interferometer [38]. Intrinsic errors include the accuracy of the laser wavelength, the measurement resolution, and optics non-linearity. Environmental errors include atmospheric compensation, material expansion, optical thermal drift, and

temperature gradients. Installation errors include deadpath error, cosine error, and Abbé error.

2.3.4.1. Environmental Errors

Changes in temperature, air pressure, and humidity cause the index of refraction of air to vary and these effects were carefully quantified and published by Bengt Eldén in 1968 [21]. Consequently, the wavelength of light changes as these fluctuations in environmental factors occur. The wavelength of light and refractive index are related as shown in equation 2.7.

$$\lambda_a = \frac{\lambda_v}{N_{air}} \quad (2.7)$$

Where λ_a is the wavelength in air, λ_v is the wavelength in vacuum, and N_{air} is the refractive index of air. Because displacement interferometers typically operate in air and use the wavelength of light as the length standard, environmental considerations must be taken into account to maximize the performance of the displacement interferometer. If a 1° C change in air temperature occurs or if a 2.5 mm of mercury air pressure change occurs or if an 80% change in relative humidity occurs, the displacement interferometer will register a measurement error of approximately one part per million. Calculating the actual index of refraction of the air based on the temperature, humidity, and pressure can reduce these errors. Once the true refractive index of the air is known, the system can actively compensate for the wavelength variations. Hewlett Packard has modified

Eldén's formulas by combining the temperature, pressure, and humidity impacts into one expression [36]. This new expression is also customized for 633nm, the wavelength of the HP distance interferometer systems and is shown in equation 2.8.

$$N = 9.74333 * P * \left[\frac{1 + P * (26.7 - 0.187 * T) * 10^{-6}}{0.934915 + 0.0020388 * T} \right] - 1.0899 * 10^{-3} * H * e^{0.032015 * T} \quad (2.8)$$

Where P is pressure in inches of Hg, H is the percent humidity, and T is the temperature in °F. Most commercially available displacement interferometers have the option to actively monitor the temperature, humidity, and air pressure and actively update the refractive index of air. Even with the actively monitored systems the measurement error of the interferometer is approximately 0.1 ppm because of the inaccuracies associated with the measurement of temperature, humidity, and air pressure [22].

Temperature effects not only cause errors associated with the refractive index of air but they also cause thermal expansion errors, optical thermal drift, and air thermal gradient errors. Thermal expansion of steel can introduce errors of 10 ppm if temperature is not controlled to within 1° C. Making measurements quickly before temperatures can change or rigorously controlling the temperature in the measurement environment can control thermal expansion errors. Introducing fans that create laminar airflow in the measurement environment can control thermal gradient errors by reducing the effects of the heat sources that cause thermal errors. Using an actively compensating

interferometer can also control errors due to thermal gradients and thermal expansions. Figure 2.14 from Hewlett Packard compares the measurement performance of a standard displacement interferometer to one that actively compensates for thermal effects.

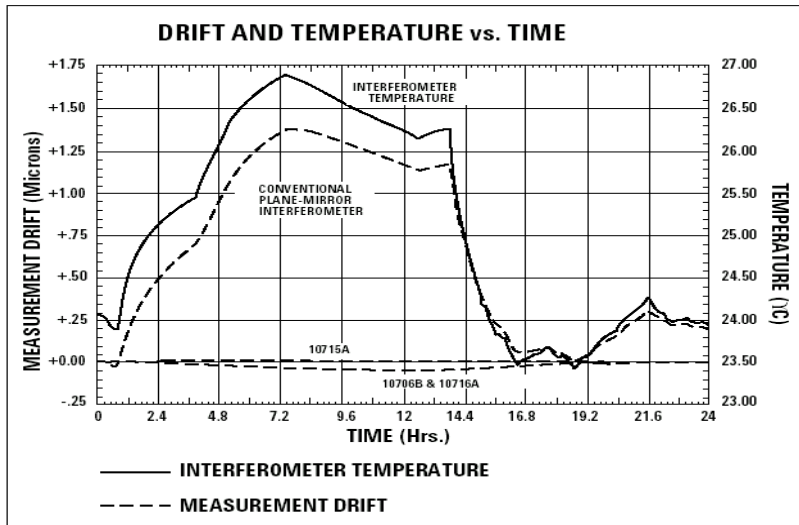


Figure 2.14. Measurement Drift vs. Interferometer Temperature [39]

2.3.4.2. Installation Errors

Installation errors are caused by the set up of particular measurements and include the cosine error, Abbé error, and deadpath error. Cosine error is similar to the beam alignment error discussed in the laser tracker theory section. A stand-alone displacement interferometer is not a tracking unit and must be properly aligned to the retroreflective target. If the machine holding the target traverses across a plane, the target must stay properly aligned to the interferometer. Misalignments cause cosine errors and the error, ε , can be expressed with the following formula:

$$\varepsilon = [(1/\cos \theta) - 1] \text{ ppm} \quad (2.9)$$

If θ is less than 2° , the paraxial approximation is valid and the error is simply:

$$\varepsilon = (1 - \cos \theta) \text{ ppm} \quad (2.10)$$

Where θ is defined in Figure 2.15.

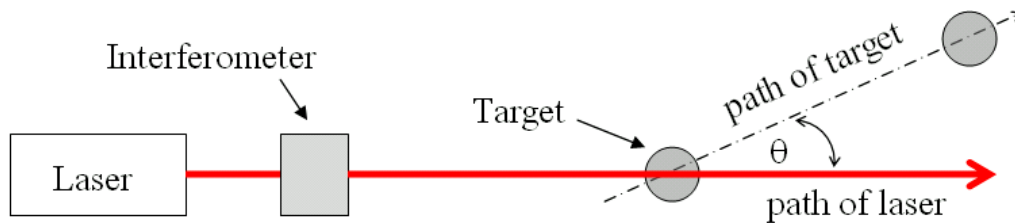


Figure 2.15. Cosine Error in Displacement Interferometers

When θ is large as is shown in Figure 2.15, the misalignment between the target path and the laser beam will cause the return beam to miss the interferometer. If the target transverses more than $35''$ and the return beam still reaches the interferometer, then cosine error will be less than 1 ppm and the cosine error can be ignored.

Abbé error is another error that can be eliminated with the proper set up. One of the most powerful applications of distance interferometry is to calibrate CNC milling machines. Most CNC machines are screw driven and violate Abbe's principle while a properly set up distance interferometer will not. Abbé error is shown schematically in Figure 2.16 and occurs because the measurement axis is not aligned to the probe path. Most machines drive probes with screws causing the probe carrier to not be normal to the

screw axis. This results in a slight measurement error known as Abbé error and can be expressed as follows:

$$\varepsilon = \delta_o \tan (\theta_o) \quad (2.11)$$

Where δ_o is the distance between the measurement axis and the probe path and θ_o is the off set angle shown in Figure 2.16. If the displacement interferometer is setup properly by placing the target along the probe path, δ_o is 0 causing the Abbé error to be 0.

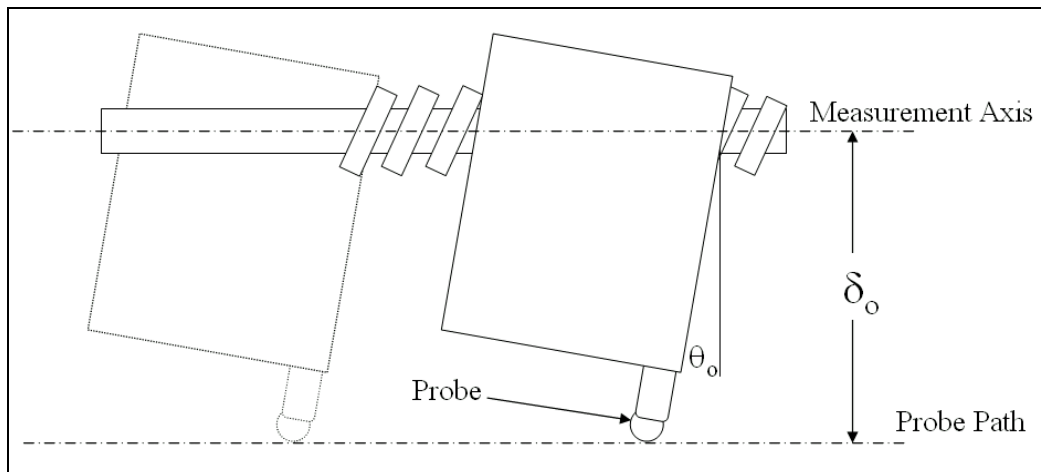


Figure 2.16. Abbé Error

Deadpath error is the final installation error that will be discussed. Deadpath errors occur when the interferometer is not located at the zero point for a given measurement. This can be corrected in most displacement interferometers because the interferometer can be physically moved to a desired location. In the case of a laser tracking system that integrates a displacement interferometer, the interferometer is fixed and deadpath error must be dealt with. Figure 2.17 describes deadpath error.

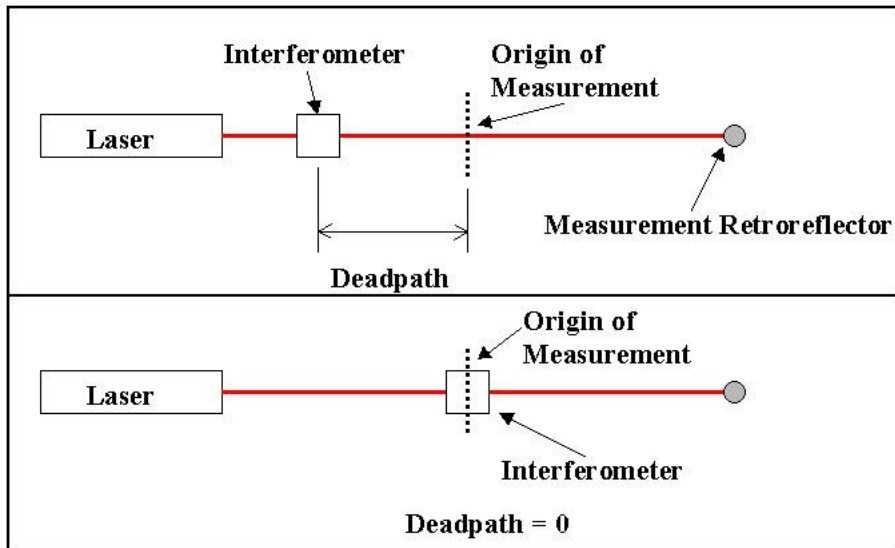


Figure 2.17. Dead Path Error in a Displacement Interferometer

Two factors cause deadpath errors, refractive index of air changes and thermal expansion of materials. These factors cause the location of the origin of measurements to shift and in turn affect any measurements from the origin. Both refractive index fluctuation and thermal expansion were discussed with the environmental errors of displacement interferometers. Reducing the distance between the interferometer and the measurement origin can minimize deadpath errors. If the measurements are made over a short period of time, deadpath errors can be minimized because the materials do not have time to expand or contract. Finally, by measuring temperature, humidity, and air pressure thermal expansion effects and index of refraction effects can be actively compensated for.

2.3.5. Specifications and Applications

Hewlett Packard's laser-interferometer systems are commonly used as the distance measuring interferometer for many prototype and commercially available laser tracking systems. Combining the HP 5517 or the HP 5501 dual frequency laser with the HP 10702 interferometer optics is a common configuration for the HP displacement interferometers. The specifications for this configuration are shown in Table 2.3.

Table 2.3. Hewlett Packard Displacement Interferometer Specifications

HP 5517 Laser Head		HP 10702 Linear Interferometer	
Type	HeNe, CW	Optical Resolution	316.5 mm
Maximum Power	1 mW	System Resolution	10 nm
Nominal Wavelength	632.991372 nm	Weight	8.2 oz.
Wavelength Stability	.002 ppm	Max Velocity	+/- 28 in/sec
Beam Diameter	6 mm		

Displacement interferometers are used in calibration applications such as calibrating the flatness of a precision surface plate, the positioning performance of CMMs and the positioning performance of precision CNC milling machines. Applications for displacement interferometers have also been developed in the photo-lithography industry that needs at least 250nm measurement resolution to measure the wafer steps found in today's semiconductors. Alex Greeleaf and Kam Lau also implemented the HP 5501A dual frequency Zeeman-split laser head in their first laser tracking systems [6, 9]

2.4. Position Sensing Detectors

The research covered in Chapters 3 and 4 employs the use of a position sensing detector or PSD. Chapter 3 describes how the PSD can be used in combination with a laser tracker to give an absolute position of an image in space. Chapter 4 uses the PSD to record image jitter. Also, PSDs are sometimes used in laser tracking systems to report the position of the return beam to the servo system.

Many different types of detectors can be used in position sensing including CCDs, quad

cells, lateral effect photodiodes, and others. The

PSD that is used in this work is a single pixel

lateral effect photodiode. The photodiode

provides an analog output that is proportional to

the location of the centroid of the incident light's

Power Density on the active area of the detector.

The output can also be thought of as the center of

gravity for all of the incident light on the

detector. The PSD offers a continuous analog

output of the position allowing the detector to

provide a fast response and high resolution. The

PSD gives a highly linear output as a spot is

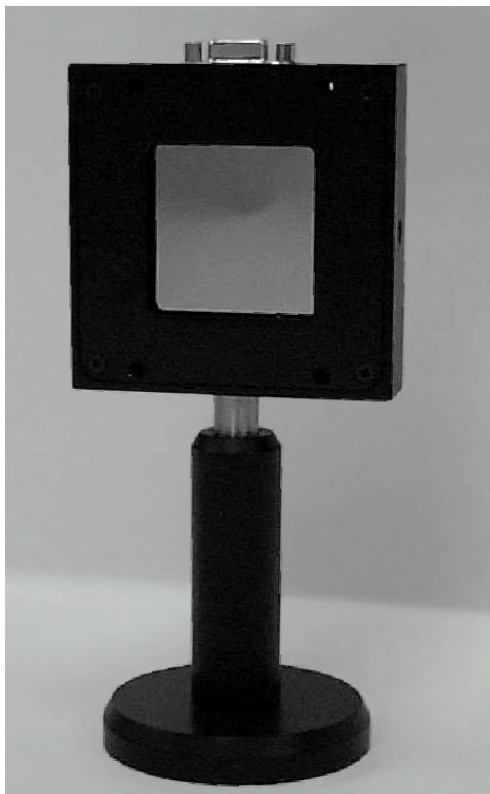


Figure 2.18. 45 x 45 mm PSD from On-Trak [40]

moved across the detector. Both 1 and 2 Axis PSDs are available and the active area for the detector ranges from 2.0 x 2.0 mm to 45 x 45 mm. Figure 2.18 shows a 45 x 45 mm PSD from On-Trak Photonics Incorporated.

The PSD integrates all of the incident light on the detector and reports the position of the center of gravity of this light. Figure 2.19 shows the response curve for the standard On-Trak PSD detector. This response curve is very similar to any standard silicon detector.

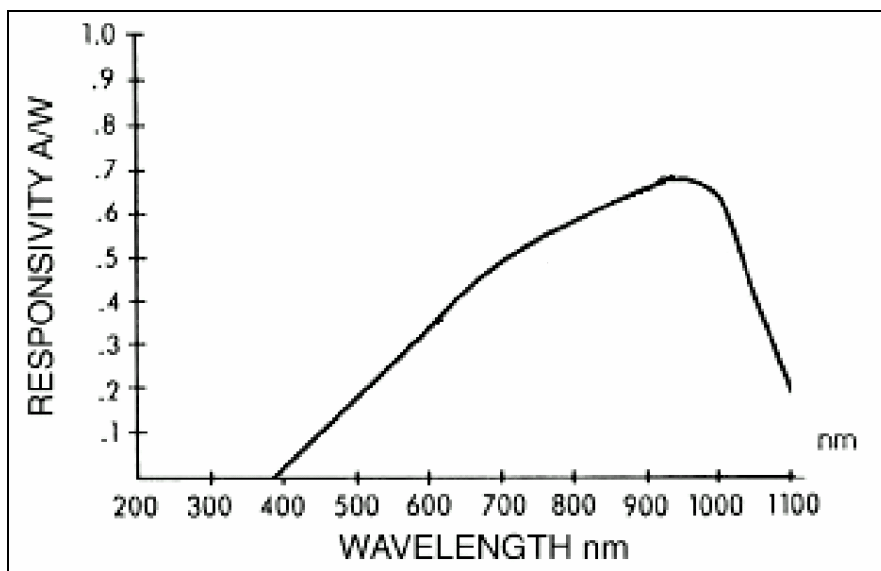


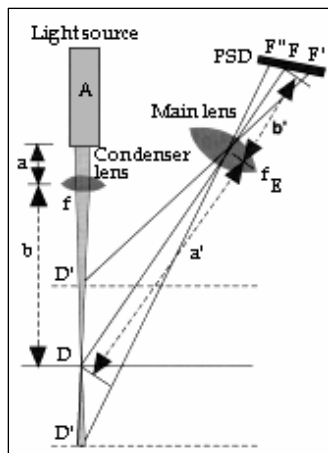
Figure 2.19. Response curve for single pixel PSD. [40]

Because the detector integrates all of the light incident on the detector, it can be used with a broad white light source or a narrow laser source as long as the wavelength of the source falls within the response curve of the detector. When PSDs are used with lasers, a

bandpass filter is typically used that allows the laser wavelength to pass but blocks out all other wavelengths.

PSDs are often confused with CCDs. Both PSDs and CCDs detect light but they do it in different ways. A PSD is a single pixel device that gives an analog output that is proportional to the location of a light spot on the detector, while a CCD is a multi pixel device that outputs digital data that can be used to image a scene. The PSD can not image it can only detect where the light is on the detector, but it can do this extremely fast and with extremely high resolution. CCDs can also detect the location of a spot on the detector but much signal processing is needed and the additional processing slows the response time of the CCD well below that of a PSD. Because PSDs are only one pixel analog devices they are much easier to manufacture than CCDs and therefore they are less expensive.

2.4.1. PSD Applications



Single axis PSDs are typically used for height and thickness measurements, wheel alignment, profile measurements, and inspection of manufactured parts. Dual axis PSDs are used for position and motion monitoring, image jitter measurements, robot calibration, straightness measurements, flatness measurements, and parallelism measurements. PSDs

Figure 2.20. Triangulation Probe from SiTek [41]

are most commonly used to measure relative movement of a surface or mirror. For example, some groups have recently used PSDs to measure the misalignments of resonator mirrors on high power lasers and used this information to actively correct the position of the mirrors [42]. Figure 2.20 from SiTek, Inc shows a typical setup that is used to measure surface movement. This setup is called a triangulation probe. Surface D is the surface of interest, and light from source A strikes the surface and is reflected back to a collection lens E. The collection lens then focuses the reflected light onto the PSD at point F. If surface D now moves to location D' then the focused spot on the detector will be moved to F' and the PSD will record this movement. The work that is included in this research uses the dual axis PSDs position and monitoring capabilities but will not be setup as a triangulation probe. A laser beam will be focused onto the PSD and relative movement of the focused spot will be recorded.

2.4.2. PSD Operation Principles

PSD is a photodiode that transforms incident light on the detector into photoelectric current. The PSD consists of a silicon substrate with two resistive layers separated by a p-n junction. The front side of the substrate is a p-type resistive layer with contacts at opposite ends and the back side is a n-type resistive layer with contacts at opposite ends. The front side contacts are orthogonal to the back side contacts. When a light spot is incident on the detector, the layers act as a homogeneous resistance causing the current

flowing through each contact to depend linearly on the location of the spot on the detector. The position of the spot on the X and Y axis is calculated as follows:

$$X_{position} = \frac{L_x}{2} * \frac{X_1 - X_2}{X_1 + X_2} \quad (2.12)$$

$$Y_{position} = \frac{L_y}{2} * \frac{Y_1 - Y_2}{Y_1 + Y_2} \quad (2.13)$$

Where L_x and L_y are the length of the detector in the X and Y directions. The currents, X_1 , X_2 , Y_1 , and Y_2 are defined in Figure 2.21.

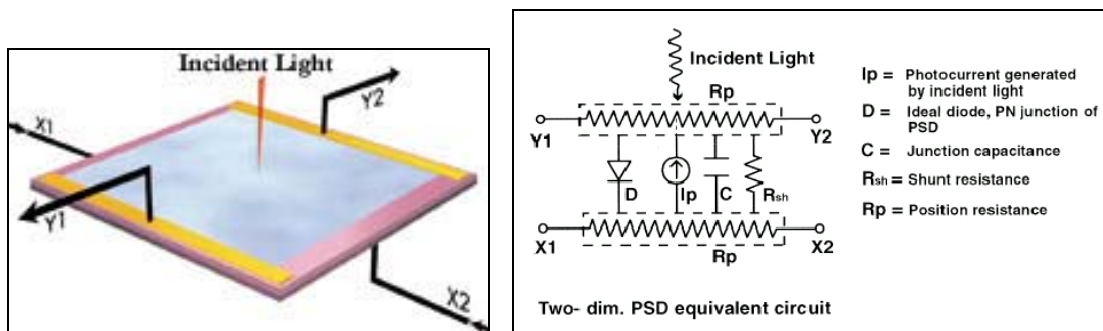


Figure 2.21. Dual Axis PSD Schematic [40]

These equations are derived from the well-known $V=IR$ equation and do not depend on the intensity of the light on the detector. As long as the intensity is below the maximum threshold for the detector and above the minimum sensitivity of the detector, the intensity of the light on the detector is not critical.

2.4.3. Specifications and Selection of the PSD

The 2.0 mm x 2.0 mm dual axis PSD from On-Trak Photonics was chosen for this research. On-Trak's PSD system was selected because its availability and it also offers a low cost solution that is easy to integrate into a measurement system. On-Trak uses a PSD from SiTek incorporated and integrates the PSD into a measurement system. The measurement system includes a packaged detector, an amplifier, and cables. This system has an ultra fast frequency response of 15kHz and sends out a 16 bit data stream between +/- 10 volts. This data stream is converted to position by measuring calibration factors and multiplying the calibration factor by the voltage from the PSD. The default calibration factors are:

$$\frac{L}{2} * \frac{1}{10} \left[\frac{mm}{V} \right] \quad (2.14)$$

Where L is the length of the side of the active area on the detector. The resolution of the Detector is 1 μ m and the linearity across the active area of the PSD is 0.8%. The maximum power density on the detector is 3 W/cm². The detector is AR coated by SiTek with a two layer coating that is optimized for 860 nm. At 633 nm the reflectance of the detector is approximately 10%, so reflections need to be considered in this work.

In addition to the PSD other items were needed to get useful data from the PSD. Table 2.4 describes the different components that are used in the PSD measurement system that has been constructed. For more detailed information on the performance of the system see the PSD Characterization section.

Table 2.4. PSD Measurement System Components

Component	Manufacturer	Part Number	Description
PSD	On-Trak	PSM2-4	4.0 mm Dual Axis PSD
Amplifier	“	OT-301	Dual Axis Amplifier
Filter	Melles Griot	03FIL224	632.8 Filter 10nm BW
Data Acquisition Board	National Instruments	6036E	16 Bit, +/- 10V
Breakout Box	“	BNC-2110	8 Channel Input
Software	“	LabVIEW	Version 6.1

Software has been developed to interface with the PSD using LabVIEW from National Instruments. For more information on the software interface see the PSD Characterization section and Appendix A.

2.5. Optical System Alignment

All optical systems must be properly aligned for maximum performance. The research presented in this thesis investigates the viability of laser trackers for optical alignment applications. Also, some conventional alignment techniques are presented with this research.

2.5.1. Geometry of Optical Alignment

An optical system is a device with more than one optical element. Alignment is critical for all optical systems from large multiple mirror astronomical telescopes to small groups of lenses used to focus light onto a fiber optic in telecommunication applications. The

examples that are investigated in this section are primarily reflective systems, but the concepts can be applied to refractive systems as well. Optical systems utilize spheres and aspheres to focus light to form an image or to illuminate a target. In most optical systems the system alignment is driven by the geometry of the system and each optical axis of the individual elements needs to be co-aligned. The optical axis for each element passes through its center of curvature and its vertex. Figure 2.22 describes the center of curvature and the optical elements in a two surface reflective system.

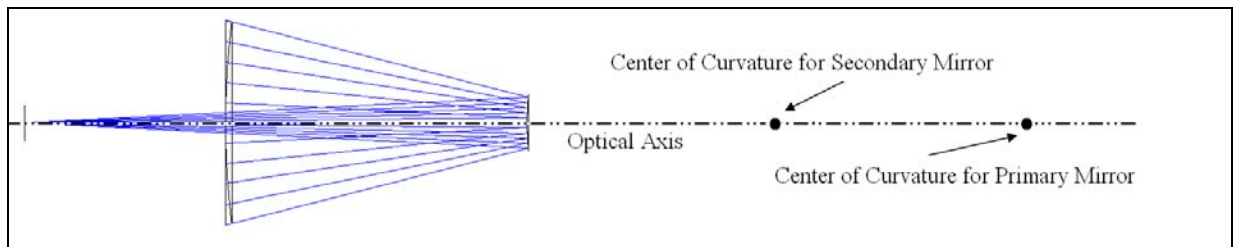


Figure 2.22. Optical Axis and Center of Curvature of an optical system.

The more elements in the system, the more complicated and critical the alignment is. Fold mirrors that change the direction of the optical axis further complicate the alignment. Additionally, the use of off-axis spheres and parabolas can make the system alignment more challenging than the actual optical design of the system.

Certain features of the geometry are more important than others in optical systems. The optical engineer must know where the optical axis is and he must develop techniques to place the center of curvature of each of the optical elements along the axis. Other points might be of interest in optical systems, for example the focal point of an off axis parabola

or the no coma point in a Ritchey-Chretien telescope, are of critical interest in specific designs.

Spheres and aspheres are used to make optical elements. Many mirrored systems utilize the geometry of a parabola because the parabola will focus collimated light to a diffraction limited point where a sphere will not. Also, off axis sections of a parabola are often used instead of a symmetrical parabola to reduce the size of the system. The use of off-axis parabolas theoretically will focus light to a diffraction limited spot but the alignment of these elements is extremely challenging. Comparing the geometry of a sphere and the geometry of a parabola can illustrate the difficulty in the alignment of off axis parabolas. Figure 2.26 compares the sphere and asphere and illustrates that the clocking of a parabola is critical where the clocking of a sphere is not.

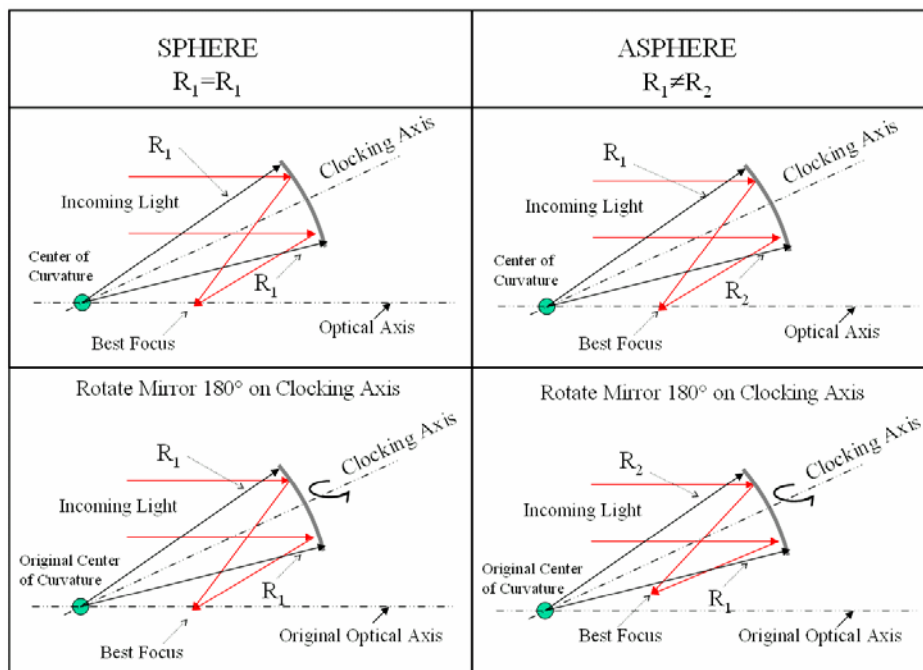


Figure 2.23. Clocking of off-axis spheres and aspheres.

Figure 2.23 illustrates that the sphere is symmetrical about the clocking axis, causing the orientation of the sphere to have no impact on the optical alignment. Figure 2.23 also shows that the parabola is not symmetrical about the clocking axis. Parabolas have unique optical axis where a sphere has an infinite number of axis because of the symmetry in the geometry. Figure 2.23 shows an extreme example where the parabola is clocked 180 degrees incorrectly the focal point of the parabola moves away from the original optical axis causing the orientation of the off axis parabola to be critical. Any clocking error will cause the focal point to move and as a result the, the alignment for a parabola requires the control of more degrees of freedom than that of the alignment of a sphere. The geometry illustrated is governed by the general sag equation:

$$Z = \frac{1}{[K + 1]} \left[r - \sqrt{r^2 - (K + 1)R^2} \right] \quad (2.15)$$

Where K is the conic constant, r is the radius of curvature of the optical element, and R is the location off axis that the sag is to be analyzed. The conic constant varies as the shape of the optical element changes and the following table lists the conic constants.

Table 2.5. Conic Constants

Shape	Conic Constant
Hyperboloid	$K < -1$
Paraboloid	$K = -1$
Ellipsoid	$-1 < K < 0$
Sphere	$K = 0$
Oblate Spheroid	$K > 0$

2.5.2. Impacts of System Misalignment

When an optical system is misaligned the system wavefront quality is affected. Even if the optical surfaces are perfect, severe aberrations can occur if an optical system is misaligned [43]. An example of the criticality of alignment is evident in the efforts to segment primary mirrors so that many small mirrors can be put together to make one large primary mirror. Figure 2.24 shows a simulated interferogram of a parabolic primary mirror made up of 36 segments that were perfectly fabricated but were improperly aligned [44].

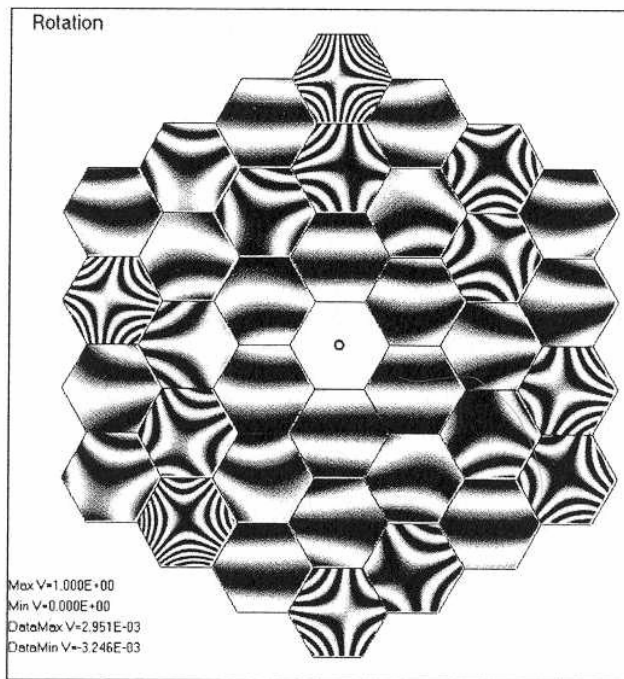


Figure 2.24. Segmented mirror with 1.5 mrad tilt between segments [44]

In a traditional system, the primary aberrations that occur due to misalignments are coma and astigmatism. In higher element systems, such as the example shown above, higher order aberrations are introduced but coma and astigmatism still dominate. Optical modeling software does an excellent job of modeling system degradation as a result of system misalignment. To demonstrate misalignment effects, a classic Cassegrain telescope was investigated. Figure 2.25 shows the telescope that was modeled in ZEMAX. The primary mirror is parabolic with a radius of curvature of 400 mm and the secondary mirror is hyperbolic with a radius of curvature of 125 mm.

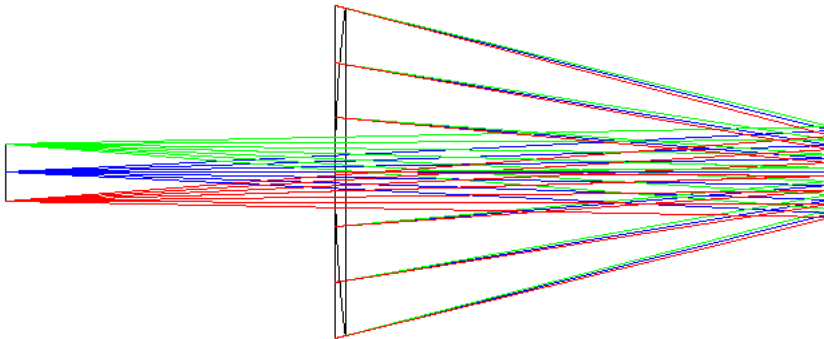


Figure 2.25. Cassegrain Telescope

Assuming that the surfaces on the telescope are perfect, the Cassegrain telescope will produce a diffraction limited spot at the on-axis field point. But when the secondary mirror is decentered by just .25mm, the focused spot is no longer diffraction limited and it has over 3 waves p-v of coma. When the off axis spot is also analyzed, the aberrations due to misalignment include astigmatism and coma. In the Ritchey-Chretien telescope

design, the secondary mirror design is modified to have high order aspherical terms and a properly aligned system will have no coma anywhere in the field. This design has an additional point of interest for the optical engineer, the neutral point. If the secondary mirror is rotated about the neutral point, only astigmatism is introduced into the system. This allows the coma and astigmatism to be separated. It has been shown that if the secondary mirror is decentered and not tilted, only coma will be introduced [45,46,47]. Other aplanatic systems such as the Offner relay system satisfy Abbe sine condition and only astigmatism is added when the optical elements are decentered or tilted.

Optical alignment effects on system performance need to also be considered in the optical testing of the surface figure of the individual optical elements. During the fabrication phase of the optical elements, interferometric testing is used to regularly check the surface figure. The optician uses the information from the test to guide him during the polishing process. If the optical element under test is not properly aligned to the interferometer, both the aberrations from the test and the aberrations from imperfections in the surface figure will be reported in the results of the test. These aberrations due to an improperly aligned test can extend the amount of time needed for fabrication because the optician is using flawed information to guide him during the polishing phase. If the misalignment of the test is repeatable in between polishing iterations, the optician will polish out aberrations that are not really there and in turn create imperfections in the optical surface. These imperfections will degrade the optical performance of the system even when the system is perfectly aligned.

2.5.3. Error Budget for Optical System Alignment

Because misalignments in the optical system cause system wavefront error, the impacts of these misalignments must be managed in an error budget. The error budget takes into account all potential sources of error and assigns a tolerance for each contribution. Each of the factors that can potentially cause wavefront errors are added up in Root Sum Square (RSS) in a system wavefront error budget. This RSS value must be less than the overall system wavefront specification. The contributions are added up in RSS because each error does not always directly impact the system performance, some errors can actually cancel out errors found in other areas of the system. The contributions from the surfaces of the optical elements, the system alignment, the design residual, and the design margin are all errors that contribute to the overall system error. Contributors to the surfaces portion of the error budget include surface figure errors, radius of curvature departures, distortions from the support frames of the elements, and testing uncertainties. The alignment portion of the error budget typically needs a separate error budget that considers the different degrees of freedom for each of the optical elements, and assigns a tolerance for each degree of freedom. To understand how the misalignments affect the system wavefront error, perturbation techniques can be used. In optical modeling software such as ZEMAX small perturbations can be applied to each of the degrees of freedom for each of the optical elements separately. ZEMAX will calculate the effect of the perturbation to the system wavefront error and a relationship relating perturbation to wavefront error can be found for each degree of freedom. Each relationship can then be

tabulated to form a set of relationships for the system. Over small perturbations as the ones found in misaligned optical systems this relationship between perturbation and wavefront error can be assumed to be linear [48]. This linear relationship gives the optical engineer an efficient method of tolerancing an optical system, because only one set of relationships is needed from the optical modeling software. If the tolerances need to be balanced, the values can be changed using the linear relationship instead of remodeling the different values in the optical modeling software. In the alignment budget each degree of freedom and its impact to the overall system wavefront specification are considered to be decoupled allowing the errors associated with each degree of freedom to be added in RSS to predict the overall impact of alignment errors to the system wavefront error.

As an example of a system wavefront error budget an Offner Relay Imager will be investigated. The Offner relay consists of a primary mirror and a secondary mirror located at the prime focus. The system that is investigated will consist of a segmented primary mirror increasing the optical elements in the system to 3 elements. The diameter for each of the primary mirrors and the secondary mirror is 2 inches for this design. This system will be investigated further in laser tracker alignment chapter of the thesis and is included here to better illustrate the mechanics of an error budget. Error budgets are typically built in spreadsheets allowing the contributions to be easily balanced and visually represented. Figure 2.26 shows the ray trace of the system and Figure 2.27 shows the top level error budget for the 3 mirror Offner Relay.

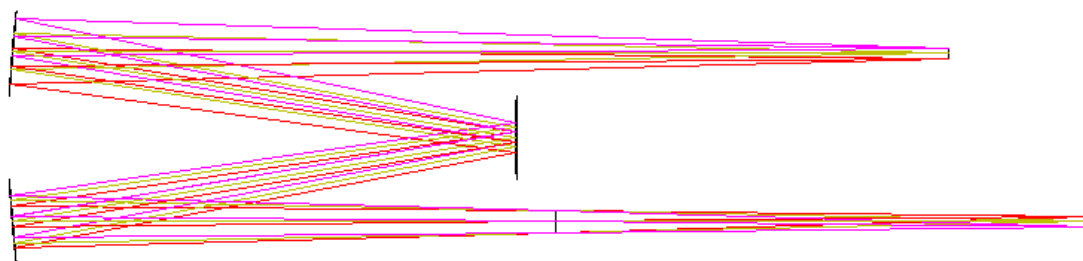


Figure 2.26. Three Mirror Offner Relay System

system error budget	RMSWE in waves	$\lambda=633\text{nm}$	
Total system	0.5		roll up
Optical surfaces	0.43		roll up
PM1	0.25		roll up
figure		0.25	.25 wave rms surface
Radius of Curvature Departure		0.01	+/- 2%
support		0.00	6.6 nm rms surface
optical test		0.01	noise, ref surface, and backout
SM	0.25		roll up
figure		0.25	.25 wave rms surface
Radius of Curvature Departure		0.00	+/- 2%
support		0.00	4 nm rms surface
optical test		0.01	noise, ref surface, and backout
PM2	0.25		roll up
figure		0.25	.25 wave rms surface
Radius of Curvature Departure		0.01	+/- 2%
support		0.00	6.6 nm rms surface
optical test		0.01	noise, ref surface, and backout
alignment	0.20		from system alignment budget
design residual	0.00		from Zemax Model
design margin	0.15		

Figure 2.27. Top Level Error Budget for 3 mirror Offner Relay System.

This top level budget assigns tolerances for the surfaces of the optical elements, the alignment, the design residual, and the design margin so that the RSS value of the

contributions add up to be less than or equal to the overall system specification of 0.5 waves tested at 633 nm. Because alignment of this system has many potential degrees of freedom that can impact the overall wavefront error of the system, the alignment is managed in a separate budget. The top level budget allots .2 waves of system wavefront error to the alignment of the system. The impacts of tilt and decenter were found and tabulated for each of the elements. Also, since the primary mirror is segmented into two pieces, impacts of the primary mirror acting as one piece are also tabulated. Figure 2.28 shows the alignment error budget that was generated for this system.

Alignment error budget (wavefront)

Error Budget (from top level error budget)		0.20 waves at $\lambda=633\text{nm}$		
Degree of Freedom	tolerance			rms waves
design residual				0.000069
Object position	1 inches			0.01
PM1 x dec	0.14 inches			0.09
PM1 y dec	0.14 inches			0.09
PM1 x tilt	0.1 degrees			0.03
PM1 y tilt	0.1 degrees			0.03
PM2 x dec	0.14 inches			0.06
PM2 y dec	0.14 inches			0.06
PM2 x tilt	0.1 degrees			0.02
PM2 y tilt	0.1 degrees			0.02
SM x dec	0.3 inches			0.05
SM y dec	0.3 inches			0.06
SM x tilt	0.3 degrees			0.01
SM y tilt	0.3 degrees			0.01
PM x dec	0.3 inches			0.05
PM y dec	0.3 inches			0.04
PM x tilt	0.2 degrees			0.01
PM y tilt	0.2 degrees			0.01
SM - (PM1&PM2)	0.1 inches			0.01
PM-SM-PM	0.1 inches			0.00
			RSS	0.19 waves
			margin	0.05 waves
			TOTAL	0.20 waves

Figure 2.28. Alignment error budget for Offner Relay system

The error budget shows that the alignment of the primary mirrors is more sensitive than that of the secondary. Therefore, the primary mirror tolerances are much tighter causing the primary mirror to need more sophisticated positioning tools than the secondary mirror. The error budget also contains an additional design margin because the assigned tolerances are less than the total allotment of 0.2 waves when the RSS of each of the tolerances are added. The tolerances were assigned using the relationships between perturbation and wavefront error that were found using ZEMAX modeling software. This relationship is assumed to change linearly as the tolerance changes allowing the tolerance to be found using the formula:

$$W_a = \frac{t}{p} W_p \quad (2.16)$$

Where W_a is the wavefront error due to the alignment, W_p is the wavefront error calculated by optical modeling software as a result of a perturbation, p is the amount of perturbation used to calculate W_p , and t is the tolerance assigned for the degree of freedom. Figure 2.29 shows the relationships between perturbation and wavefront error that were used to generate the alignment error budget shown in Figure 2.28. The mechanics of the error budget shown in this example can be used to tolerance other aspects of an optical system including pointing accuracy, image jitter, thermal drift, and others.

Degree of Freedom	perturb		dWsim
Object position	0.7	inches	0.005
PM1 x dec	0.1	inches	0.066
PM1 y dec	0.1	inches	0.066
PM1 x tilt	0.05	degrees	0.013
PM1 y tilt	0.05	degrees	0.013
PM2 x dec	0.1	inches	0.045
PM2 y dec	0.1	inches	0.046
PM2 x tilt	0.05	degrees	0.009
PM2 y tilt	0.05	degrees	0.012
SM x dec	0.2	inches	0.032
SM y dec	0.2	inches	0.038
SM x tilt	0.1	degrees	0.003
SM y tilt	0.1	degrees	0.003
PM x dec	0.3	inches	0.048
PM y dec	0.3	inches	0.041
PM x tilt	0.2	degrees	0.013
PM y tilt	0.2	degrees	0.013
SM - (PM1&PM2)	0.1	inches	0.008
PM-SM-PM	0.1	inches	0.004

Figure 2.29. Perturbation to Wavefront error relationships

2.5.4. Optical Alignment Tools

Many tools and techniques are utilized that assist in optical alignment. These tools range in accuracy and sophistication and include tape measures, micrometers, alignment lasers, autocollimators, alignment telescopes, interferometers, wavefront sensors, computer generated holograms, and others.

Because the optical alignment is dictated by the geometry of the system, traditional measuring tools such as tape measures and micrometers can be used to align optical surfaces and to set proper spacing between elements. The level of accuracy from these techniques is limited and can damage the optical surfaces because they often require the surfaces to be touched by the measuring tool.

A technique often used in optical alignment is to create a reference axis and align the optical axis of each of the elements in the system onto this axis. Alignment lasers can be used to generate this reference axis. The size of the laser beam and the diverging properties of the beam are two primary limitations of the alignment laser. When the laser beam passes through optical elements, the beam is no longer collimated causing the beam to expand the further the beam is propagated. When the beam is expanded, the center of the beam is difficult to accurately determine and the accuracy of the alignment laser is reduced. Alignment lasers are useful in the alignment of fold mirrors and slow optical elements that do not cause the beam to diverge rapidly.

A different tool that is often used to create an optical axis is the alignment telescope. An alignment telescope is a powerful tool that can focus on object as close as 1" from the end of the telescope to objects at infinity. The optical axis generated by the alignment telescope and the mechanical axis of the telescope is typically aligned to within 3 arc seconds. Figure 2.30 shows an alignment telescope manufactured by Taylor Hobson.

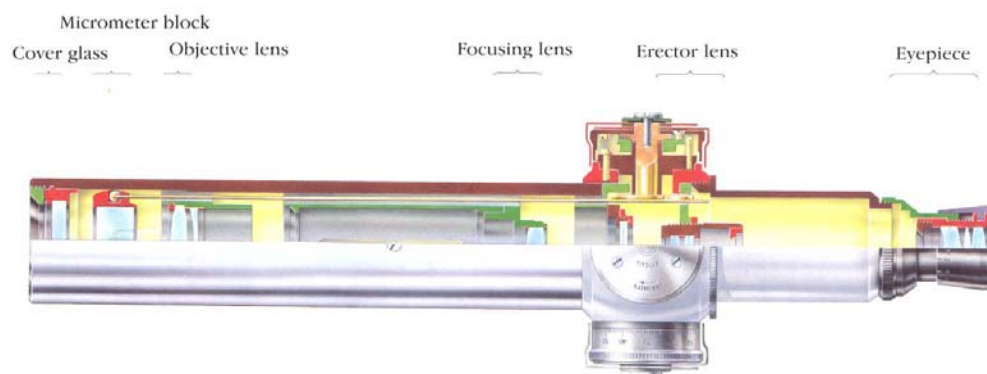


Figure 2.30. Taylor Hobson Alignment Telescope [49]

To create a reference axis the alignment telescope is typically aligned to a datum target and then the optical elements to be aligned are placed in the optical axis. When the optical elements are placed on the reference axis, they cause the focus of the datum target to change and they cause the optical axis between the telescope and the target to bend. This causes the telescope and the target to no longer be aligned. To align the optical element, the telescope must refocus on the datum target and the optical element must be positioned so that telescope is realigned to the datum target. Only the focus of the alignment telescope should be changed when new elements are added, moving the optical element that is being aligned should allow the target to be realigned to the telescope. A typical setup of an alignment telescope is shown in Figure 2.31.

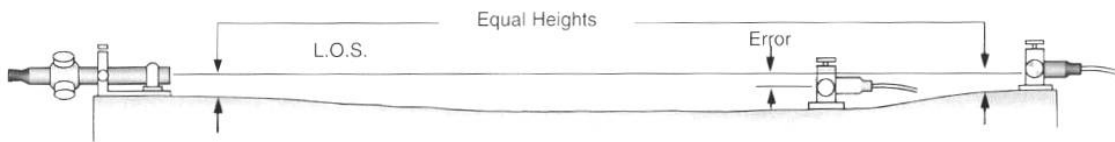


Figure 2.31. Alignment telescope setup [49]

If the alignment telescope to be placed on the optical axis of an existing system the alignment process can be complicated. Aligning fold mirrors in an optical system also complicate the alignment process. These complicated scenarios sometime need to utilize an autocollimator to better orient the alignment telescope to the optical system. Most alignment telescopes act as an autocollimator when they are focused at infinity. An autocollimator sends out a collimated beam and when the autocollimator is aligned perfectly normal to a reference flat, the reflected beam will be aligned to the beam

leaving the auto collimator. Autocollimators are also available as stand alone pieces of equipment and are used to align multiple flats or measure the wedge in prisms or parallel windows.

Interferometers can also be used to align optical systems. In the case of a segmented mirror the interferometer can be used to ensure the center of curvature of each of the segments is properly aligned. In the example of the Offner relay shown in the error budget section, the budget says that the mirrors center of curvatures need to be aligned to within 0.1 degrees or 1.7 mrad. For this alignment the interferometer can be configured similar to the way needed for the spherical surface test as shown in Figure 2.32. If one of the mirrors is nulled out with zero fringes and the other mirror is aligned to have less than 10 fringes, then the total tilt between the two mirrors will be 10 waves. The mirrors in this example are 2" diameter and the testing wavelength is 633 nm. Consequently, 10 waves of tilt translates into .127 mrad, which is much less than the 1.7 mrad that the error budget requires, therefore the Primary mirrors are aligned within tolerance.

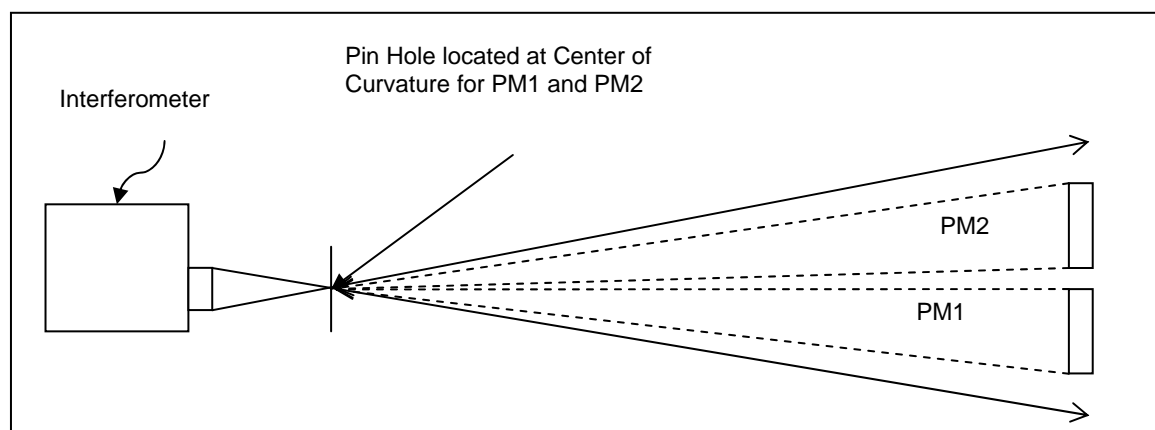


Figure 2.32. Interferometer used to align segmented primary mirrors.

Interferometers can also be used as a wavefront sensor to measure the amount of aberrations from the optical system. Much research has been done in recent years to try to optimize the technique of aligning optical systems by using aberrations as a measure of how much misalignment is in an optical system. [45, 46, 47, 50] The surfaces of each of the elements that make up a system are well known and these surfaces can be input into optical modeling software. The modeling software can then predict the residual wavefront error and Zernike coefficients. These coefficients can be backed out of the system test data and the remaining wavefront errors should be due to misalignments in the system. Understanding the dynamics of the optical system and their effects on system wavefront error is critical when these techniques are employed. For example, in the Ritchey-Chretien system mentioned previously in this section decentering the secondary to produce coma and tilting the secondary about the neutral point to produce astigmatism can separate the coma and astigmatism. This separation of aberrations is critical in helping the optical engineer apply the information provided by the interferometer so that the system can be aligned.

Computer generated holograms (CGH) have also been investigated to assist with alignment [51]. CGHs have been used for years to assist in the testing of aspherical mirrors and recently alignment fiducials have been incorporated into the CGHs for alignment purposes. These fiducials can help with the difficult clocking problems associated with off-axis parabola alignment during testing and could also have potential applications in system alignment. A CGH with alignment features typically has the information needed to test the aspheric mirror on the circular pattern near the center of

the hologram and the alignment information is embedded in the square pattern surrounding the circular pattern. Figure 2.33 shows a photograph of one of the alignment fiducials produced by the CGH.

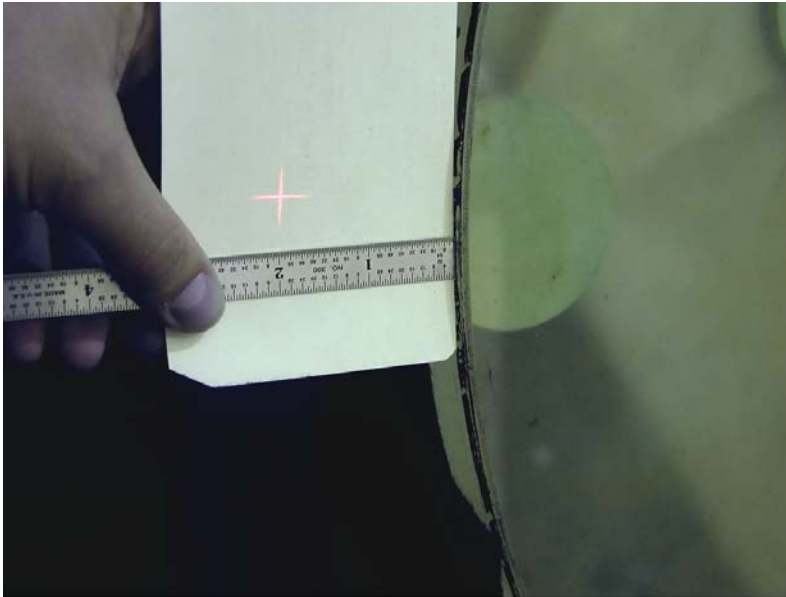


Figure 2.33. Photograph of alignment fiducial produced by CGH.

The location of these fiducials must be known in reference to other features of the part or system that is being aligned. For some applications, the location only needs to be known to within .050" and a ruler is acceptable for locating the fiducials in these applications. For applications that require more accuracy, CCD cameras have been used to locate the fiducial on CCD chip, allowing the fiducials to be located to within a tolerance of 50 microns.

The research in this thesis looks at a new tool that can potentially have powerful applications in optical system alignment. This research investigates the viability of using

a laser tracking system in combination with a position sensing detector to easily locate alignment fiducials produced by a CGH. The tracker has the ability to relate the location of these fiducials to other features in the system. This research will also look at the viability of using laser trackers to align an optical system by using the surface profiling features of the laser tracker to find and track the center of curvature for different optical elements.

CHAPTER 3. EVALUATION OF TRACKER AS AN OPTICAL TOOL

To test the viability of the tracker for optical applications, three applications were targeted for investigation. The three targeted applications were radius of curvature measurement of an optical surface, alignment of optical elements, and image tracking. Experiments were designed and executed that would help draw conclusions on whether or not the tracker would be a useful tool in the optical shop. Many of the error sources that were identified were not corrected because of the limited time that the tracker was available for experimentation. This chapter presents the results and the analysis of the experiments that were performed.

For the experiments presented in this chapter, the SMX 4500 laser tracker was used and the Absolute Distance Meter (ADM) was turned on. Table 3.1 shows a summary of the specifications for the SMX laser tracker, section 2.1.3 goes in further detail on the specifications of the SMX laser tracker.

Table 3.1. Specifications for SMX 4500 laser tracker

	Radial Interferometer	Radial ADM	Transverse Encoders
Resolution	0.16 μm	0.5 μm	0.25 μm
Repeatability	1 μm + 1 $\mu\text{m}/\text{m}$	7 μm + 1 $\mu\text{m}/\text{m}$	3 μm + 1 $\mu\text{m}/\text{m}$
Accuracy	10 μm + 0.8 $\mu\text{m}/\text{m}$	20 μm + 1.1 $\mu\text{m}/\text{m}$	18 μm + 3.0 $\mu\text{m}/\text{m}$

3.1. Gauge Block Investigation

To demonstrate the measurement capability of the laser tracker a simple test was performed that used the laser tracker to measure a 2 inch gauge block. A grade two Gauge block from Mitutoyo that is 2.0 ± 0.000008 inches long was used for this demonstration. To perform this test a 1.500" tracker ball was used. A tracker ball is a corner cube that is housed inside of a tooling ball. The tracker ball is a true retroreflector that is calibrated such that the beam is reflected exactly from the center of the 1.500" tooling ball.

In this experiment the gauge block was measured at many different distances from the tracker. To make the measurement, the ball was simply put on one side of the gauge block and the tracker was instructed to find a Cartesian coordinate of the tracker ball. The tracker ball was then moved to the other side of the gauge block and again the tracker was instructed to find a Cartesian coordinate of the location of the ball. After the tracker found the two data points, the tracker's software can find an absolute distance between the two coordinates that were measured. To ensure that the tracker ball was touching the gauge block at exactly the radius of the ball, a jig was constructed so that the ball could be held against two flat surfaces and along the gauge block. Figure 3.1 shows the jig that was constructed for this measurement.

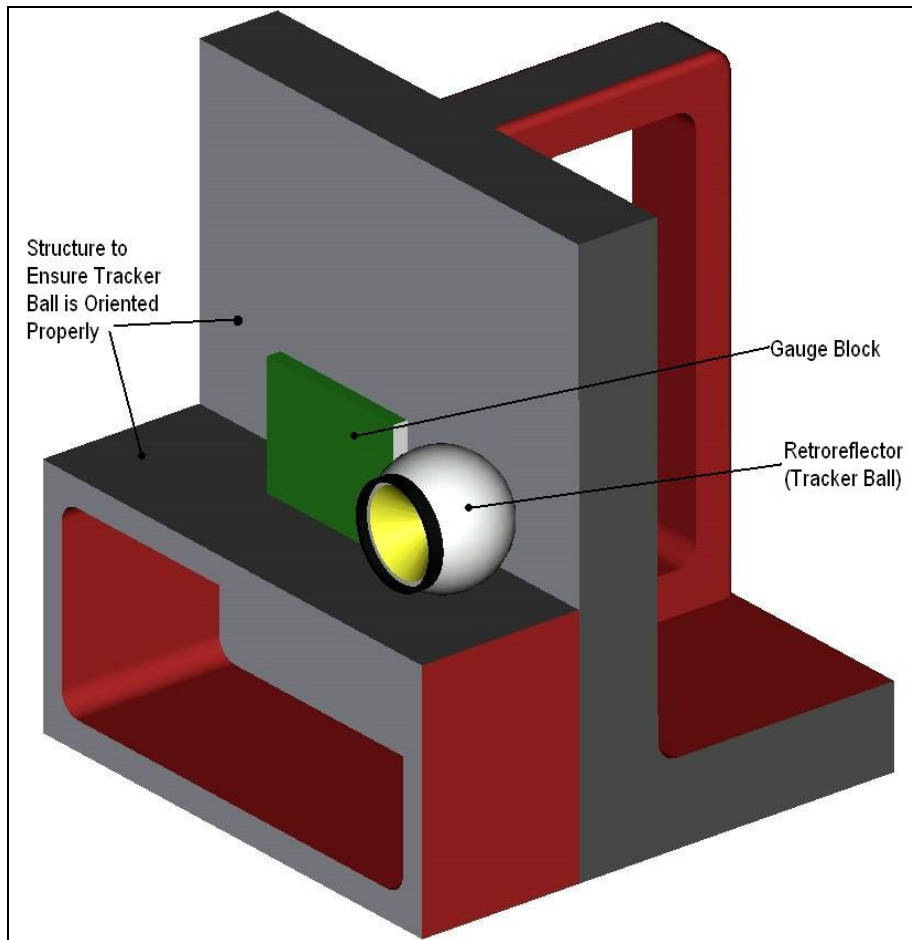


Figure 3.1. Setup for gauge block test

The setup shown in Figure 3.1 was placed at many different distances away from the tracker and the length of the block was measured. To increase the accuracy, the tracker was set to record 2000 data points for each measurement. The tracker's software averages these data points and reports the average as the location of the ball. Figure 3.2 shows the results of this test and compares the results to the expected performance based on the SMX tracker specification. Because the ADM was enabled for this test the expected accuracy was $20\mu\text{m} + 1.1\mu\text{m}/\text{m}$ as stated in Table 3.1.

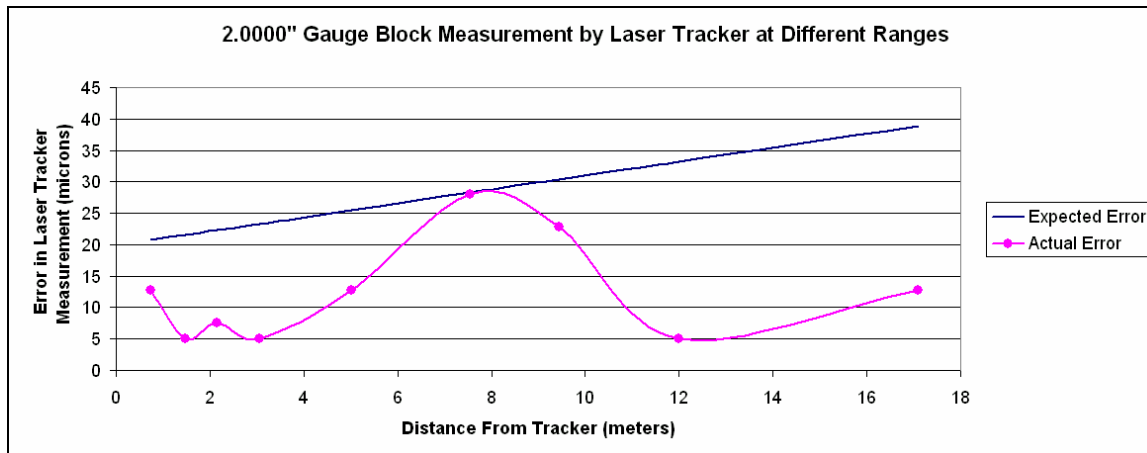


Figure 3.2. Results of Gauge Block Measurement at different ranges.

Figure 3.2 shows that the laser tracker performs remarkably well, even at extended ranges of 17 meters, the tracker still measured the ball to within 12 micron accuracy. The last measurement of 17 meters was the longest line of site that was available in the shop where the tests were performed. There were two main measurement error sources that were introduced into this test that could be eliminated. The first error source is that the gauge block could have been held more rigidly, it was attached to the base with hot glue, as the tracker ball was placed against the block, the block could have slightly moved. The second error source was that the tracker ball was held by hand against the gauge block introducing errors from an unsteady hand. Even with these two significant error sources, the tracker still performed better than it's specification for this test.

3.2. Radius of Curvature Investigation

The first optical application investigated was the application of measuring the radius of curvature of an optical element. To perform these measurements the profiling features of

the laser tracker were used. When a surface is profiled with a laser tracker, the tracker ball is generally rubbed across a surface and the tracker is set to make a measurement each time the ball is moved by more than a set increment such as 0.25". The tracker's software then generates a point cloud that describes the surface that has been profiled. This profiling technique is not ideal for measuring an optical surface because the contact of the tracker ball to the optical surface can damage the surface and the contact needs to be minimized. Instead of rubbing the surface with the tracker ball the surface was profiled by taking individual points at set locations and having the software fit the data to a sphere. This technique still requires the optical surface to be touched with the tracker ball but the contact is minimized to just a few points that are needed to define the surface.

For this experiment, a single mirror was used but it was tested in many different scenarios. The mirror used was a 10.5" diameter concave spherical mirror with a radius of curvature of approximately 16.7". Three variables on the testing technique were varied to generate a series of tests that indicate the tracker's ability to measure the radius of curvature of an optical element. The three variables were: (1) location of tracker with respect to the surface being measured, (2) number of data points used to generate a surface, and (3) the percentage of the complete sphere that is being used to fit the data to.

The radius of curvature for the 10.5" diameter mirror that was used for the tests presented in this section was first measured with a spherometer and then with an autostigmatic test. The autostigmatic test was performed with a Wyko 6000 interferometer equipped with a

high precision measurement rail. The spherometer measurement is an easy measurement to perform and gives a rough idea of what the radius of curvature is. The measurement with the interferometer is one of the most precise ways that a radius of curvature can be measured and can report a radius of curvature with an accuracy of better than 5 microns. The following table compares the two measurements.

Table 3.2. Radius of Curvature Measurements with traditional techniques.

Measurement	Spherometer	Interferometric Autostigmatic Method
Radius of Curvature	16.983 in.	16.7243 in.

The radius of curvature measurement using the autostigmatic method with the Wyko 6000 interferometer will be considered the standard for which the laser tracker will be compared to in the following sections.

3.2.1. Location of Tracker with Respect to Surface Being Measured

The first test was to investigate the effect that the location of the tracker had with respect to the surface being profiled. In chapter 2 the error sources of the tracker were thoroughly discussed and it was determined that the radial measurement capabilities of the tracker are incredibly precise and the transverse encoders are what limits the tracker's accuracy. As the tracker is moved to shallower angles with respect to the surface under measurement, the angular encoders are needed more to profile the surface and the tracker's performance is expected to decrease. To make this series of tests, the tracker

was placed in 5 different locations with respect to the mirror. At each tracker location, 10 data points were used to define the surface and the surface was profiled 10 times so that an average radius could be calculated. Figure 3.3 shows the test setup and how theta is defined for the different measurements. For the case where the tracker is looking directly at the mirror, theta equals zero.

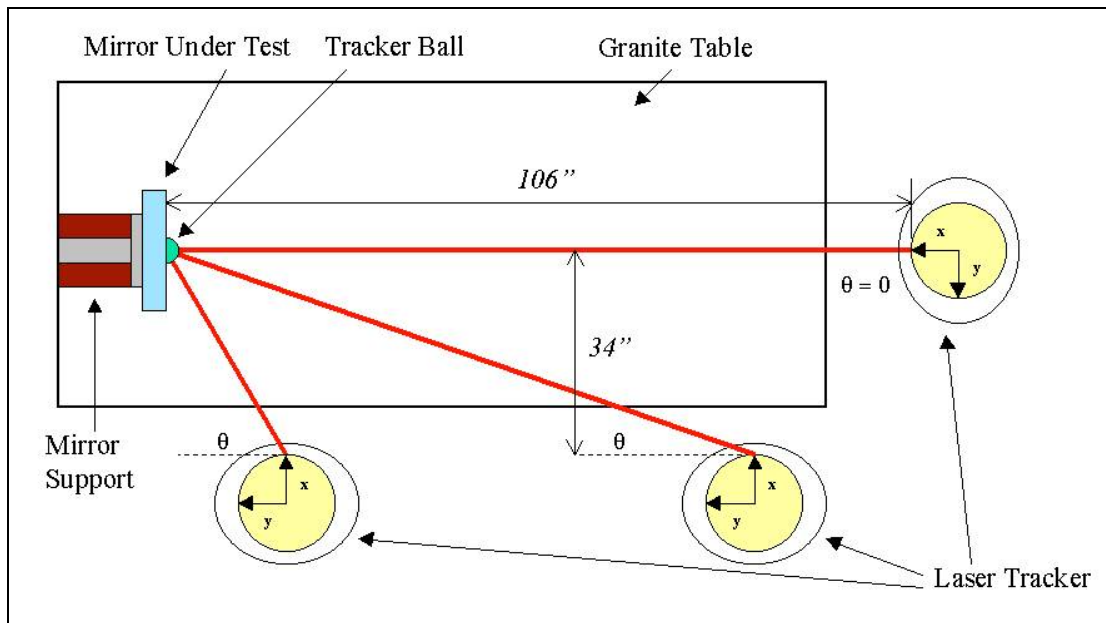


Figure 3.3. Tracker Locations with Respect to the Mirror Under Test.

The five different tracker locations were theta equal to 0° , 27° , 37° , 46° , and 55° where theta is defined in Figure 3.3. The results of this series of tests are presented in Figure 3.4.

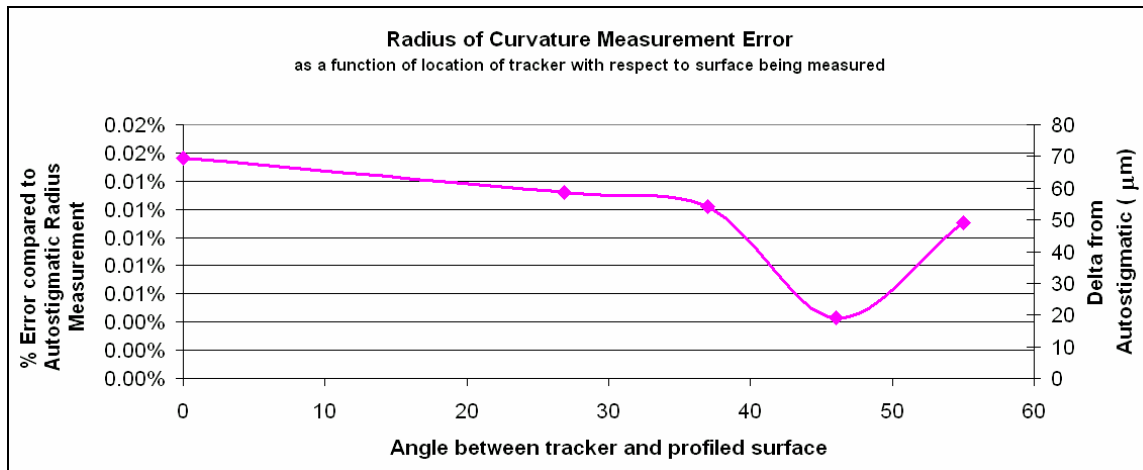


Figure 3.4. Radius Measurement Error as a Function of Tracker Location

Figure 3.4 shows that the tracker performs remarkably well, matching the autostigmatic measurement to within 0.016% or 70 microns when the tracker is at normal incidence to the mirror. Figure 3.4 shows that the performance of the tracker does not degrade as it is moved at shallower angles to the surface under measurement and the data shows that the performance also gets slightly better. This improvement in performance could be because the tracker was moved closer to the surface to produce the shallow angles or it could just be measurement noise. The difference between the reported radius of curvature from 0° incidence and 55° incidence is only 21 microns and this translates into a sag difference of 1.0 microns. Section 3.2.3 will go into a more in depth discussion on sag difference.

To make a more careful analysis of the effects of the tracker location on the measurement performance, the standard deviation of the reported radius was analyzed. The standard

deviation of the radius reported for each the 10 profiles that were generated at each tracker location was calculated and the standard deviation was found to steadily increase as the incident angle was increased. Figure 3.5 shows this trend and it indicates that making a series of measurements and averaging the results can compensate for the effect of tracker position.

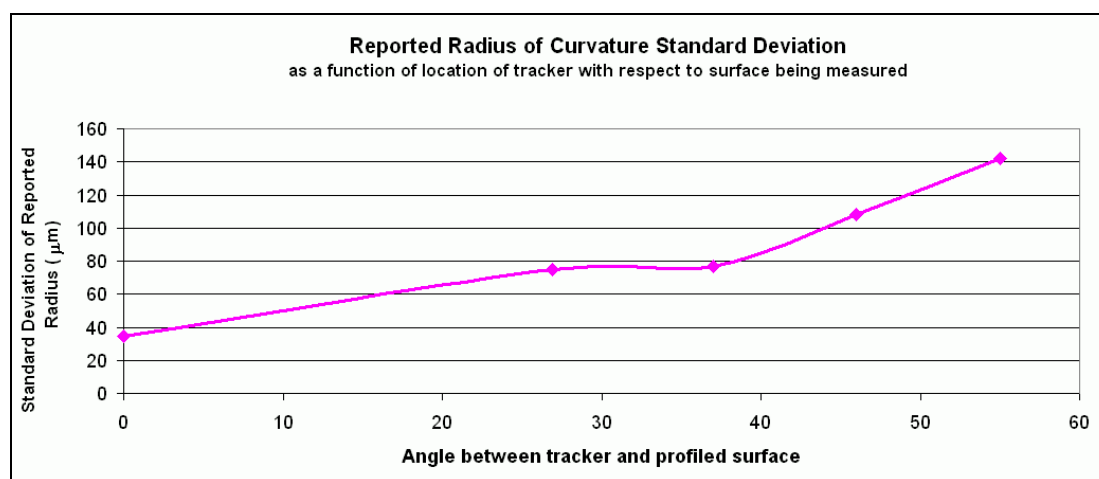


Figure 3.5. Standard Deviation of Radius Report as a Function of Tracker Location.

3.2.2. Effects of Number of Data Points used to Generate a Surface

The most common way for the laser tracker to profile a surface would be to physically rub the tracker ball across a surface and have the tracker make measurements at set intervals. Because of potential damage to the optical surface, the touching of the surface needs to be minimized making the preferred technique to profile an optical surface to be the pick and place technique. The pick and place technique is to put the tracker ball on the surface, make a measurement, remove the ball from the surface, place the ball on the surface at a different location, make a measurement, etc. Because this process is time consuming and can still potentially damage the optical surface, the number of locations

that are needed to generate a surface needs to be minimized. Four different scenarios were investigated and they were 20 points to define a surface, 10 points, 7 points, and 5 points. A pattern was used to scan the surface for each of the different scenarios and the scanning patterns are shown in Figure 3.6.

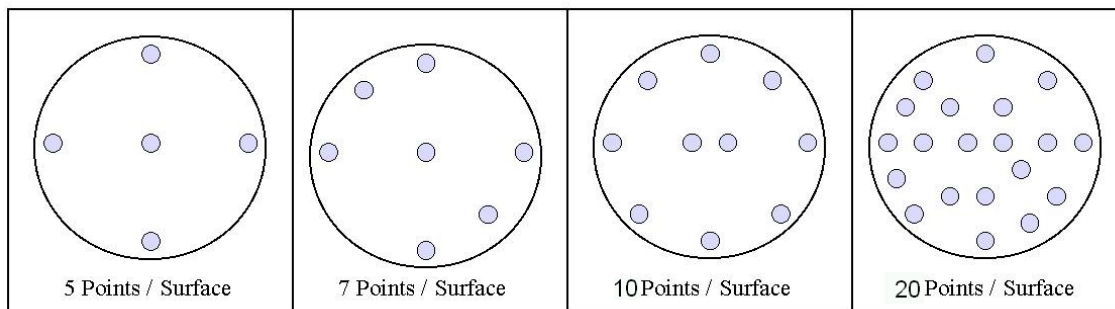


Figure 3.6. Scanning patterns for different measurement techniques.

Initially the tests were run with the tracker at 0° incidence (see Figure 3.3), and approximately 10 profiles were performed so that the data could be averaged. The tracker was then moved to 37° incidence and 10 profiles were made for each of the patterns shown in Figure 3.6. Figure 3.7 shows the results of this series of tests.

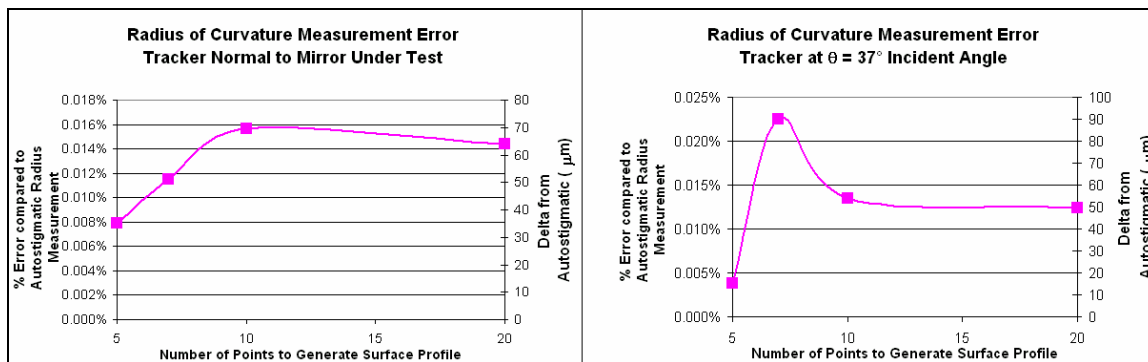


Figure 3.7. Radius Measurement Error as a Function of Points to Generate Surface

Figure 3.7 shows that the measurement error is fairly constant over the different scenarios with the best performance using only 5 data points to define the surface. This is the optimum scenario because the best performance requires the least amount of touching of the optical surface. Figure 3.7 also shows that when the angle of incidence is increased the performance slightly improves as shown in Section 3.2.1. This improvement is due to the tracker being physically closer to the surface being measured or because of measurement noise as discussed in the previous section.

3.2.3. Effects of Reducing the Area Scanned to Produce Profile

The final effect that was investigated was the effect of reducing the area of the surface that defines the surface. The software of the tracker takes the point cloud that is generated during the measurement and mathematically fits the points to a shape. As the percentage of the total shape is increased to generate the point cloud, the software will do a better job of fitting the data and reduce the error. To calculate the percentage of the sphere the surface area of the mirror can be divided by the surface area of the entire sphere as shown in the following equations.

$$\%_{sphere} = \frac{Area_{mirror}}{Area_{sphere}} \quad (3.1)$$

$$\%_{sphere} = \frac{2\pi RS}{4\pi R^2} \quad (3.2)$$

$$\%_{sphere} = \frac{S}{2R} \quad (3.3)$$

Where R is the radius of curvature of the surface being profiled and S is the sag of the mirror and can be calculated using the general sag equation presented with equation (2.15) in the optical alignment section of chapter 2. If the paraxial approximation is used, the mirror sag can be approximated and the percentage of the sphere that is being profiled can be written in terms of $R/\#$ as shown in equation (3.4).

$$\%_{sphere} \approx \frac{1}{16\left(\frac{R}{\#}\right)^2} \quad (3.4)$$

Where $R/\#$ is equal to the radius of curvature over the diameter of the surface of interest. The parameter of $R/\#$ was chosen to represent the surface instead of $f/\#$ because mirrors or surfaces are better described by the radius instead of the focal length. There is a discrepancy in convention in that some groups use the term $f/\#$ instead of $R/\#$ to describe a surface but still call $f/\#$ the radius over the diameter instead of the focal length over the diameter.

To make this series of tests, the 10.5” diameter mirror with a 16.7” radius mirror was again used. The scan area was reduced for each of the measurements by scanning the ball over smaller apertures. The data was generalized by calculating the percentage of the sphere that was being used to define the sphere. The tests were performed with the tracker at 0° incidence and approximately 10 profiles were performed for each scenario so that the data could be averaged. Figure 3.8 shows the results of this series of tests. The tracker was then moved to 37° incidence, and the series of tests were repeated. As

with the previous tests, the results did not significantly change when the angle of incidence was changed.

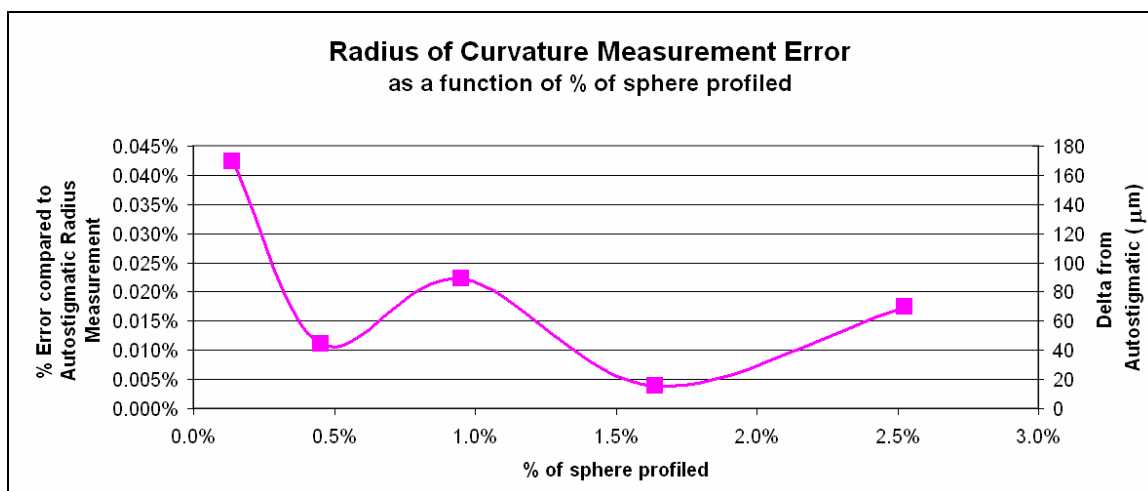


Figure 3.8. Radius Measurement Error as a Function of % of sphere profiled

Figure 3.8 shows that the laser tracker performs very well when measuring mirrors that encompass more than 0.5% of the total sphere with the tracker data matching the Wyko data with in 90 microns. Figure 3.8 shows that when less than 0.5% of the total area of the sphere is used to define the surface, the error in the measurement starts to rapidly increase.

Another way to look at % of sphere or R/# of the mirror being measured would be to investigate the sag in the surface that is being measured. When the tracker is measuring radius of curvature it is actually measuring points on a surface and using the sag between these points to calculate a radius. Sag and radius are related by the general conic formula

presented with equation 2.15 in the optical alignment section of chapter 2. If the paraxial approximation is used then sag and radius are related by the following well known formula as shown in equation 3.5.

$$S \approx \frac{y^2}{2R} \quad (3.5)$$

Figure 3.8 reports absolute radius of curvature error between the autostigmatic measurement and the laser tracker system. A small change in radius translates to a smaller change in sag making the delta sag associated with a given delta radius an interesting parameter to investigate. To find the relationship between delta sag and delta radius, the derivative of the sag equation is taken with respect to radius and is as follows.

$$\frac{dS}{dR} \approx -\frac{y^2}{2R^2} \quad (3.6)$$

Using the relationship in equation 3.6 and setting dR as the difference in the radius measurement from the autostigmatic measurement and the laser tracker measurement the 5 scenarios plotted in Figure 3.8 are plotted in Figure 3.9.

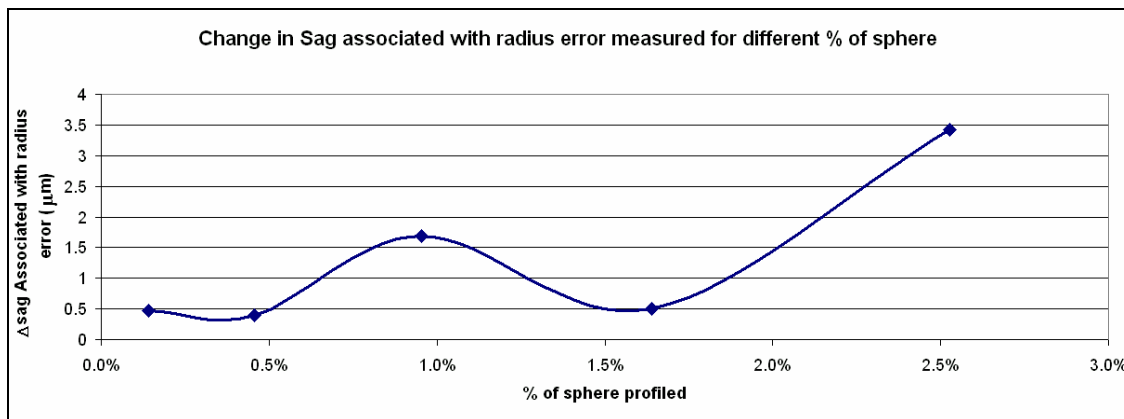


Figure 3.9. Change in Sag Error as a function of % of sphere profiled

Figure 3.9 does not show a clear trend and the change in sag that the laser tracker is measuring is less than 3.8 microns for the five cases that were measured. There were 19 different tests performed on the 16.7 inch radius mirror that investigated the effects of location of the tracker, number of data points used to define a surface, and amount of the total sphere profiled on the measurement performance of the tracker. The delta sag associated with all of these tests was calculated and was found to be independent of the test conditions. To report this effect the average and standard deviation of the different delta sags was calculated and is reported in Table 3.3.

Table 3.3. Average and Standard Delta Sag on 16.7 inch mirror

	Inches	Microns
Average	8.93E-05	2.27
Standard Deviation	5.00E-05	1.27

Table 3.3 shows that the standard deviation for the measured sag error is low. If the delta sag is assumed to be constant then a relationship between expected radius error versus R/# of the optic being profiled can be derived. Taking equation 3.6 and substituting R/# for y and R then the following relationship is found.

$$dR \approx 8 \left(\frac{R}{\#} \right)^2 dS \approx \frac{1}{2(\%_{sphere})} dS \quad (3.7)$$

Delta sag is set equal to 2.3 microns and equation 3.7 is plotted in Figure 3.10. The scale on the y axis is set as logarithmic to highlight the measurement performance for fast R/# optics.

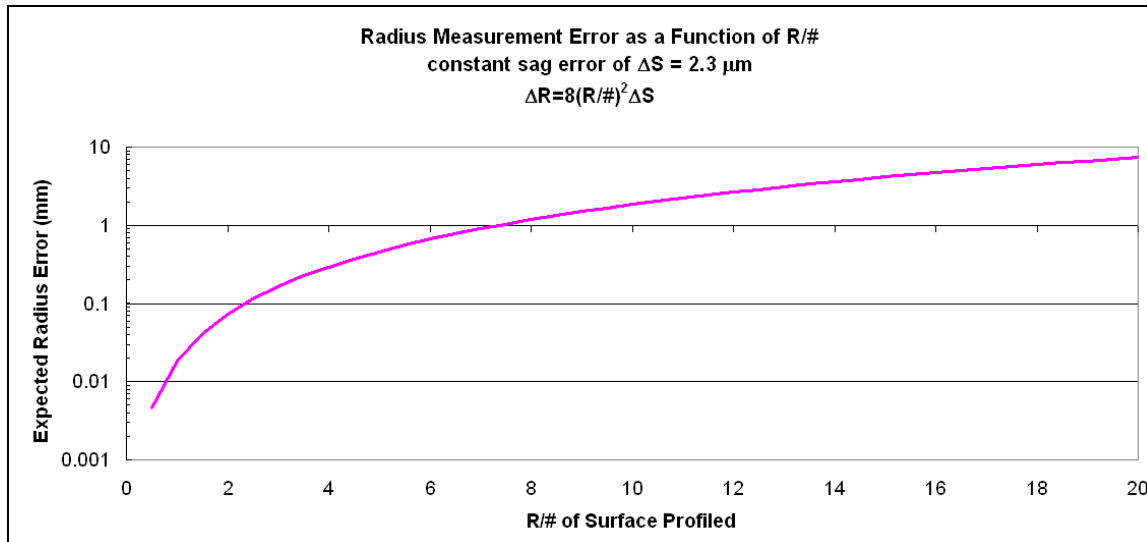


Figure 3.10. Radius Measurement Error as a Function of R/#

To verify the relationship shown in Figure 3.10 an R/18 mirror with a 2794 mm radius was profiled. The surface was profiled 10 times and the average radius error was found to be 6.62 mm. Using equation 3.7 this radius error translates into a sag error of 2.5 microns and this is consistent with the average sag error presented in Table 3.3. As a further check, Figure 3.10 can be used to calculate an expected radius error for an R/18 optic and the figure predicts 5.9 mm of radius error and this is also consistent with the actual measured radius error. To achieve measurement performance of better than 0.5 mm accuracy on the reported radius of curvature, Figure 3.10 shows that R/#s faster than R/5.5 should be measured with the tracker.

3.2.4. Radius of Curvature Summary

Data has been presented that shows that the laser tracker does an excellent job of reporting the radius of curvature for an optical element with an R/# of R/5.5 or faster. The slower R/# mirrors do not use a very large percentage of the total sphere to fit a cloud of points to a sphere and measurement errors are introduced. A relationship between R/# and expected measurement error and has been derived and is shown in equation 3.7. Two other variables were investigated, the orientation of the tracker to the surface being measured and the number of data points required to fit a sphere to. Both of these variables proved to be insignificant and their negative affects could be averaged out by several measurements.

Even though it has been shown that the number of data points needed to touch the surface is minimal, touching the optical surface still presents a risk. To mitigate this risk, protective low residue tape can be placed on the surface in the locations that the tracker ball will touch the surface. This technique was investigated and zero residue tape from American Bilrite Inc. (ABI) was placed at 10 locations on the surface and the surface was profiled. The tape was measured to be .0025” thick and this offset was removed from the data. Model 9148 from ABI was used because of its Polyester film backing that leaves zero or low residue and will not break or tear during application or removal. Figure 3.11 shows a photograph of the surface with the protective tape installed.



Figure 3.11. Photograph with tape

The surface was profiled 5 times and the average radius was measured to be 16.72057" or 94 microns different than the autostigmatic measurement. This performance is comparable to the performance without the protective tape. The thickness of the tape needs to be minimized because thicker tape has more of a chance to compress when the tracker ball is placed on the tape and could introduce measurement error. The tape that was used for this experiment was a good choice because it was only 0.0025" thick and did not impact the measurement performance of the laser tracker.

The radius of curvature measurement features of the tracker could prove to be very powerful. Techniques of using spherometers, inside micrometers, plumb bobs and other mechanical measurement techniques are often used to measure radius of curvature and

these techniques are sometimes difficult and inaccurate. The use of the autostigmatic method using the Wyko 6000 interferometer equipped with a lens rail is an extremely accurate technique but is limited by the length of the rail and the $f/\#$ of the transmission sphere on the interferometer. The laser tracker has been shown to have similar measuring performance as the autostigmatic method when measuring low $R/\#$ optics. The tracker has an added benefit in that it does not need to have a polished surface in order to measure the radius of curvature with high accuracy. This would be beneficial in the early stages of manufacturing when a mirror is ground and ready for polishing and can not be accurately measured with an interferometer. An ideal application for the tracker would be to measure the radius of curvature for large astronomical mirrors that are 8 m in diameter that typically have $R/\#$ s less than 1.5. The tracker could also be used to measure the flatness of the back side of mirrors by fitting the cloud of data to a plane instead of fitting the data to a sphere as would be needed for the powered side of an optical element.

Further studies are required to test the laser tracker's ability to test aspherical surfaces and report the location of the vertex and center of curvature. Also, investigating the tracker's ability to only use part of a surface to report a radius of curvature would be interesting. This would be useful to test the radius of curvature of an annular mirror or scanning a surface entirely outside of the clear aperture to reduce the risk of damaging the surface

3.3. Optical Alignment

The next general application that was investigated with the tracker was its viability as an optical alignment tool. Theoretically the tracker would be an extremely valuable alignment tool especially on large systems that are difficult to adjust and work with. The profiling features of the tracker not only report a radius of curvature but they give a location of where the center of curvature is in X, Y, Z coordinates. This location is extremely critical to any optical alignment and is in general a difficult point to find because it is not a physical thing that can be touched. The tracker can not only locate the center of curvature but the moveable coordinate frame features of the tracker also allow for the location to be related to other mechanical features in the system that is being aligned.

Because this location can not be compared to a standard as in the radius of curvature investigation, the performance of the tracker was determined by making many measurements and recording the standard deviation of the reported location of the center of curvature. As with the radius of curvature investigation, three variables were investigated. They were: (1) tracker location with respect to the surface being measured, (2) number of data points measured to generate a surface, and (3) the percentage of the complete sphere that is being used to fit the data to.

3.3.1. Effects of Tracer Location on the Repeatability of the Tracker

Five different tracker locations with theta equal to 0° , 27° , 37° , 46° , and 55° were used to quantify the trackers performance. Theta is defined in Figure 3.3. At each tracker location the surface was scanned 10 times and the tracker's software calculated the X, Y, Z coordinate that defines the location of the center of curvature for the element. The standard deviation of the 10 measurements was found and the results of this series of tests are presented in Figure 3.12.

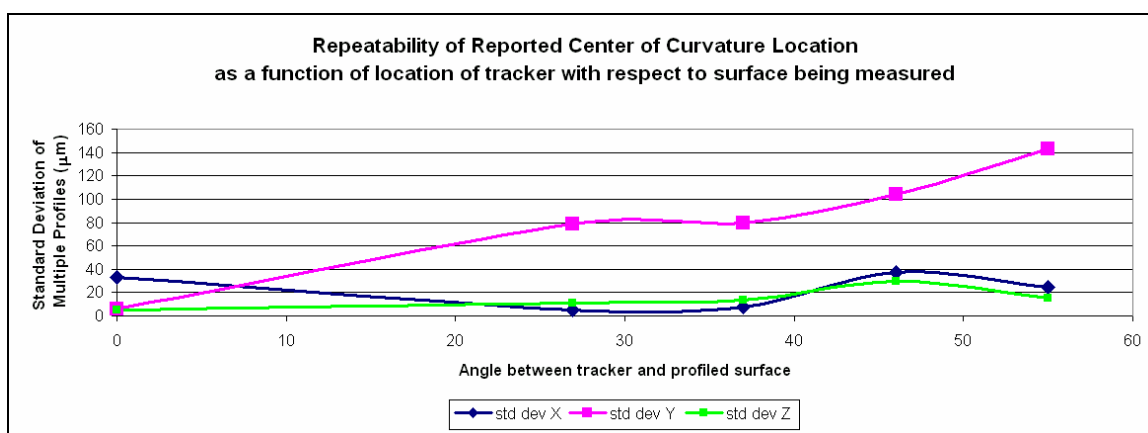


Figure 3.12. Center of Curvature Location vs. Tracker Location

Figure 3.12 shows that the Z axis stays flat until the angle of incidence is increased to approximately 45° when the error increases to approximately 25 microns. The X axis data is shown to improve then it follows the data for the Z axis. The Y axis data shows to be low at normal incidence but it dramatically increases when the tracker is moved away from normal. This is because when the tracker is at normal incidence the mirror is being pushed on in the X direction and when the tracker was moved to angles that were not

normal, the Y direction is the direction that the mirror is pushed on. The data that was taken for this set of measurements was taken with a mount that was attached to the table with hot glue. This glue could have been slightly compliant causing small errors in the direction the tracker ball is pushed onto the mirror. This compliance in the glue is why the repeatability in the X direction is high at normal incidence and why the repeatability in the Y direction is high when the tracker is not at normal incidence. If the mount is rigid the tracker should be expected to perform as shown with the Z axis data. The repeatability in the Z direction is less than 15 microns for all angles with the exception of 45° where the repeatability increases to approximately 25 microns. This data leads to the conclusion that the location of the tracker with respect to the surface did not significantly affect the performance of the tracker for this measurement

3.3.2. Effects of Number of Data Points used to Generate a Surface

Next the affects of the number of data points used to define the surface was investigated. The tracker was placed at normal incidence and the surface was profiled with different numbers of data points. As with the radius of curvature investigation, 20, 10, 7, and 5 points were used to define the surface and were scanned with the patterns shown in Figure 3.6. For each dataset the surface was profiled 10 times and the standard deviation of the reported location of the center of curvature was recorded and the results are presented in Figure 3.13.

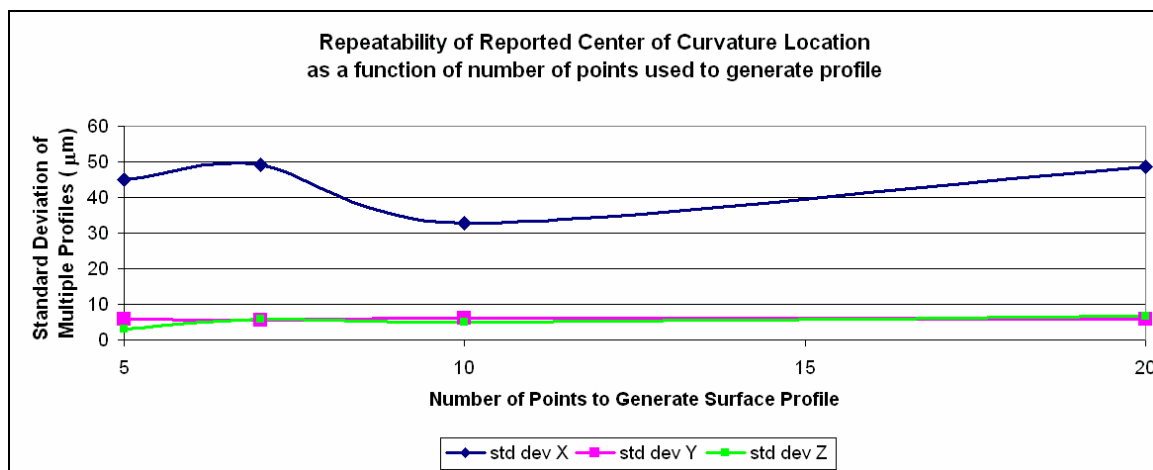


Figure 3.13. Center of Curvature Location vs. Number of Points to Generate Surface

As with the radius of curvature measurement, the repeatability of the location of the center of curvature is fairly flat. All data sets were taken at normal incidence so the instability in the mount will cause the X axis performance to be worse than the other axis. Figure 3.13 shows that the repeatability of the tracker is better than 50 microns for all of the different scenarios. This high performance could be because an optical surface is extremely accurate with less than a micron of departure from a sphere and increasing the number of points to profile the surface is not necessary because the optical surface is already almost perfect.

3.3.3. Effects of Reducing the Area Scanned to Produce a Profile

The last variable investigated was the laser tracker's ability to produce a repeatable location of the center of curvature as the R/# of the surface being measured is increased or the percentage of the total sphere is decreased. To make this series of measurements,

the tracker was set at normal incidence and the clear aperture of the optical element was reduced to increase the R/#. The results of this series of measurements are shown in Figure 3.14.

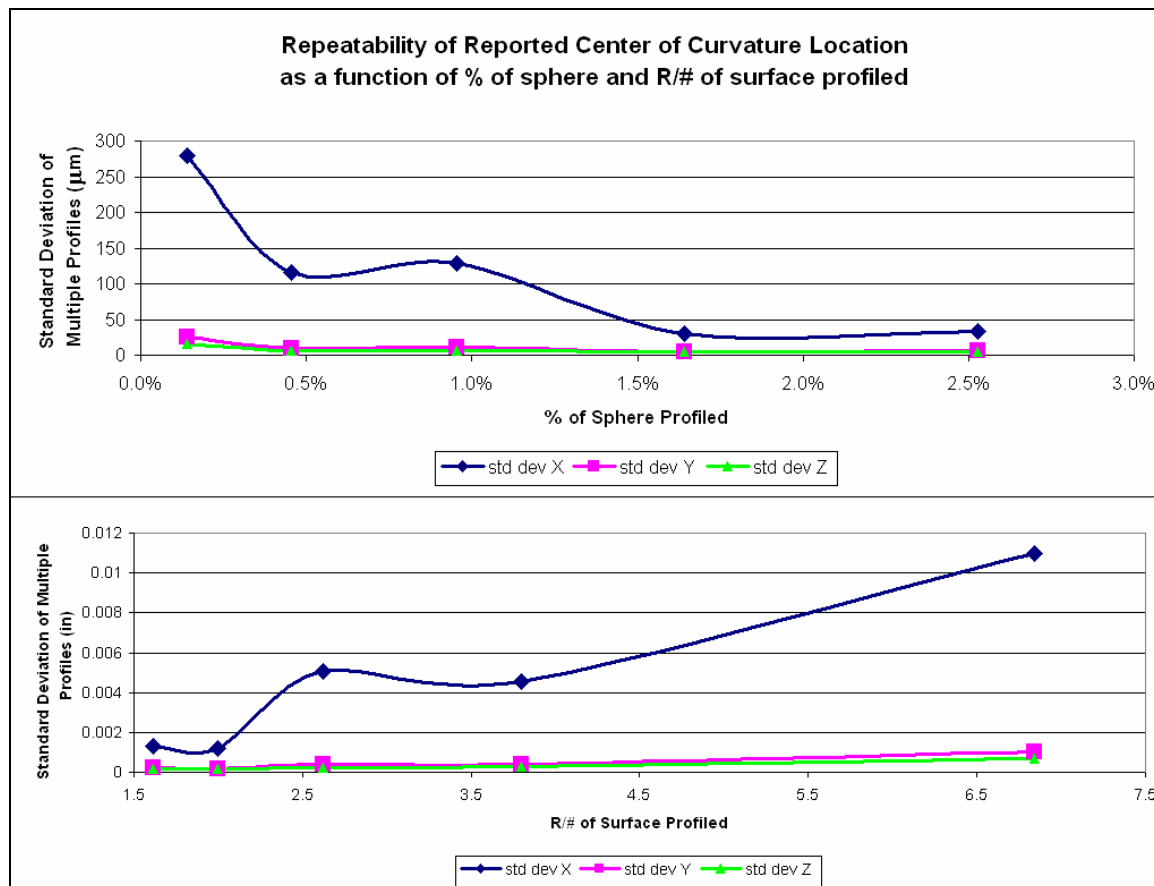


Figure 3.14. Center of Curvature Location vs. Mirror R/#

Figure 3.14 again shows that the Y and Z axis perform much better than the X axis. This error is due to the setup and with a stiffer mount the error could be expected to improve. For a rigid mount the X axis data should be expected to perform as well as both the Y and the Z axis. The trend shown in Figure 3.14 for the x axis is similar to the radius of curvature trend shown in Figure 3.8 implying that the x axis data drove the radius of

curvature error that the tracker was reporting. A delta sag analysis was performed on all repeatability data taken on the 16.7 inch mirror and the average sag error for the X and Y axes of the tracker. The average sag error for the axis that was being pushed on during profiling was compared to the average sag error for the axis not being pushed on and the results are shown in Table 3.4.

Table 3.4. Comparison of Sag Error for Different Axes of Laser Tracker

	Inches	Microns
Average for Axis the mirror was pushed on	1.30E-04	3.294969
Average for Axis the mirror was not pushed on	2.78E-05	.707332
Average for both Axis	7.87E-05	2.001151

Table 3.4 shows that the average sag error for the direction that the mirror was pushed on was higher than the error for the axis that was not pushed on. Table 3.4 shows that the average sag error when the two axes are averaged is approximately 2.0 microns and this value correlates well to the average sag error reported in Table 3.3 regarding the sag error for the radius of curvature measurement. If the mount for the optic was made rigid the performance of the tracker would be expected to drive towards the data that was taken for the axis that was not pushed on. Using the trends shown for the different axis of the tracker, the constant sag error can be reduced to 1.15 microns then the expected radius measurement error as a function of R/# can be recalculated and the results are shown in Figure 3.15.

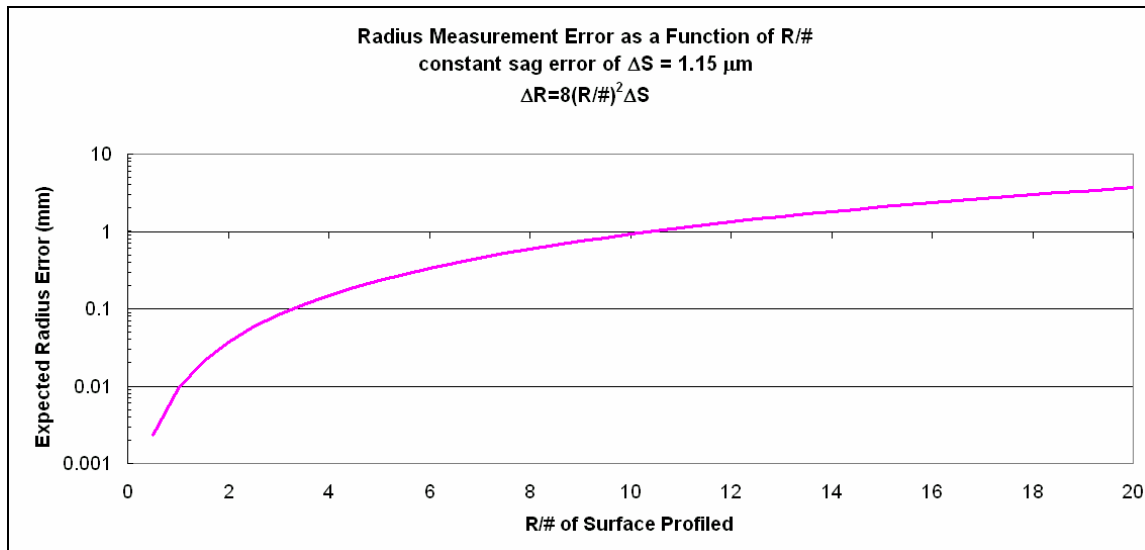


Figure 3.15. Corrected Radius Measurement Error as a Function of R/#

The trends that are shown in this section show that the repeatability of the reported location of the center of curvature correlates well with the tracker's capability of measuring radius of curvature. If the sag error is corrected then $R/7.4$ and faster optics can be measured with accuracies better than 0.5mm for both the radius of curvature and center of curvature location measurements.

3.3.4. Active Alignment

In addition to checking for repeatability to investigate the trackers ability to perform as an optical alignment tool, the tracker's active alignment features were also investigated. To use the active alignment features of the tracker, watch windows are used. The watch window displays the X, Y, Z location of the tracker ball and can be set so that when the window reads 0, 0, 0, the tracker ball is in the exact right location. To set up the active

alignment of an optical element, either a reference sphere can be generated or the surface can be fiducialized and the fiducials tracked.

3.3.4.1. Active Alignment by Creating a Reference Sphere

To make a reference sphere, a sphere is created in software and the radius of the sphere is set equal to the optic that is being aligned. The origin of the sphere can be set at any point when the reference sphere is being generated. If concentric elements are being aligned, the origin of the reference sphere would be set at the center of curvature of the first element. After the reference sphere is set up, the optical element to be aligned is profiled and the software compares where the element is compared to the reference sphere. Watch windows can now be used to track the tracker ball. The watch window will report how far the tracker ball is from the reference sphere when the ball is on the surface. Alignment of a mirror is achieved by holding the tracker ball on the surface and adjusting the surface until the tracker ball is on the reference sphere. The tracker ball is then moved to a new location and the adjustments are repeated. The mirror is aligned when the tracker ball can be moved to any point on the mirror and the deviation from the reference sphere is zero. This technique is very efficient when the adjustments are easy to make, but it requires the tracker ball to be constantly contacting to the surface that is being aligned. Because contact between the tracker ball and the optical surface needs to be minimized to reduce risk of damaging the surface, the technique of using a reference sphere is not the preferred alignment method.

3.3.4.2. Active Alignment with Fiducials

Fiducializing the surface is the technique of scanning a surface and relating the surface to a minimum of three points and tracking the three points during the alignment instead of tracking the surface. This technique is not as efficient as the reference sphere technique because the software needs to keep changing the point it is tracking. However, it minimizes the amount that the surface needs to be contacted because it only needs to be profiled once.

This technique was simulated with the SMX 4500 laser tracker. To simulate an alignment three tracker ball seats were hot glued to the mirror. These seats will be used as the alignment fiducials. Figure 3.16 shows the mirror with three tracker ball seats that are used as alignment fiducials.

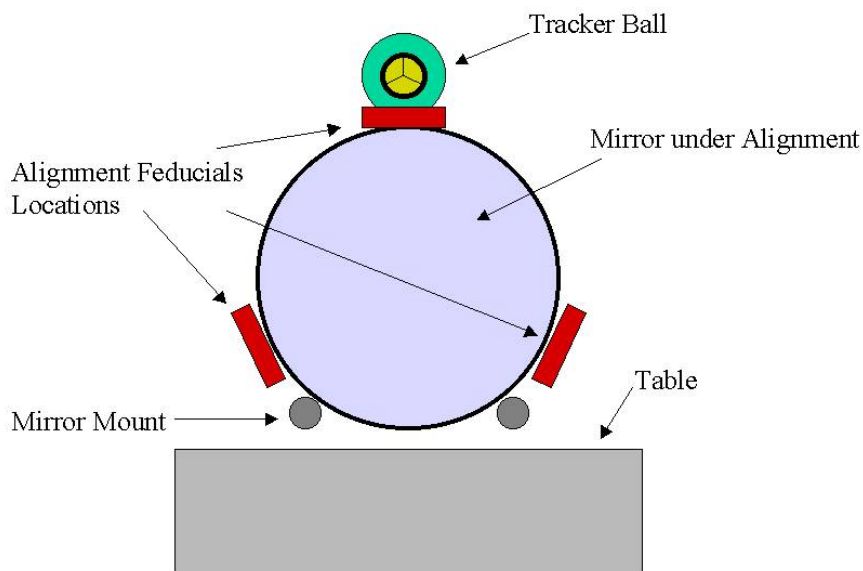


Figure 3.16. Mirror with alignment fiducials.

To run this simulation the mirror was first profiled to create a sphere and locate the center of curvature for the mirror. A coordinate frame was then built with the origin of the coordinate system at the center of curvature. The table that the mirror was mounted on was used to orient the X, Y, and Z axes. Next the three fiducials were measured with the tracker using the “measure point” feature in the software. The software then needed to be tricked to orient the fiducials in the correct coordinate frame. To do this the fiducial locations were exported and then imported into the measurement file. When imported, they are correctly oriented in the active coordinate frame. Next the mirror was moved or misaligned and then the active alignment features of the tracker were used to position the mirror back in the correct location.

The watch windows were activated and used to move the mirror back to the correct location. The mirror position was adjusted by sliding the mirror on the table and alternating the tracker ball in the three fiducial locations and moving the mirror until the three fiducial locations read close to zero. The final fiducial locations are shown in Table 3.5. After the fiducial locations were minimized in the watch windows, the surface was profiled again to check how close to zero the center of curvature of the mirror is after it has been aligned. This check is also presented in Table 3.5.

Table 3.5. Results of Active Alignment Simulation

	X	Y	Z
Fiducial 1	0.19558	0.1143	-0.0051
Fiducial 2	0.04064	0.13716	-0.0152
Fiducial 3	0.0508	0.15748	0.01016
Verification	0.09398	0.14478	0.2032

- Note: All Dimensions in millimeters

Table 3.5 shows that the fiducial locations were minimized. They could not be driven to zero because of limitations with the setup and making all of the adjustments by sliding the mirror mount by hand on the table. The verification shows that this technique is effective; the center of curvature was placed to within 0.20 mm of the targeted value even with this limited setup. This simulation did not take full advantage of the spherical mirror because the clocking of the fiducials was critical to make this alignment successful. The clocking of a spherical mirror should not be a factor when aligning spherical mirrors. To compensate for this, the alignment could have been done in spherical coordinates instead of Cartesian and the radial distance between the fiducials and the center of curvature could have been driven to zero. Using the spherical coordinates would be more effective with optical alignments because it allows the tracker to track only the parameters that are critical for aligning spherical mirrors. Because of limited availability of the SMX 4500 laser tracker, the use of spherical coordinates to align the mirror was not simulated.

The use of watch windows would be a powerful feature to assist with optical alignment of elements that can be easily adjusted during alignment. Some alignment tasks do not use knobs to align elements but use shims which are more difficult to adjust. For these difficult alignment tasks, the active features are not as ideal but the tracker is still very attractive optical alignment tool. The tracker can be used to measure the misalignments and these misalignments can be taken to a CAD model. The CAD model can then simulate the misalignments and calculate the shim sizes that are necessary to put the system in the proper alignment.

3.3.5. Alignment Summary

As with the radius of curvature investigation the data presented in this section shows that the tracker could be used as a powerful optical alignment tool. To measure the performance of the tracker as an alignment tool the repeatability of the reported center of curvature location was measured. Different variables were investigated including location of the tracker, number of data points used to define the surface, and percent of the total sphere used to define the surface. As with the radius of curvature investigation the number of data points used to define the surface was found to be not critical. The location of the tracker with respect to the surface being measured also had little impact to the measurement performance of the tracker. As with the radius of curvature investigation, the percent of the total sphere or the mirror R/# played the largest role in the performance of the tracker. If the mirror R/# is faster than R/6 then the repeatability

of the tracker is less than 25 microns. The data presented in this section highlights that the stiffness of the mirror mount is critical. This is evident because the data shows that the axis that the mirror is pushed on during measurement is the least repeatable axis. The data also shows that when the mirror mount is stiffened, the repeatability improves. The final capability of the tracker that was investigated in this section was its active alignment features. An alignment was simulated using the watch windows and the mirror was aligned to within 0.20 mm with a crude setup. The active alignment features of the tracker have been shown to be very useful with alignments that are readily available adjustments. For alignments that require shims or difficult iterations, analyzing the data provided by the tracker would prove to be a more efficient means of aligning the system.

Many optical systems can be aligned to within 25 microns and still have acceptable performance. For example the Offner Relay system that was presented in chapter 2.5.2, the error budget for the alignment said that the center of curvatures of the two primary mirrors need to be aligned to be within 3.6 mm and this is well within the performance range of the laser tracker. The performance of the system that was presented to demonstrate error budget mechanics was not well corrected allowing 0.2 waves of wavefront error due to the misalignments in the system. A different Offner Relay system was looked at to better understand how well the tracker could align a system. A model of an Offner Relay was built using the 16.7" Radius mirror that much of the tracker testing has been done on as the primary mirror. For this system a secondary with an 8.35" radius

would need to be installed at the focal point of the primary mirror. The layout of the system is shown in Figure 3.17.

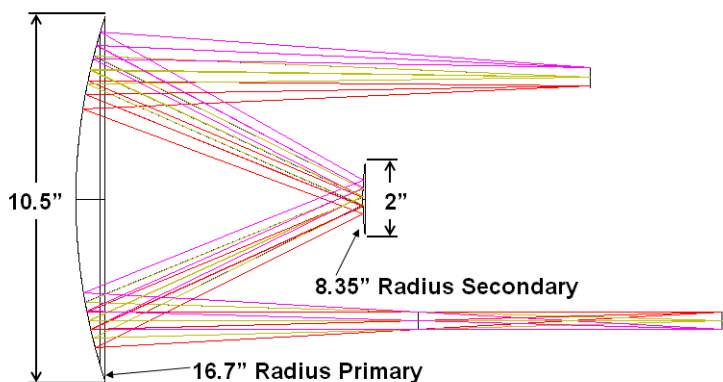


Figure 3.17. Offner relay system using 16.7" primary mirror.

Using the relationship that has been derived for radius error and $R/\#$ the expected errors on the reported location of the center of curvature were calculated. For the $R/1.59$ primary mirror the expected error was calculated to be 2 microns and for the $f/4.175$ secondary mirror the expected error was calculated to be 160 microns. For the worst case scenario these numbers can be directly added to find the overall expected error and is 162 microns. This error was then taken to the ZEMAX model and entered as a decenter and then as a tilt. The model predicts that 162 μm of decenter of the secondary will contribute 3.4 nm of RMS wavefront error and the tilt associated with 162 μm will introduce 3.1 nm of RMS wavefront error. These wavefront errors are remarkably low and this analysis shows that the error budget for secondary mirror decenter and tilt could allocate less than 5 nm of wavefront error for these degrees of freedom if this system was to be aligned with a laser tracker.

One more system will be investigated as a potential candidate to be aligned with the laser tracker and is the LSST system. The Large-aperture Synoptic Survey Telescope (LSST), often called the Dark Matter Telescope, is a proposed 8.4 meter, 7 square-degree field, synoptic survey telescope. The LSST telescope design has three large reflective optics and a refractive corrector and is shown in Figure 3.18.

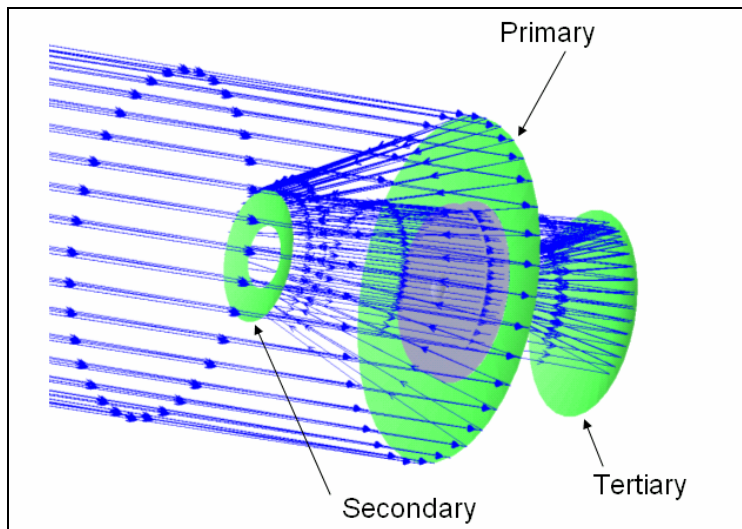


Figure 3.18. Optical Layout of the LSST telescope

Because this system has three reflective elements instead of the traditional two, the alignment of this system will be extremely challenging. A sensitivity analysis of the error budget has been performed by Scott Ellis with Photon Engineering, LLC and is summarized in Table 3.6.

Table 3.6. Error Budget for LSST mirror alignment.

	Max Tilt		Max Decenter	Max Defocus
Primary Mirror	0.05 mrad	0.887 mm	0.250 mm	0.030 mm
Secondary Mirror	0.05 mrad	0.307 mm	0.500 mm	0.030 mm
Tertiary Mirror	0.05 mrad	0.420 mm	0.500 mm	0.030 mm

To analyze whether or not the laser tracker would be an effective tool that could be used to align this system, first the method of profiling the surfaces and finding their center of curvature will be looked at. The mirrors for the LSST are all conic mirrors and the experiments performed for this thesis have investigated spherical mirrors. For the purpose of this analysis, the mirrors will be assumed spherical and the results will recommend if further investigation is warranted. The expected radius error has been shown to correlate well with center of curvature location and assuming that the sag error is constant, the expected errors were calculated and shown in Table 3.7.

Table 3.7. Expected Radius Error from Tracker Measuring LSST Mirrors

	R/#	Expected Error
Primary Mirror	2.11	0.0407 mm
Secondary Mirror	1.84	0.0310 mm
Tertiary Mirror	1.68	0.0258 mm

The expected errors shown in Table 3.7 are much less than the requirements for maximum tilt and decenter but are near the defocus requirements. This simple analysis says that this technique could measure the misalignments of the system near the precision required to align the LSST system. Techniques would need to be developed to take the misalignment data from the tracker and use it to correct the positions of the mirrors. This preliminary investigation shows that further investigation would be warranted to ensure that the R/# vs. error relationships shown in this thesis would scale to large 8 m optics. Also further investigation is needed to research how the tracker interfaces with aspherical surfaces.

The profiling technique is time consuming and the adjustments for the LSST system are more suited for an active alignment technique. Active alignment could be done without touching the surface of the mirrors by having three tracker balls located on the mirrors and these ball locations could be related to the geometry of the mirror during fabrication.

To align with this method, the active alignment method presented in 3.3.4 would be utilized. The first step would be to define a common reference for the mirrors and this could be the optical axis and could be found by scanning the central hole in the primary mirror. The tracker could measure the points that define the location of the mirrors and reference them to the optical axis. Because this technique is measuring individual points instead of fitting data to a sphere, each measurement would contribute an error and the errors could be root summed squared. The errors would be similar to the errors presented in the gauge block test shown in Figure 3.2. For the tilt and decenter measurements only four errors would contribute and they are the measurement of the optical axis and the measurement of the individual tracker ball locations for the mirror of interest. For the defocus measurement, the optical axis measurement is not necessary but the tracker must be related to a different mirror and errors from the measurement of both mirrors would contribute making 6 error sources. Assuming that the average range for measurement will be approximately 17 meters, the specified error using the laser tracker specification and the expected error using data shown in Figure 3.2, the error sources are RSSed and summarized in Table 3.8. The table does not differentiate between primary, secondary,

and tertiary because the actual profile of the surface is not being considered in this analysis. Because of this, the tracker's ability to measure tilt, decenter, and defocus will be equal for all three mirrors.

Table 3.8. Predicted Error using Active Alignment Features of Laser Tracker

	Error Sources	Specified Error	Expected Error
Tilt	4	0.077 mm	0.050 mm
Decenter	4	0.077 mm	0.050 mm
Defocus	6	0.095 mm	0.061 mm

Table 3.8 shows that the tracker should be expected to do a good job of measuring tilt and decenter for the LSST system and the tracker's performance is well below what the error budget allocates for the allowable tilt and decenter for the system. To measure defocus, the active alignment technique needs to relate two mirrors and therefore introducing more error sources making this the least accurate of the measurements. This is unfortunate because the defocus has the tightest alignment requirements. Even though the tracker's accuracy will not meet the requirements for defocus, the tracker still looks to be a powerful tool for rough alignment that can almost align the system to within tolerance. Many assumptions were made for this brief analysis but the analysis shows that a more careful analysis would be warranted that would investigate in detail the viability for the laser tracker system to align the LSST system that is being proposed.

3.4. Image Tracking

A potentially powerful application for the laser tracker is for the tracker to track images. The need to track images arises in scanning optical systems where a point source is

imaged at a focal plane and then scanned in a line. In a scanning system, the image is generally given a tolerance on how straight of a line the image must scan in. Other potential applications for image tracking include locating alignment fiducials that can be projected by optical elements such as computer generated holograms.

The tracker can not directly track an image because an image is not a physical thing that the tracker ball can be attached to. A CCD camera or a photodiode can locate an image but the detectors themselves need to be located in a meaningful coordinate system before the information on the detector is meaningful. The tracker is an ideal tool to locate the detector that finds the image. Using some of the coordinate frame building features of the tracker, the tracker can be used to locate the detector and the information from the detector and the laser tracker can be combined to output the location of the image. This research employs a lateral effect position sensing detector (PSD) to locate the image. The characterization of the PSD, the hardware and methodology to relate the data from the tracker and the PSD, and a simulation using the SMX 4500 laser tracker are presented in this section of the chapter. Figure 3.19 shows the general concept of image tracking.

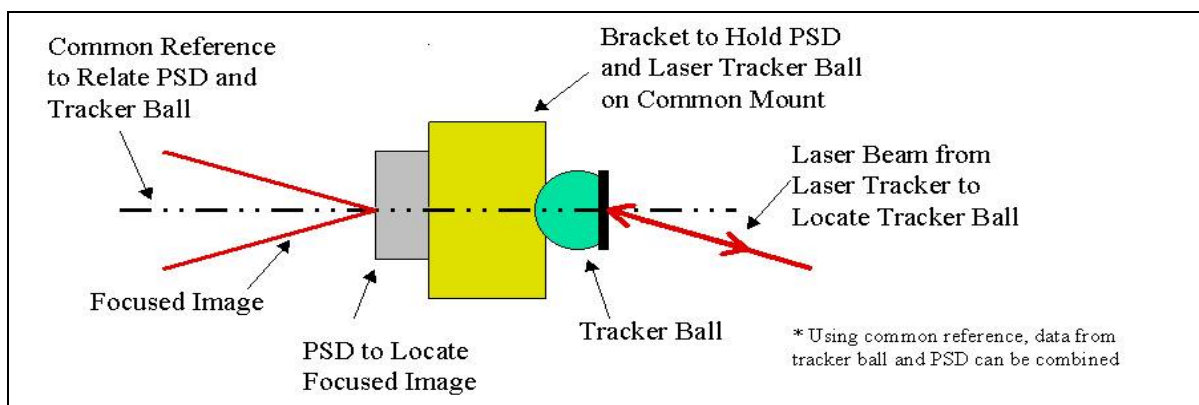


Figure 3.19. Conceptual diagram of image tracking.

3.4.1. PSD Characterization

The Position Sensing Detector (PSD) will be integrated with the Laser Tracker to track an image. Before this integration can be performed the PSD must be understood and characterized. This section presents a summary of the characterization that was performed on the PSD. The setup and software interface, the stabilization investigation, the incident power investigation, measurement of calibration coefficients, and other considerations will be presented in this section of the report.

3.4.1.1. Setup and Software Interface

Much care was taken to ensure that the setup was very stable. Many setups were used, but this section will look at the final setup that was used to perform the characterization.

Figure 3.20 shows the setup schematically.

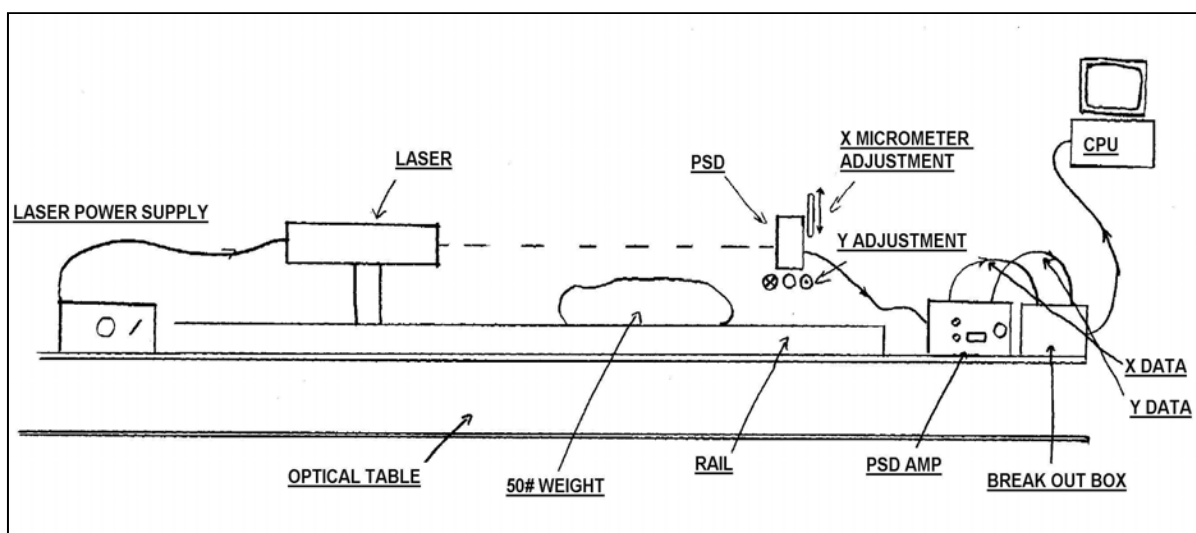


Figure 3.20. PSD Characterization Schematic

Both the Laser and the PSD are mounted onto a rail that is mounted onto the optical table. A 50 pound bag of lead is also placed on the rail to help stabilize the setup. Because the PSD is capable of making sub-micron measurements the stability of the setup is critical. The PSD is mounted on two stages that allow movement in the X and Y directions. The PSD is connected to the amplifier. The amplifier sends the X and Y voltages to the breakout box and the breakout box sends the data to the Data Acquisition Card (DAC) inside of the computer. The following table summarizes the PSD components and also the other equipment used for the characterization.

Table 3.9. Key Components used in PSD Characterization.

	Component	Manufacturer	Part Number	Description
PSD	PSD	On-Trak	PSM2-4	4.0 mm Dual Axis PSD
	Amplifier	“	OT-301	Dual Axis Amplifier
	Filter	Melles Griot	03FIL224	632.8 Filter 10nm BW
	Data Acquisition Board	National Instruments	6036E	16 Bit, +/- 10V
	Breakout Box	“	BNC-2110	8 Channel Input
	Software	“	LabVIEW	Version 6.1
Other	Laser	Spectra-Physics	117A	Stabilized, 633nm, 1.5 mW
	Positioning Stage	Newport	433 Series	Ball Bearing, Low Profile
	Micrometers	“	SM-25	Metric Vernier Micrometer

The PSD sends different voltages to the amplifier depending where the laser spot is on the detector. As the X and Y micrometers are adjusted the spots moves on the detector and different voltages are sent to the amplifier. These voltages can be read by attaching a multimeter directly to the amplifier. If the voltage data is to be converted to position data, the amplifier must send the voltage data to a computer that will make the

conversion. This conversion is done by finding calibration coefficients and using software to multiply the coefficient by the voltage from the PSD. The manufacturer of the PSD recommends an initial setting of the calibration coefficient to be 0.00787 inches per Volt. This corresponds to a 4.0mm detector with voltages ranging from +10 V to -10 V. The software can also be used to log data to a text file for manipulation with a spreadsheet program or to average readings to get the best position data.

LabVIEW software was chosen to interface with the PSD. LabVIEW was chosen because it interfaces well with the Data Acquisition Board (DAQ) that was needed to interface with the amplifier. Figure 3.21 shows the interface that was developed to interface with the PSD.

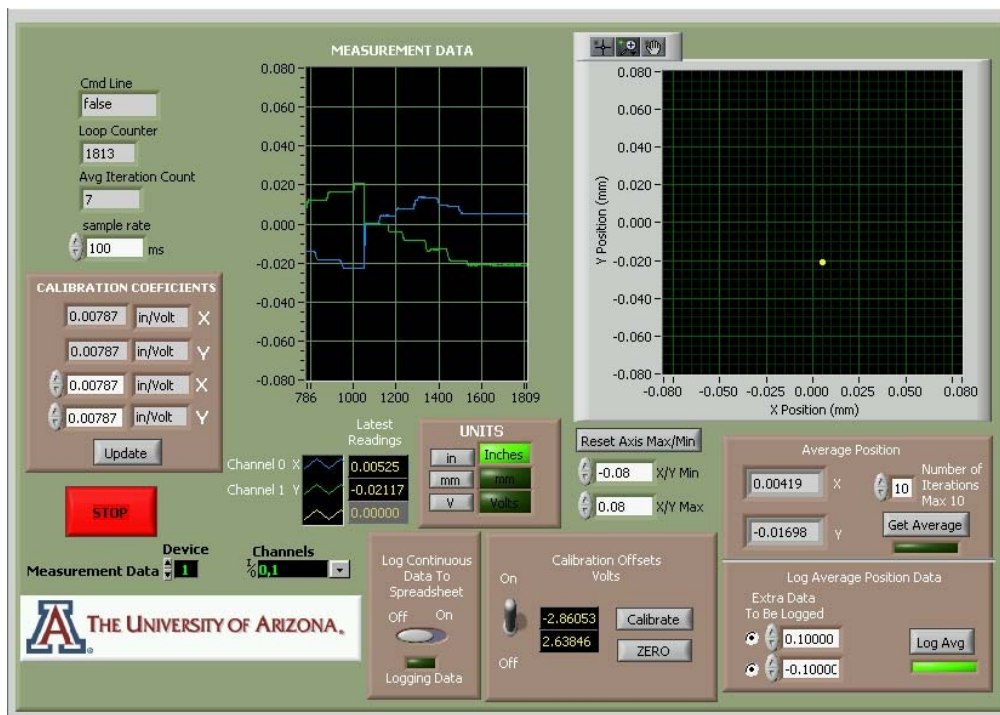


Figure 3.21. PSD Interface Developed in Lab View.

Features of the interface include real time and historical graphical position information, average position indication, data logging, calibration coefficient modification, resetting the origin and others. Appendix A contains a more detailed discussion of the features of the software, how to use the software, and the source code for the LabVIEW interface that has been developed.

3.4.1.2. Stabilization Investigation

Before the calibration coefficients were measured the stability of the setup was confirmed and characterized. Because of the extreme sensitivity of the PSD's measuring performance, the setup had to be carefully constructed so that the setup was not introducing measurement error into the PSD. Many different setups were evaluated before an optimal setup was found. Figure 3.22 shows the evolution of the setup. Many scenarios were investigated to find what combination produced the least amount of random jitter. Data sets were recorded with and without the filter, more and less stable setups, room lights on and off, a frequency stabilized laser and a standard laser, a focused spot and a non focused spot, and others. The figure plots how the standard deviation for a data set changes for different scenarios.

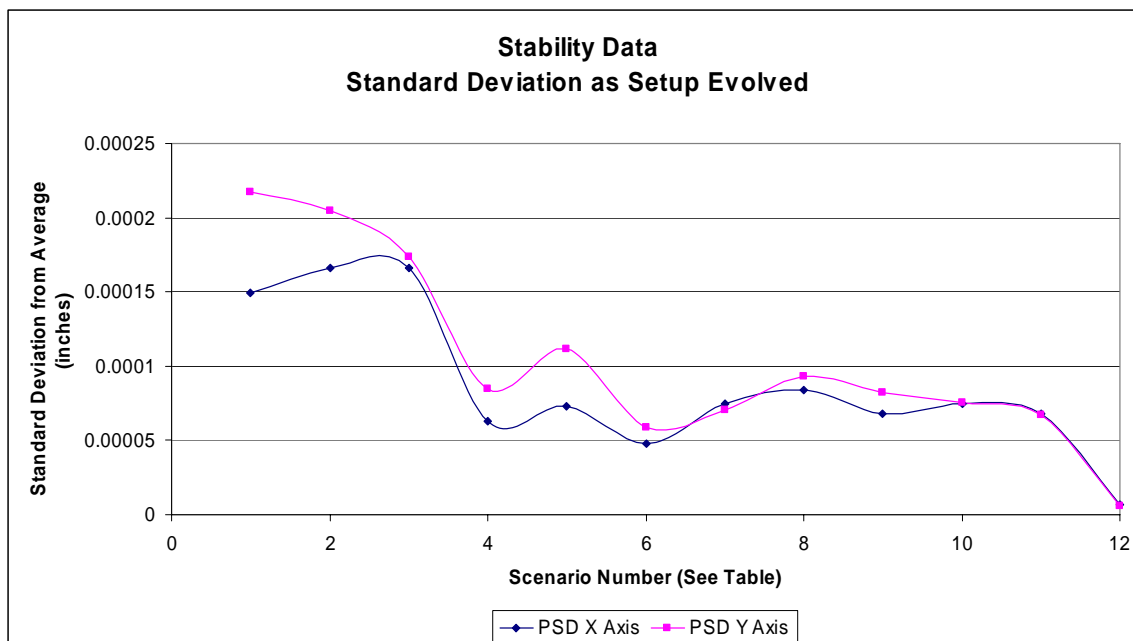


Figure 3.22. Standard Deviation of Data Set as Setup Evolved

Figure 3.22 shows how the standard deviation of the measurements went down and the X and Y values converge to the same value as the setup improved. Once the gross errors in the setup were fixed, the data got much better with the standard deviation of the data set falling from .0002” to .00008”. It was not until a focusing lens was introduced between the laser and the PSD that the standard deviation dropped well below .00005”. This level of sensitivity is needed to make system jitter recordings on the order of .0001”

The best combination of variables was found to be the focused stabilized laser with the filter in, the lights on, and mounted to the isolated optical table. The following figure shows the stabilization data from this combination of variables.

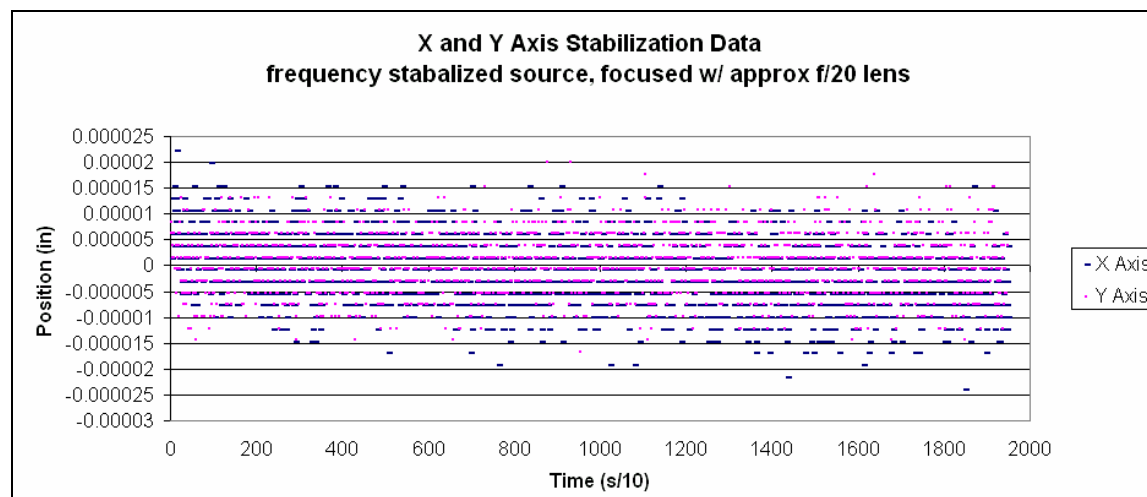


Figure 3.23. Final Stabilization Test Data

Figure 3.23 shows that most of the data points are within ± 0.00001 of zero with a few data points that fall outside ± 0.000015 . The standard deviation for the data set shown in Figure 3.23 is 6.5×10^{-6} inches for the X axis and 5.5×10^{-6} inches for the Y Axis.

3.4.1.3. Incident Power on the Detector Characterization

The next characterization that was performed on the PSD was to characterize how the PSD performs at with low incident power on the detector. The data presented in the previous section all used an unattenuated laser with the total power reading 1.5 mW. The power of the laser has been attenuated to different values and data sets similar to the ones taken in the stabilization section were recorded. The standard deviation of the jitter of the focused spot is plotted in Figure 3.24.

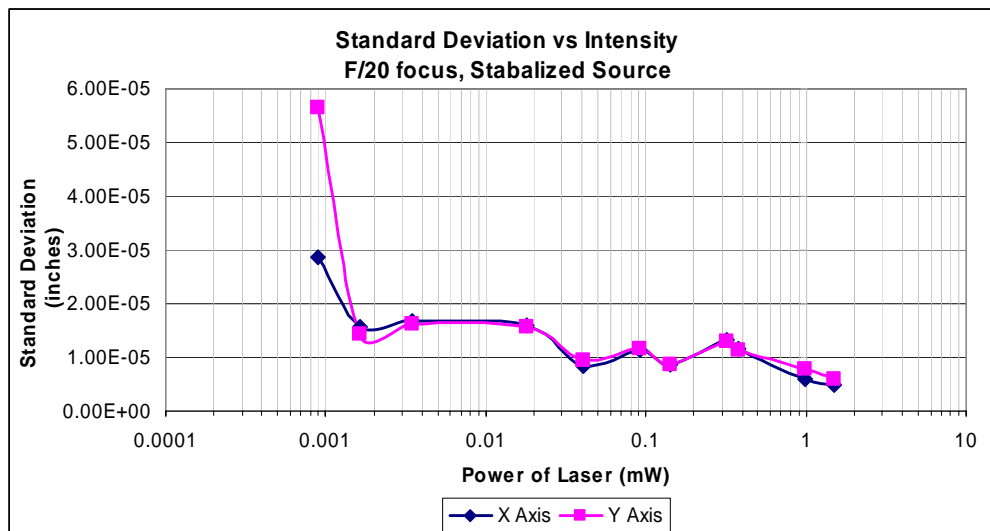


Figure 3.24. Standard Deviation vs. Laser Intensity

Figure 3.24 shows that if the power on the detector was held above $1.5 \mu\text{W}$, the standard deviation of the spot is less than $.0000175''$. At the lower power levels the gain on the detector was increased so that the PSD could still make good measurements. Values lower than $.1 \mu\text{W}$ could not be compensated with the gain adjustment. All of the data was taken with the room lights on and a 633nm filter installed in front of the detector.

3.4.1.4. Calibration Coefficients

Once the stability of the setup for the PSD has been characterized the calibration coefficients were calculated. The calibration coefficient is what is used to convert the Voltage read from the detector into inches or millimeters. To run the calibration coefficient tests the setup shown in Figure 1 was used with the log average position feature in the interface software. To record the data the following steps were taken: (1) the beam was put close to the center of the detector, (2) an average of 10 data points were

recorded using the “Log Average” button on the software, (3) the micrometer was adjusted in one axis and not the other (.10 mm increment is typical), (4) the micrometer information was logged into the extra data field of the software, (5) the micrometer position was adjusted and more data was logged, (7) etc.

Figure 3.25 shows the curves for the X and Y Axis Voltage vs. Position. The chart labeled “X axis Voltage vs. Position” represents the data that was recorded when the PSD was moved along the X axis with the micrometer and the Y axis was held constant. Similarly, the chart labeled “Y Axis Voltage vs. Position” represents the data where the PSD was moved along the Y axis of the detector and the X axis held constant.

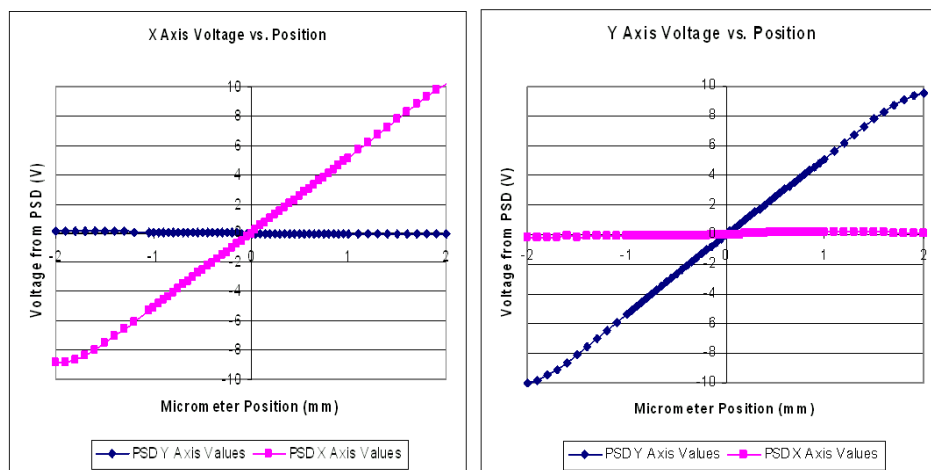


Figure 3.25. X and Y axis Voltage vs. Position.

Figure 3.25 shows that the Slope of the curve for both the X and Y axis is linear. At the edge of the detector, above ± 1.8 mm the detector no longer performs linearly. To get

meaningful data from the PSD, the region of the PSD between +/- 1.5 mm or +/- 0.06 in. should be used.

To calculate the calibration coefficients for the detector the slope of the curve was calculated in the region between -1.0 mm and +1.0 mm. Figure 11 shows the X and Y axis Calibration Coefficients with the corresponding Y and X values held constant at zero.

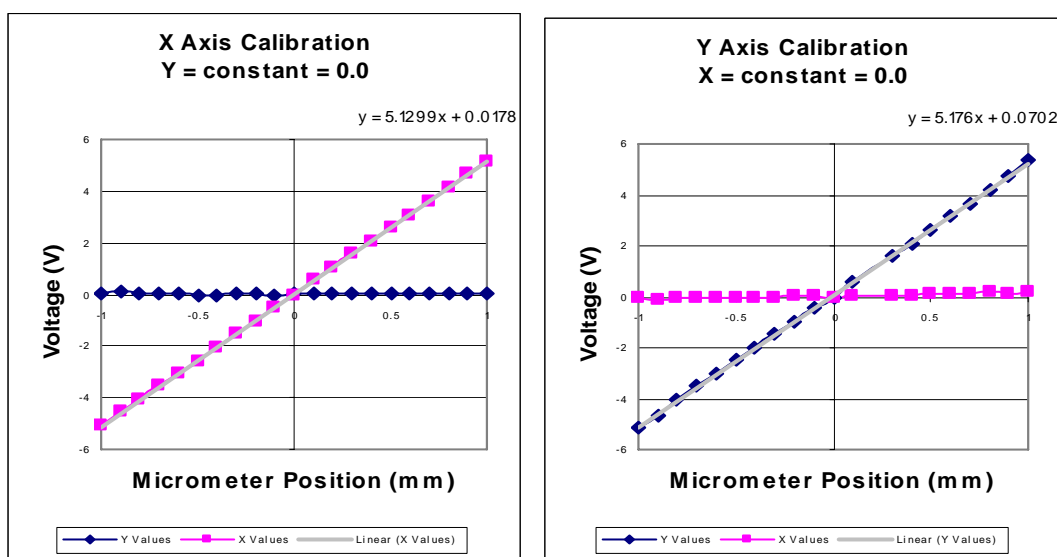


Figure 3.26. X and Y Calibration Coefficients across center of detector.

Figure 3.26 shows that the slope of X Axis curve is 5.1299 Volts/mm and the slope of the Y Axis curve is 5.1760 Volts/mm. Since there are no offsets the slope of these curves are the calibration coefficients. For ease of calculation the calibration coefficients are needed in the form of mm/Volt or in/Volt. In this form the calibration coefficients are 0.19494

mm/Volt or 0.007675 in/V for the X axis and 0.19320 mm/V or 0.007606 in/V for the Y axis.

The next step of the characterization was to find the slope of the curves at different constant values of Y and X. The plots for these calibration coefficients can be found in Appendix A. Table 4 summarizes the calibration coefficients for different regions on the detector. Appendix A also has a summary chart for the calibration coefficients in millimeters.

Table 3.10. Calibration Coefficients across the detector

		X AXIS OF PSD (in)						
		-0.06	-0.04	-0.02	0.00	0.02	0.04	0.06
0.06	0.007678	0.007678	0.007678	0.007678	0.007678	0.007678	0.007678	0.007678
	0.007447	0.007460	0.007469	0.007606	0.007555	0.007493	0.007433	
0.04	0.007683	0.007683	0.007683	0.007683	0.007683	0.007683	0.007683	0.007683
	0.007447	0.007460	0.007469	0.007606	0.007555	0.007493	0.007433	
0.02	0.007613	0.007613	0.007613	0.007613	0.007613	0.007613	0.007613	0.007613
	0.007447	0.007460	0.007469	0.007606	0.007555	0.007493	0.007433	
0.00	0.007675	0.007675	0.007675	0.007675	0.007675	0.007675	0.007675	0.007675
	0.007447	0.007460	0.007469	0.007606	0.007555	0.007493	0.007433	
-0.02	0.007621	0.007621	0.007621	0.007621	0.007621	0.007621	0.007621	0.007621
	0.007447	0.007460	0.007469	0.007606	0.007555	0.007493	0.007433	
-0.04	0.007621	0.007621	0.007621	0.007621	0.007621	0.007621	0.007621	0.007621
	0.007447	0.007460	0.007469	0.007606	0.007555	0.007493	0.007433	
-0.06	0.007613	0.007613	0.007613	0.007613	0.007613	0.007613	0.007613	0.007613
	0.007447	0.007460	0.007469	0.007606	0.007555	0.007493	0.007433	

X Axis Calibration Coefficient (in/V)
Y Axis Calibration Coefficient (in/V)

Table 3.10 shows how the calibration coefficient changes for different regions of the detector. If a test is going to be working on one specific region of the detector the calibration coefficients for that region should be input for the most accurate data. For example, if a beam is focused in the (-.02,.04) region of the detector the calibration

coefficients should be input as .007683 in/V for the X axis and .007469 in/V for the Y axis. If multiple regions are to be used, best engineering judgment should be used to pick the coefficients. The maximum difference calibration coefficients recorded for the X axis is between the 0.02 region and the 0.04 region with a 0.9% difference in values. This value corresponds well to the maximum of 0.8% non linearity specification provided by the supplier of the PSD. Our recorded value may be slightly higher because of limitations from our set up stability or resolution on micrometer adjustments.

The PSD is performing within the manufacturer's tolerance of 0.8% non linearity across the detector.

3.4.1.5. Other PSD considerations

System warm up time and the effects of tilt were also investigated during the PSD Characterization phase of the research. A drift in the PSD readings were noticed when the system was first turned on. Many scenarios were investigated and it was proven that the detector itself did not require a warm up but rather the laser itself needed to warm up. When the laser that was used in the characterization was converted to a frequency stabilized source, as soon as the laser stabilized, the PSD data stabilized. Figure 3.27 shows that the laser for this set up needed approximately 30 minutes or 1800 seconds for warm up time.

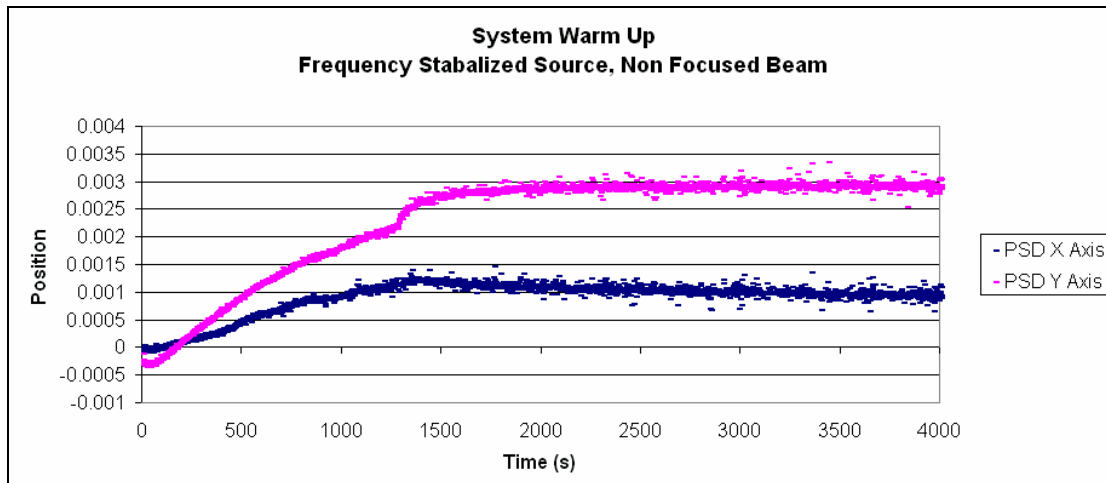


Figure 3.27. System warm up time

The final affect that was investigated in the characterization was the effect of tilt between the incident beam and the detector. Kelly Canham did much of the work investigating this characterization of the PSD for her Senior Independent Study project. Figure 3.28 shows a summary of her findings.

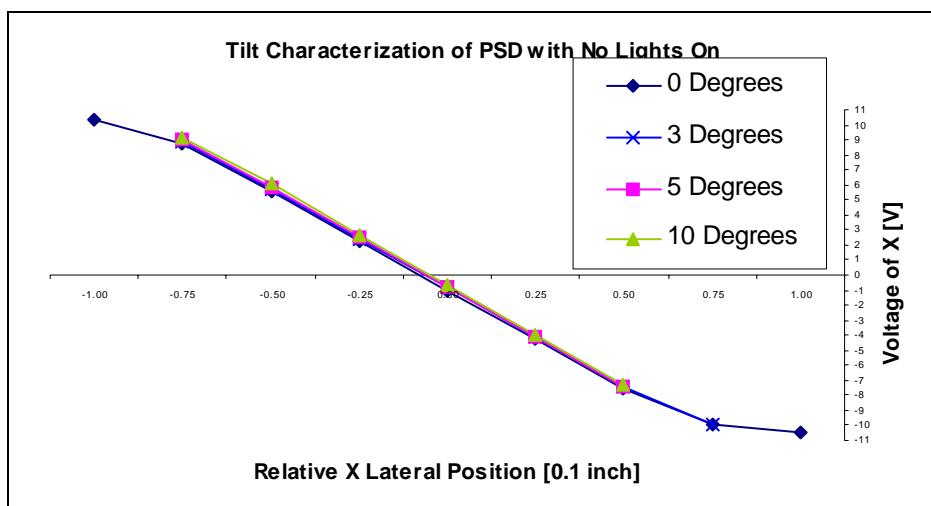


Figure 3.28. PSD Tilt Characterization, without room lights and filter

Figure 3.28 shows that effect of tilt in the incident beam has little affect on the calibration coefficients of the system. Incident angles from 0 to 10 degrees were investigated and all show that the same calibration coefficients are used. This data implies that the PSD does not need to be aligned accurately to make precision measurements.

3.4.1.6. PSD Characterization Summary

A careful characterization has been performed on the PSD that will be used with the laser tracker to track images in space. This exercise has led to the following conclusions:

- The PSD is capable of make measurements below 0.0001” but the set up is extremely critical to make measurements of this level.
- Meaningful data can be recorded with the PSD as long as the incident power on the detector is above 1.5 μW .
- The PSD does not require a warm up time to make repeatable measurements.
- The laser warm-up time needs to be characterized.
- Calibration Coefficients have been mapped for the entire detector.
- The Calibration Coefficients for the center of the detector are :
 - 0.007675 in/V for the X axis
 - 0.007606 in/V for the Y axis
- The non-linearity across the detector is a maximum of 0.8% just as the supplier has specified.
- Affects of tilt between the incident beam and the PSD have little effect.

The characterization that has been performed gives confidence that this device will be able to accurately track an image across the detector and will be useful for image tracking, pointing repeatability, and image jitter tests.

3.4.2. Relating the PSD data and the Laser Tracker data

To track an image as shown in the conceptual diagram in Figure 3.19, the data from the PSD locates the image on the detector and the laser tracker locates the detector to a global coordinate frame. If the image location is to be reported in a global coordinate frame, the data from the PSD and the data from the tracker must be combined to report the location of the image. To combine the data from these two data sources a common reference must be found and utilized. If the tracker ball and the PSD were mounted on a common rotation stage, the axis of rotation could be found and the axis of rotation could be used as the common reference.

3.4.2.1. PSD/Tracker Ball Bracket Design

The Newport 481-A rotation stage was chosen as the common rotation stage that the PSD and the tracker ball were to be mounted to. This stage was chosen because it had 0 backlash, a range of 360 degrees, could be side loaded, and the stage has an access hole that allows access to the rotating part of the stage from both the top and bottom of the stage. Figure 3.29 shows a photograph of the stage.



Figure 3.29. Photograph of Newport Rotation Stage.

The hole through the middle of the stage allows for a bracket to be built that would hold the PSD on one side of the stage and the tracker ball on the other. Furthermore, the bracket could be designed such that the part that holds the tracker ball could hold the ball exactly on the rotation axis of the stage. Only the PSD would be required to be calibrated to the axis of rotation.

Several designs of the bracket were analyzed and an exploded view of the final bracket design is shown in Figure 3.30. The custom adapter that was fabricated was a two-piece bracket that bolted together and is shown in green in Figure 3.30.

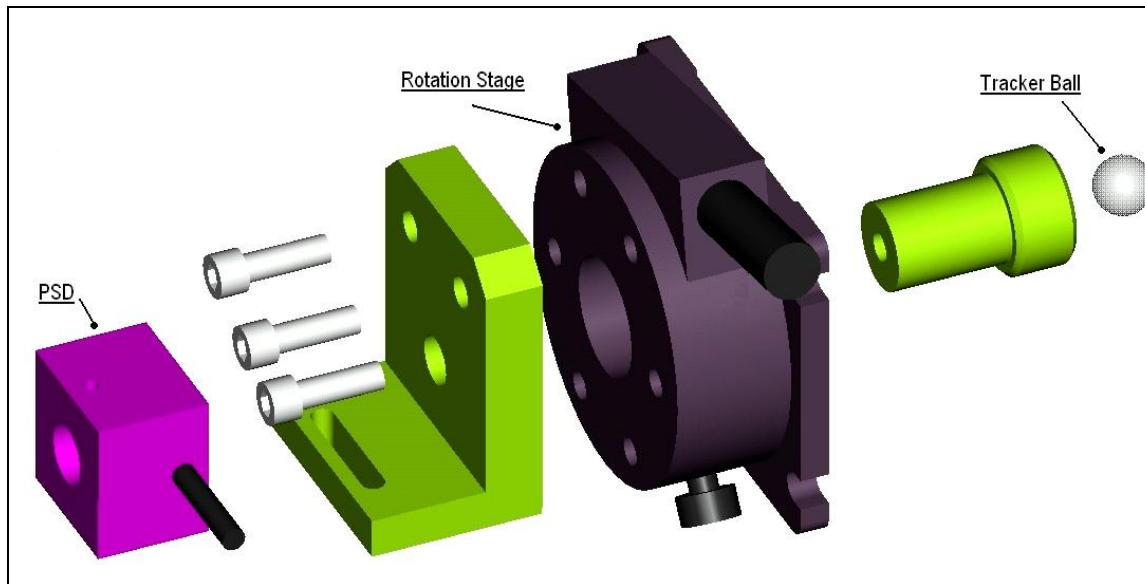


Figure 3.30. Exploded view of PSD/Tracker Ball mount

The adapter in green is a two-piece adapter that bolts together with one screw that seats in a counter bored hole in the L shaped portion of the bracket. The L shaped portion of the adapter bolts into the rotation stage and the PSD seats in the right angle portion of the bracket. It then is secured with a bolt from the side of the bracket. The tracker seats in a 90 degree conical seat to ensure repeatability from when the ball is removed and replaced. The ball is held in place with a small Neodymium magnet that is epoxied inside of the adapter. The magnet allows for the tracker ball to easily be removed and replaced and securely holds the ball in its seat.

This design is ideal because it is easy to fabricate and only 4 tolerances are needed to be tightly held. The original design was a one-piece adapter but the adapter was going to be difficult to fabricate. The two-piece design is good because both pieces are simple and

can be made to high precision with standard lathes and mills found in any machine shop. The four tolerances that had to be held tightly were the flatness of the two surfaces that interfaced when the bracket was bolted together, the location of the tracker ball seat, and the diameter of the rod that protruded through the rotation stage. To reduce the difficulty of the part that protruded through the rotation stage, the diameter was stepped so only a small length of the diameter had to be held to tight tolerances. See Appendix B for the fabrication drawings. This two piece design was also ideal because allows for the piece that protrudes through the stage to be switched out depending on the application. The adapter design shown in Figure 3.30 works best if the tracker is directly behind the adapter but does not work well if the tracker is located to the side of the adapter. Figure 3.31 shows an alternate bracket design that could be used if the location of the tracker could not be behind the adapter. Because the bracket design is a two piece design, different posts can be installed to customize the adapter for a given application.

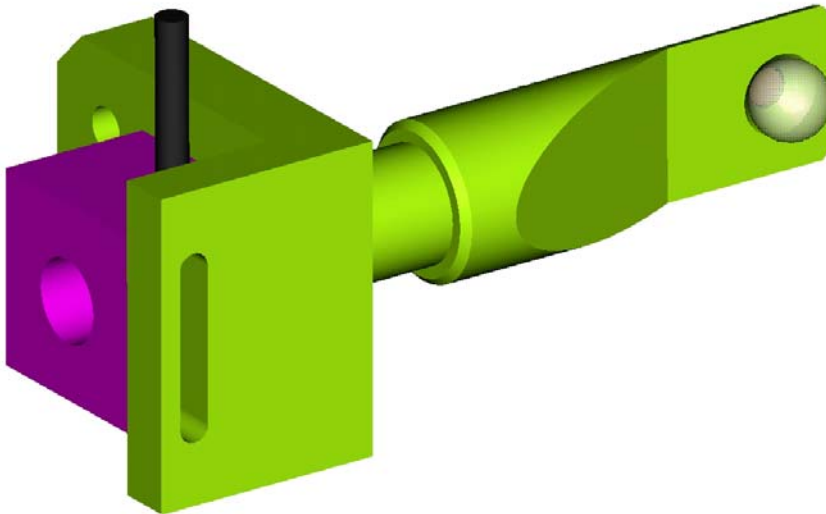


Figure 3.31. Bracket design for use when tracker is located to the side of the adapter

3.4.2.2. Relating the PSD to the Axis of Rotation

The bracket design presented in the previous section does not accurately locate the PSD onto the bracket and does not use any mechanical features to locate the detector with respect to the axis of rotation.

This orientation can be accomplished with the PSD itself. One technique would be to mount the adapter/rotation stage shown in Figure 3.30 on an X-Y translation stage and illuminate the PSD with a laser with a setup similar to the one shown in Figure 3.20 in the PSD characterization section. With the PSD illuminated with the laser, the rotation stage can be rotated and the movement of the beam on the detector can be observed. The X-Y translation stages are then adjusted until the laser beam does not move while the stage is rotated. When no image movement is recorded then the laser beam is on the axis of rotation. Because the interface software for the PSD allows for the origin to be reset at various locations on the detector, the origin can now be reset to the axis of rotation and all future measurements that the PSD reads out will be from the axis of rotation.

The first technique to find the axis of rotation can be time consuming and inaccurate, especially when trying to make the final alignments to the axis of rotation. To expedite the process of finding the axis of rotation, the PSD interface software was modified so that two data points on an arc could be recorded and the software will calculate where the axis of rotation is. The geometry of this problem is shown in Figure 3.32.

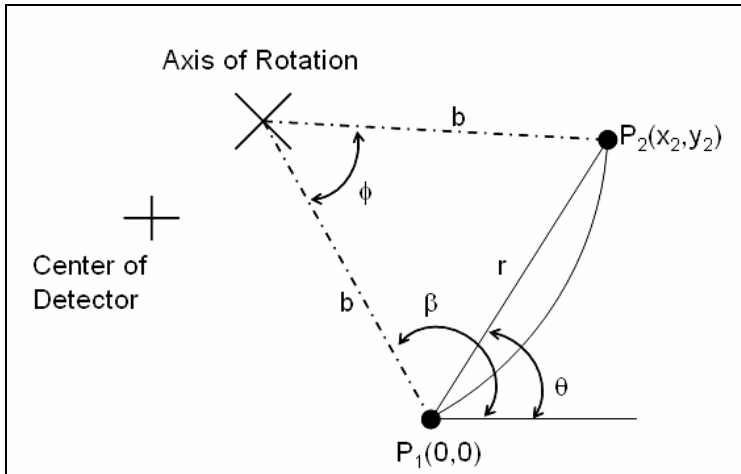


Figure 3.32. Geometry of the Axis of Rotation

Figure 3.32 defines the center of the detector, the axis of rotation of the stage, P1 as the first point of the arc and new origin, P2 as the second point on the arc, ϕ as the amount the PSD was rotated, r as the distance between P1 and P2, and the angles α , β , and θ . The software can be used to find P1 and P2 and the rotation stage can be used to measure ϕ . This information is then sent to a routine in the PSD interface software that calculates where the axis of rotation is. This routine uses the following formulas to find the location of the axis of rotation.

$$r = \sqrt{x_2^2 + y_2^2} \quad (3.8)$$

$$\theta = \tan^{-1}\left(\frac{y_2}{x_2}\right) \quad (3.9)$$

$$\alpha = \beta - \theta \quad (3.10)$$

$$b = \frac{r}{2 \cos(\alpha)} \quad (3.11)$$

$$\begin{cases} x_c = b \cos(\beta) \\ y_c = b \sin(\beta) \end{cases} \quad (3.12)$$

The above formulas use mathematical techniques to locate the axis of rotation and are useful when an X-Y stage is not available to perform a calibration by adjusting the position of the bracket or they are useful to use as a guide as to where to locate the PSD during the manual alignment of the PSD to the axis of rotation. This series of formulas was implemented into the PSD software interface and many different scenarios were investigated. Data sets were built that investigated the software's ability to report a repeatable axis of rotation. To measure the performance, over 50 data sets were taken and the standard deviation of the repeatability of the location of the center of curvature was found to be 0.0027". This value could be improved with a better setup, a weak 90 degree mount was used for this measurement and a stiffer mount should improve this data.

3.4.2.3. Relating the Tracker Ball to the Axis of Rotation

The tracker ball also has to be related to the axis of rotation so that the data from the tracker and the data from the PSD will have a common reference. The calibration of the tracker ball is much simpler than the calibration of the PSD.

The design of the post assumes that the hole that goes through the center of the rotation stage is concentric to the axis of rotation and the tolerances for the post are based on this assumption. Using mechanical tolerances, the seat for the tracker ball can be placed

along the axis of rotation of the stage to within 0.006". The features of the post that drive how well the tracker ball is placed on the axis of rotation are the clearance between the post and the hole in the rotation stage, how close the center of the tracker ball seat is centered on the post, the perpendicularity of cone seat to the axis of the rod, and the perpendicularity of the mounting surface of the post to the axis of rotation. When all of these tolerances are stacked up, the tracker ball should be placed on the axis of rotation to within 0.006" by using mechanical tolerances.

If the location of the image that the PSD and the laser tracker is tracking needs to be known with better tolerances than 0.006" then the tracker itself can be used to measure how far the tracker ball is misaligned from the axis of rotation of the stage. The simulation of image tracking in section 3.4.3 will show that this is an easy measurement to make.

3.4.2.4. Combining Tracker Data with PSD Data

The methodology for calibrating the PSD and the tracker ball to a common reference has been presented in the previous two sections. After careful calibrations have been performed the reporting of the absolute position of an image in space is straight forward.

To combine the data, the coordinate systems of the PSD and the tracker need to be aligned so that a movement in the X direction on the PSD translates to a movement in the X direction on the laser tracker. The laser tracker's software allows for coordinate

systems other than the default coordinate system to be built. This feature of the software can be used to relate the PSD data and the tracker data. The simplest approach to build the coordinate system would be to find the axis of rotation for the stage, then scan the top of the PSD surface to build the X vector, and to scan the side of the PSD to build the Y vector. An origin for these two vectors is needed to define the Z axis and would be set along the axis of rotation of the stage and be offset from the tracker ball so that the origin would be in the plane of the detector. Figure 3.33 shows the concept of where the origin of measurement can be set. With this configuration the X, Y, Z coordinate can be built by adding the X and Y data from the PSD and the Laser Tracker and then directly using the Z coordinate from the tracker.

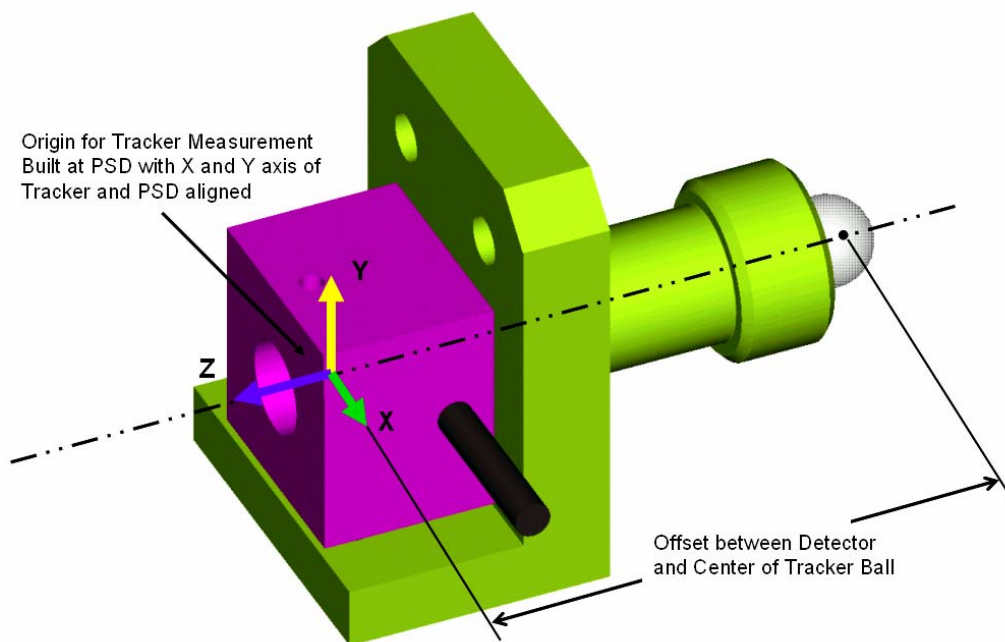


Figure 3.33. Origin of Measurement when PSD and Tracker ball are combined

The accuracy of the method mentioned above will be well below the accuracy of the PSD or the laser tracker because the detector inside of the PSD package is not exactly aligned to the outside planes that were used to build the X and Y vectors. Also the manufacturer specifies the location of the detector in the package to be $\pm 0.010''$ causing the Z coordinate of the image location to be no better than $0.010''$. Often only the X and Y coordinates are critical because it is often difficult to determine exactly where best focus is making the Z axis accuracy not as important. Many techniques can be used to improve the X and Y alignment of the two axes and consequently improve the X and Y accuracy of the reported image location. One example would be to mount the PSD/Tracker ball assembly on a rail and illuminate the PSD with a laser. The rotation stage could be adjusted until only X movement was recorded on the PSD. The position of the rotation stage would then be locked and the rail scanned to produce the X vector. Depending on the required accuracy of the image location, the alignment of the accuracy can be completed so that the accuracy of the image location will approach $0.001''$ or the accuracy limit of the tracker.

3.4.3. Simulation of Image Tracking

To verify the concepts previously presented a simulation was run to track an image. To track an image the setup shown in Figure 3.34 was built. The setup utilized two rails and a HeNe laser was mounted on one rail and the PSD/Tracker ball assembly was mounted on the other. To simulate image tracking, readings would be taken from the PSD and tracker at an initial point, then the laser would be moved a known distance, readings

would again be taken from the PSD and laser tracker, the data would be combined, and the calculated movement would be compared to the actual movement of the laser. The setup shown in Figure 3.34 was built on a granite table and care was taken to make the two rails parallel by using the edge of the table as a reference.

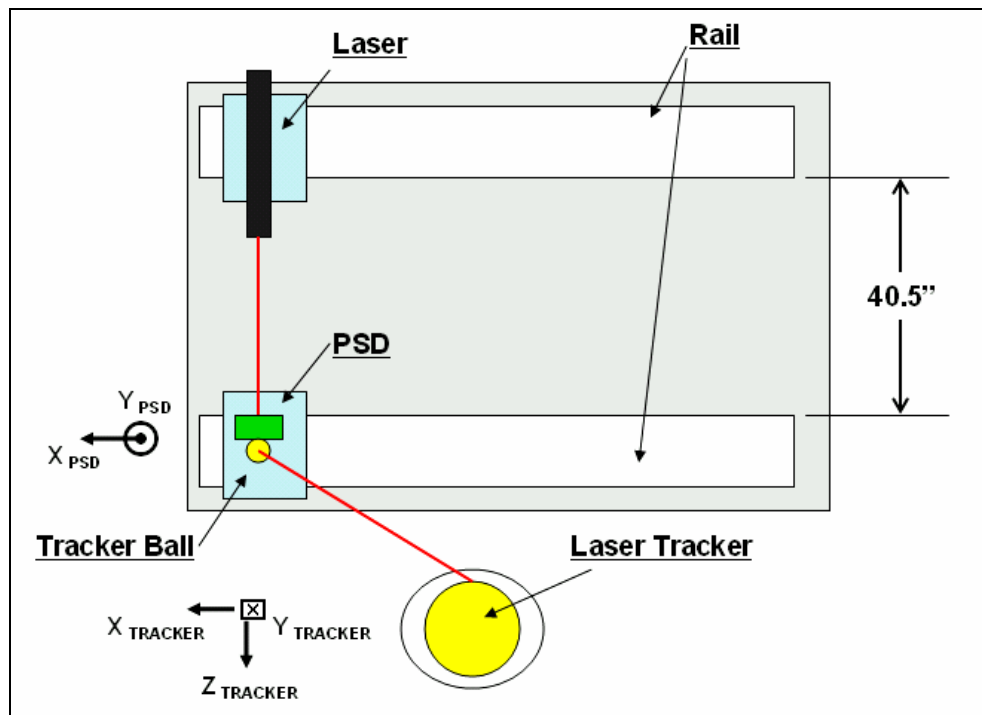


Figure 3.34. Setup for image Tracking Simulation

3.4.3.1. Calibration of PSD and Tracker Ball

Before measurements could be taken with the laser tracker the PSD and the tracker ball seat had to be calibrated to the axis of rotation for the stage and the axes for the tracker and the PSD were aligned. To calibrate the PSD the mathematical routine presented in section 3.4.2.2 was attempted because an X-Y stage to find the axis of rotation was not available. There was a problem with the software causing this routine to be ineffective. The location of the PSD was then found by adjusting the direction of the laser until the

position of the laser spot did not change as the PSD was rotated on its stage. The laser was aligned to the axis of rotation of the PSD to within 0.003” and the Voltage readings from the PSD were recorded and shown in Table 3.11. These offsets were then entered into the PSD interface software so that all subsequent measurements made by the PSD were made from the axis of rotation.

Table 3.11. PSD Offsets

PSD Offsets	Axis
-1.43V	X
0.87V	Y

The PSD/tracker ball bracket assembly was then calibrated to the axis of rotation with the laser tracker. The assembly was placed in a 90 degree bracket and mounted on the rail as shown in the photograph in Figure 3.35.



Figure 3.35. PSD/Tracker Ball Assembly mounted on Rail

To find the axis of rotation the tracker ball was seated in the bracket and the tracker was set to measure a circle. 20 points were used to define the circle and the tracker measured a circle with a diameter of .0078” meaning the tracker ball was displaced from the axis of rotation by 0.0039”. This value matches well to the predicted value presented in section 3.4.2.3 regarding the relationship between the tracker ball and the axis of rotation.

The axis of the tracker and the PSD were then aligned so that a coordinate frame could be built. To build the coordinate frame the origin with two vectors option was chosen. The Y vector was set by profiling the table that the rail was resting on, the Z vector was set by profiling the flat surface surrounding the tracker ball seat on the PSD/tracker ball bracket, and the origin was set at the center of the circle that defined the axis of rotation. The offset distance between the center of the tracker ball and the location of the detector as shown in Figure 3.33 was manually subtracted from the Z axis data. To orient the PSD to the rail, the PSD was translated on the rail and the rotation stage was adjusted until movement along only the X axis was recorded.

3.4.3.2. Simulation Procedure and Results

To perform the simulation an initial point was measured with both the PSD and the Laser Tracker. The laser was then translated 200 mm on its rail. The PSD/tracker ball assembly was translated on its rail so that the laser registered on the PSD but no care was taken to ensure that the assembly moved 200 mm. Measurements were again recorded

with the PSD and the laser tracker. Because the coordinate frame for this set of measurements was carefully built, the true image location was found by simply adding the X data and subtracting the Y data from the tracker and the PSD and simply taking the Z data from the tracker and adding the offset between the tracker ball and the detector surface. The results of the simulation are shown in Table 3.12. The True and Error columns are based on the rail reading off of the rail that the laser was mounted on.

Table 3.12. Results of Image Tracking Simulation

		1st Data Point	2nd Data Point	Δ	True	Error
Laser Tracker Data	X_L	212.804	12.733	-200.071		
	Y_L	-0.008	-0.066	-0.058		
	Z_L	65.697	66.355	0.658		
PSD Data	X_P	0.012	0.757	0.745		
	Y_P	0.012	-0.555	-0.543		
Combined Location	X (X_L + X_P)	212.816	13.490	-199.326	-200	0.674
	Y (Y_L - Y_P)	-0.020	-0.489	-0.509	0.0	0.509
	Z (X_L + O)	-0.673	-0.015	0.658	0.0	0.658

▪ Note: All Dimensions in Millimeters

Table 3.12 shows that the simulation tracked the image to within 0.674 mm along the X axis and 0.509 mm along the Y axis. This performance is not very good but there were many error sources that entered into this simulation that degraded the performance of the

simulation. Due to limited availability of the tracker, these error sources could not be corrected but will be addressed in this report. The simulation was successful because the concept has been shown and the coordinate frames were related. A more robust setup should cause the performance to dramatically increase.

3.4.3.3. Error Sources for Image Tracking Simulation

Many error sources contribute to the error presented in Table 3.12. They include but are not limited to lack of precision on the scale that was used to define 200 mm of image movement, rails not parallel, misalignment between the PSD x axis and the rail, misalignment between surface used to define Z and the rail, PSD offsets not exactly set along axis of rotation, rails not parallel to surface, and others. The impact of these errors is summarized in Table 3.13.

Table 3.13. Summary of Error sources for image tracking simulation.

Error Source	IMPACT	
	Axis	Magnitude
Resolution of Scale on Rail	X	0.50 mm
Rails not Parallel	X	1.03 mm/mrad
Misalignment PSD X axis and Rail	Y	0.509 mm
	X	0.013 mm
Misalignment between Z and rail	Z	0.658 mm
	X	0.013 mm
PSD Offsets not exactly on Axis of rotation	X and Y	0.075 mm
Rails not parallel to surface	Y	0.025 mm

Using the measured performance from Table 3.12 some of the impacts from the misalignments are known and are presented in Table 3.13. The impact of the rails not being parallel is significant and this is not known and is presented as a ratio in Table 3.13.

3.4.4. Image Tracking Summary

The concept of image tracking has been presented along with a methodology of how one can go about to track an image. To track an image, data from two measurement devices must be combined and much of the challenge associated with image tracking is the process of combining the data. To make the combination, careful considerations must be given to the coordinate frame for both the laser tracker and the position sensing detector. The most effective way to combine the data is to use a common reference and align the coordinate frames for each of these devices around that reference. Also presented in this section was a simulation of image tracking. The results of the simulation were less precise than anticipated, but the error sources have been identified and can readily be corrected. Due to limited availability of the tracker, these corrections were not made and will be corrected with further use of this image tracking system.

There are many potential uses for image tracking. Large scale lithographic systems scan a focused spot or an image in a line and the scanning performance of the system is difficult to quantify. The image tracking system presented in this section could quantify

the performance of a large scale scanning system. If the PSD/tracker ball assembly is mounted at the moving image plane, the scanner could then be scanned and the PSD/tracker ball assembly could be moved to find the new location of the image. The scanner could be moved to many different points and the tracker would be able to find all of these points and generate a profile of how well the scanning system is working.

An additional application would be to locate alignment cross hairs or fiducials that can be projected through computer generated holograms. These fiducials are used to help align and orient difficult optical elements such as off axis parabolas. Because a pattern generated by CGH is not circular, the PSD might not be the best choice to locate this reticle. If part of the pattern falls off of the PSD, the PSD would not report the correct location of the fiducial because the PSD reports the location of the spot as the center of all of the incident light on the detector. For this application, a CCD camera could be used in place of the PSD and the CCD would be able to determine where the center of the cross hair is.

Applications in optical testing could also potentially use image tracking. A difficult task in optical testing is off-axis parabola testing. Before and off-axis parabola can be tested by an interferometer, it must be precisely aligned to interferometer. The image tracking system presented in this section would be able to locate the position of the focal point of the interferometer and the off-axis parabolic surface could then be profiled with the tracker and the center of curvature could be compared to the location of the focal point of

the interferometer. For this application a more precise version of laser tracker would be required both for the reported location of the interferometer focal point and the profiling of the parabola.

3.5. Miscellaneous

In addition to the radius of curvature, alignment, and image tracking capabilities of the tracker two other applications were examined. Both diffraction gratings and fold mirrors are often used in the optical shop and the way that the tracker interfaces with these elements was investigated.

3.5.1. Diffraction Grating Investigation

The goal for the test was to see if the tracker could track through the 0th, -1st, and +1st order of a diffraction grating. The diffraction grating could be useful to increase the sensitivity or accuracy of the tracker or allow the tracker to track multiple targets at once. Once the tracker's ability to track the -1st and +1st orders through the grating was established, the tracker's output was to be monitored as the diffraction grating is slightly shifted. The tracker was expected to record movement of the tracker ball when the grating was shifted, if the tracker was able to see this movement this feature could be used to increase the trackers transverse sensitivity. Also, if the tracker was able to track multiple targets through multiple orders, the ability of the tracker to measure pose would be increased.

To investigate how the tracker interfaces with a diffraction grating a 25mm square grating with 92 grooves/mm was selected. The grating was rated for 633 nm light and was made from crown glass. The grating sends 45% of the incident light to the 0th order and 20% of the incident light to both the -1st and +1st orders. For the test the grating was attached to a rotation stage so that it could be added and removed from the beam. The system was aligned and the grating was put in the beam and the 0th order was sent to the tracker ball. The process of inserting the grating into the beam broke the beam and the tracker needed to be reset. The absolute distance meter is used to reset the tracker and it uses an IR laser to do this. The IR laser was not able to see through the grating therefore the tracker could not output a coordinate. Even though the tracker would not output a coordinate, it would still track the target through the grating. As the tracker ball was moved, the tracker stayed aligned to it. To further investigate the tracker's ability to track through the grating, the tracker ball was aligned to track the 1st order beam. The tracker would not track the 1st order beam. This is probably due to the severe loss of signal when the grating is used in double pass. The beam is diffracted once when it is going to the tracker ball and again when the beam goes back to the tracker. The grating sends only 20% of the light to the 1st order therefore, the tracker would only see 4% of the initial power when the light is diffracted the second time on the return path. Figure 3.36 describes this effect.

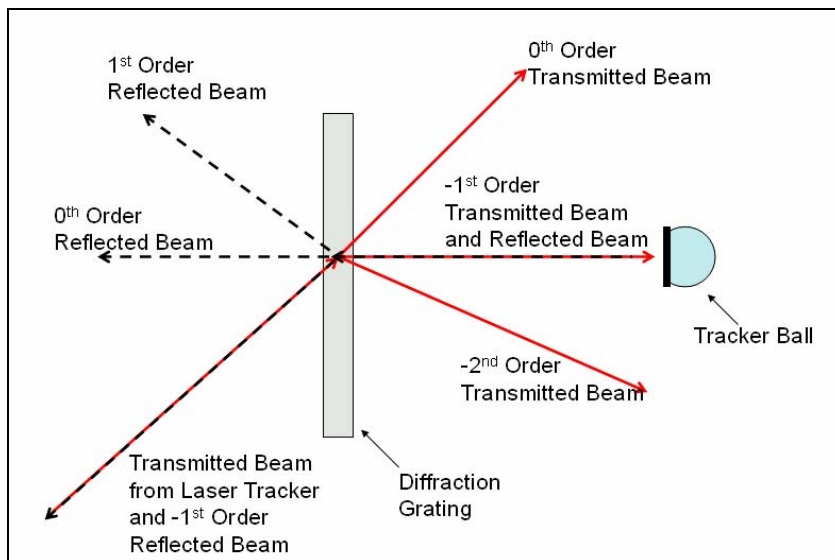


Figure 3.36. Diffraction Grating when used in Double Pass.

3.5.2. Fold Mirror Investigation

The final experiment that was performed with the laser tracker was to investigate how the tracker interfaced with a fold mirror. To set up this test a simple setup was constructed where the tracker's beam was folded and aligned to the tracker ball. The Tracker ball was mounted on a translation stage that was driven by a micrometer so the ball could be moved known amounts during tracking. A figure of the setup is shown in Figure 3.37.

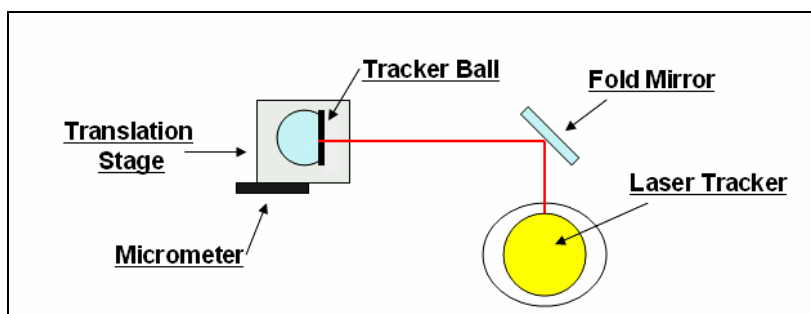


Figure 3.37. Fold Mirror Test Setup.

As the ball was moved on the translation stage, the tracker was able to track the movement. To ensure that the tracker was tracking correctly the tracker acquired a datapoint, the stage was adjusted by a set distance, and the tracker acquired a second data point. The software of the tracker calculated the distance between the two points that were acquired and this number matched the reading from the micrometer on the translation stage to within 0.0001” or the resolution of the micrometer.

The ability of the tracker to track through fold mirrors could potentially be used to measure the line of sight distance of a folded optical path. Making this measurement is traditionally difficult because the exact location of where the optical axis intersects a fold mirror is difficult to determine.

3.6. Summary of Laser Tracker Evaluation

This chapter has shown that the laser tracker has potentially powerful applications in the optical shop. The capabilities of the laser tracker to profile spherical surfaces and relationships between expected measurement error and R/# have been derived. The tracker’s ability to measure radius of curvature has been compared to an interferometric autostigmatic test and the tracker has been shown to perform remarkably well for optics faster than R/2.0 with predicted accuracies better than 40 microns. For R/7.5 optics the predicted accuracy is better than 0.50 mm.

The tracker was also looked at as an optical alignment tool, and the tracker's ability to report a repeatable center of curvature of a spherical surface correlated well with its ability to measure radius of curvature. The same error vs. R/# relationships can be used to judge how well a tracker can report the location of the center of curvature. The repeatability section highlighted the importance of a rigid mount when profiling a surface, any movement of the surface during profiling introduces measurement error. Two examples were investigated as potential candidates to have their optics aligned with the laser tracker.

The final capability that was investigated was image tracking and the data from the tracker and a position sensing detector was combined to report the location of an image. This capability could be used test the scanning performance of a scanning system or to locate alignment fiducials that can be projected. Hardware was built and a simulation was performed that demonstrated this capability of the tracker.

CHAPTER 4. OTHER TESTING AND ALIGNMENT TECHNIQUES

This chapter is included in this thesis to document some of the other work I have done with optical testing and alignment. Although the techniques do not involve the laser tracking system, they are novel testing and alignment techniques that could be applied in future work. Three sections are included in this chapter. They investigate real time power spectral density analysis of image jitter data, aligning auxiliary optics to an alignment telescope, and utilizing an adjustment matrix to expedite difficult alignments.

4.1. Power spectral density analysis of image jitter

The resolution and sampling frequency capabilities of the position sensing detector (PSD) presented in the PSD characterization section of chapter 3 enable this device to make line of sight (LOS) jitter measurements. The detector used in this research has a resolution of 250nm and a maximum sampling frequency of 15 kHz. The software that interfaces between the computer and the detector was modified to exactly set the sampling frequency and display statistics in real time. The statistics that the software displays are the mean spot position, position standard deviation, position histogram, and a power spectral density plot for each axis of the position sensing detector.

4.1.1. Measurement Techniques and Impacts of Line-of-Sight Jitter

Line-of-Sight (LOS) Jitter is the time-varying motion of an image on a detector. Jitter is caused by internal or external dynamic loads and can be measured by pointing a system at a target and measuring how well the system points at the target. External loads that can cause jitter not only include extreme vibrations seen by vehicles when they are in motion but also include minute vibrations of the floor of a building that an optical system is mounted on. If there is jitter in a system, the system's pointing ability will vary and the system will not always point exactly where it is expected to point. Many methods can be used to make jitter measurements including monitoring the encoder readouts of a gimballed system and monitoring accelerometers that can be attached to the system under measurement. Other methods are used depending on the amount of jitter to be measured and the configuration of the system that is being measured. The method that will be investigated in further detail will be the technique of sending a light source through an imaging system and measuring the image movement at the image plane. This technique is the most direct way to measure line of sight jitter and extremely small amounts of image motion can be detected.

Depending on the application of the system, there are many ways that jitter can degrade an optical system's performance. In a video system the most fundamental effect is aesthetics. If there is significant jitter in a system the user will observe the image jumping on a viewing screen, and this effect is not desirable. Jitter can also affect the pointing accuracy of a system. If a system is designed to track a target, system jitter will

degrade the systems ability to report the location of the target. Examples of these types of systems are laser tracking systems, which have been extensively investigated in this thesis, and military targeting systems. Jitter has other degrading effects on systems, but the last one that will be discussed is the impact to the image quality of an imaging system. Image jitter degrades the image quality of a system by increasing the blur diameter of the point spread function causing the MTF of a system to degrade. The decrease in system MTF due to jitter depends both on the amount of image motion in the system and the exposure or integration time of the detector. Figure 4.1 describes the effects of jitter on an imaging system.

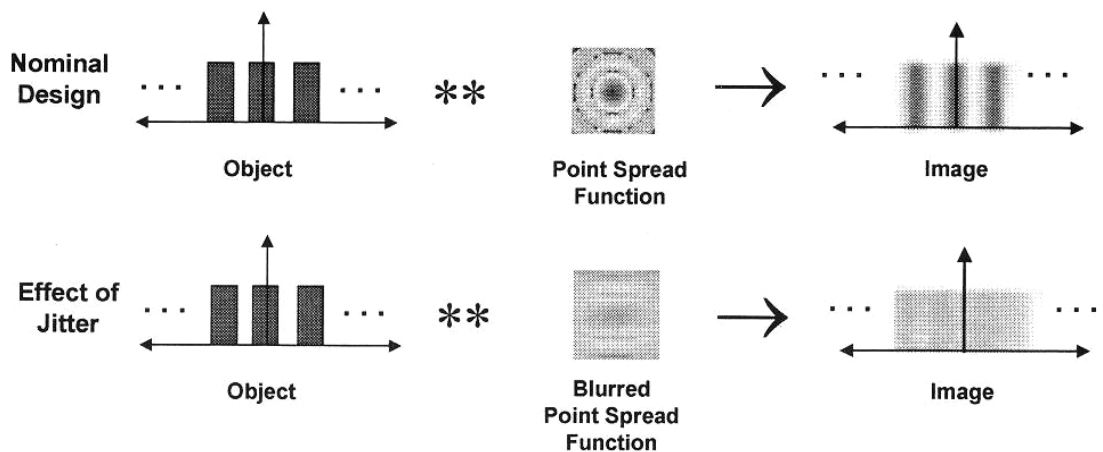


Figure 4.1. Effects of jitter on an imaging system [52]

Impacts of jitter can be modeled during the design phase of a project. A perturbation analysis and error budget similar to the one discussed in section 2.5.3 can be generated for LOS jitter. Instead of wavefront effects for each perturbation, the image motion for each perturbation will be recorded. A set of relationships between perturbation and

image motion can be tabulated for each degree of freedom and the allowable amount of movement for each element can be tolerated in an error budget. To predict if the system will perform to the tolerances allotted by the error budget, finite element analysis can be used. The system can be input into finite element model and the model can be excited by a range of external forces similar to the forces that the actual system is expected to see. The finite element model will then predict the movement of each of the optical elements and this movement is compared to the movement allotted by the error budget.

4.1.2. Power Spectral Density

To describe a random time domain signal, power spectral density can be used to analyze the frequency response of a system. The power spectral density (PSD) statistically represents the energy content of the signal as a function of frequency. The PSD is especially useful when dealing with random functions because system performance information can be pulled from data that is interpreted as random noise when analyzed in the time domain. To convert a time domain signal to a frequency domain signal, the Fourier transform is utilized. If a computer is to be used to capture discrete data points, the fast Fourier transform (FFT) is an efficient method to calculate the conversion from time domain to frequency domain. The power spectrum of a time domain signal is computed with the following equation.

$$G(\text{signal}) = \frac{FFT^*(\text{signal})FFT(\text{signal})}{N^2} \quad (4.1)$$

Where $G(\text{signal})$ is the power spectrum, $\text{FFT}(\text{signal})$ is the fast Fourier transform of the signal, $\text{FFT}^*(\text{signal})$ is the complex conjugate of the fast Fourier transform, and N is the number of discrete data points that were collected from the signal. N is calculated by multiplying the sampling frequency by the length of the measurement. To generate the PSD plot, the power spectrum is divided by the frequency interval, Δf , and is expressed in the following equation.

$$PSD(\text{signal}) = \frac{G(\text{signal})}{\Delta f} \quad (4.2)$$

Where $PSD(\text{signal})$ is in units of $[\text{Amplitude}^2/\text{Hz}]$. Because the power spectrum is the Fourier transform of the signal multiplied by the complex conjugate of the Fourier transform the power spectrum is always real and symmetric about zero. Traditionally, only the positive half of the PSD curve is displayed because the negative frequency portion of the curve has no physical meaning. Because only half of the power spectrum is useful, the sampling rate of the time domain must be twice that of the maximum frequency to be analyzed.

The power spectral density of a signal is related to the variance and standard deviation of the time domain signal. The variance of the time domain signal, denoted by x^2 , is simply the area under the curve of the PSD plot as shown in the equation 4.3.

$$x^2 = \int_0^{\infty} PSD(\text{signal})df \quad (4.3)$$

The standard deviation, σ , of the time domain signal is simply the square root of the variance as shown in equation 4.4.

$$\sigma = \sqrt{x^2} \quad (4.4)$$

4.1.3. Software

Line of sight jitter is a result of random vibrations in a system and can be represented with a power spectral density plot. To generate a PSD plot that represents LOS jitter, image movement must be recorded at set time intervals to create a dataset that represents a random time domain signal. Because the position sensing detectors can report image position at high sampling rates, this type of detector was chosen to provide LOS jitter information. Software was developed in LabVIEW® to interface between the position sensing detector and the computer.

The software interface allows the user to set the sampling frequency and the length of measurement and after the data set is collected, the software will report a power spectral density plot for each axis on the detector. Before the PSD plot is generated, data arrays for each axis of the position sensing detector are built. To build the arrays, position information is recorded at set intervals over the length of measurement. For example, if the sampling rate is set at 1000 Hz and the length of measurement is 10 seconds there will be 10,000 data points collected for both the x and y axis of the detector. Because jitter is typically specified in radians, these arrays of position information are converted

to arrays of angular information by simply scaling each position by $1/D$, where D is the distance between the detector and the rotational point of the optical system. The array of angular information is a time domain signal that can be converted into a frequency signal with the methods described in Section 4.1.2. Figure 4.2 shows the LabVIEW® block diagram that was used to compute the power spectral density plots.

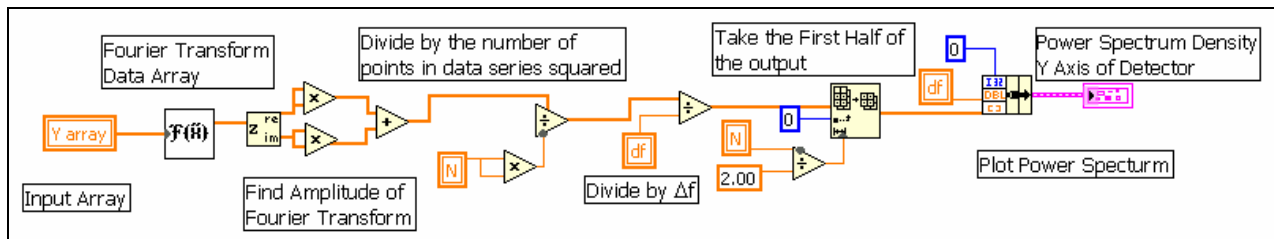


Figure 4.2. Power Spectral Density Computational Block Diagram

To minimize computational time the amplitude of the Fourier transform of the input array is found by splitting the transformed array into the real and imaginary parts. Each part is then squared and added together to find the amplitude. This technique provides the same answer as the technique presented in equation 4.1 but only requires the computer to make one Fourier transform of the dataset. The following equations show that the two techniques produce the same result.

$$\begin{aligned}
G(s) &= \frac{FFT^*(s)FFT(s)}{N^2} \\
G(s) &= \frac{[FFT(real) - iFFT(imaginary)] * [FFT(real) + iFFT(imaginary)]}{N^2} \\
G(s) &= \frac{FFT^2(real) - iFFT(im)FFT(real) + iFFT(im)FFT(real) - i^2 FFT^2(im)}{N^2} \\
G(s) &= \frac{FFT^2(real) + FFT^2(im)}{N^2}
\end{aligned} \tag{4.5}$$

Figure 4.2 shows that after the amplitude is divided by the number of data points squared and by Δf only the first half of the resulting data set is used to generate the power spectral density plot. Because only half of the data is used, the signal must be sampled at twice the maximum frequency of interest to generate a PSD curve that fully describes the system.

To ensure that the software was operating correctly, the input array shown in Figure 4.2 was replaced with a sine wave and a power spectral density plot was generated. In addition to generating the plot, the PSD curve was integrated to find the variance and standard deviation. The frequency of the sine wave was set at 100 Hz and the amplitude was set at 1. Because this is an infinite signal in the time domain, a spike at 100 Hz was expected on the PSD plot. Also, the square root of the integral of the PSD curve should be equal to $\frac{1}{\sqrt{2}}$ because this is the standard deviation of a sine wave with amplitude equal to 1.

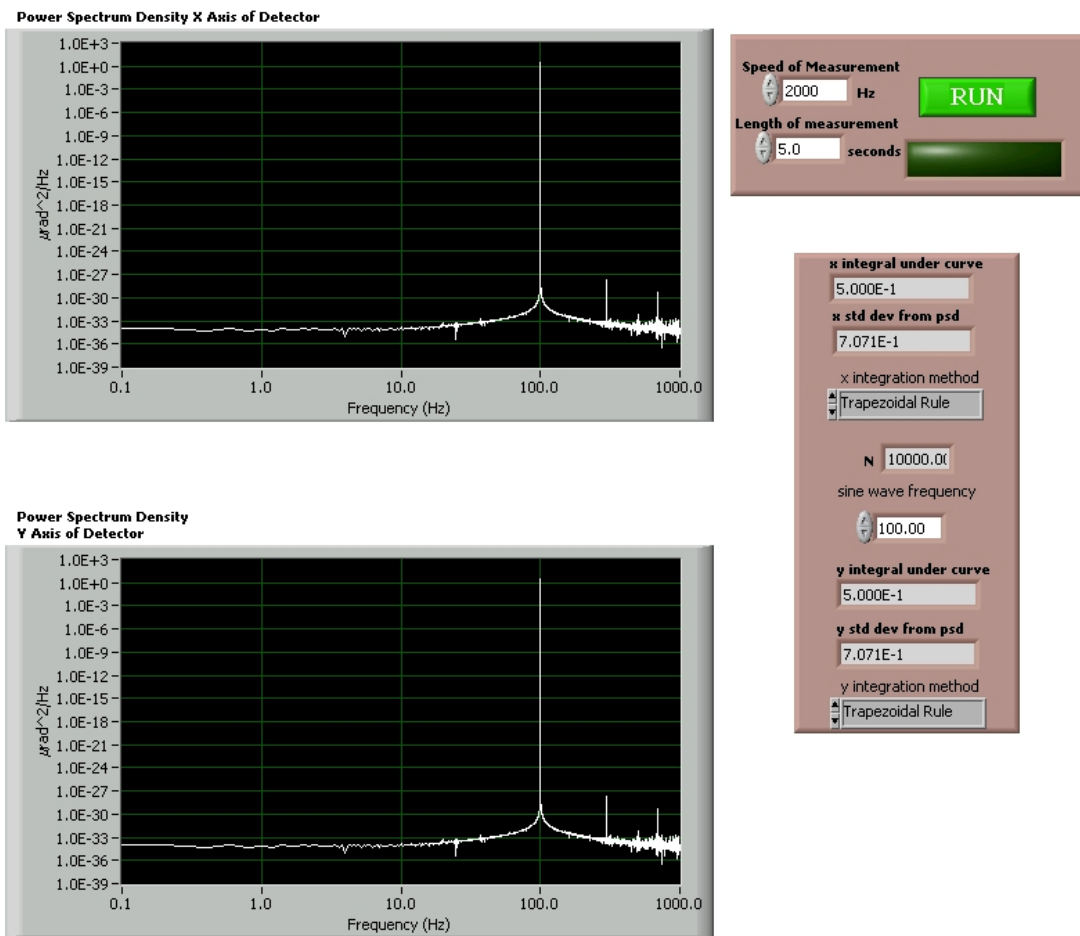


Figure 4.3. Power Spectral Density Software verification.

Figure 4.3 shows the results of the verification and shows that the software performs as expected. A sharp spike shows up on the PSD Plot exactly at 100 Hz. To the right of the PSD plots in Figure 4.3, the result of the integration of the two curves is displayed. Again, the software performs as expected because the square root of the integral equals 0.707 and this is equal to the standard deviation of a sine wave.

4.1.4. Line-of-Sight Jitter Measurements with Software

After the software's ability to generate power spectral density plots was verified, the software then interfaced with the position sensing detector and line-of-sight jitter measurements were taken. To demonstrate the position sensing detector's ability to measure jitter, a system similar to the one presented in the PSD (Position Sensing Detector) Characterization was constructed and is shown in Figure 4.4.

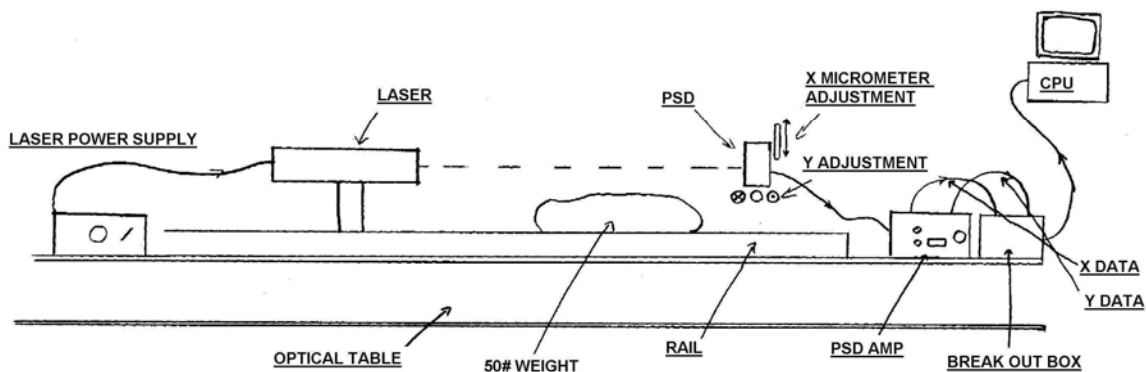


Figure 4.4. LOS Jitter Test Setup

A laser was mounted on a table that was isolated with air and was pointed at the position sensing detector. Spot motion on the detector was then recorded. Jitter is typically specified in radians so the distance between the center of the laser mount and the detector was measured and found to be 27.75 inches. The position information on the detector is simply converted to radians by dividing the image movement on the detector by 27.75". A data set was taken by sampling the detector at 2000 Hz for 10 seconds. Figure 4.5 shows the raw data for each axis, a total of 20000 data points were collected in 10 seconds, this data makes up the time domain LOS jitter signal.

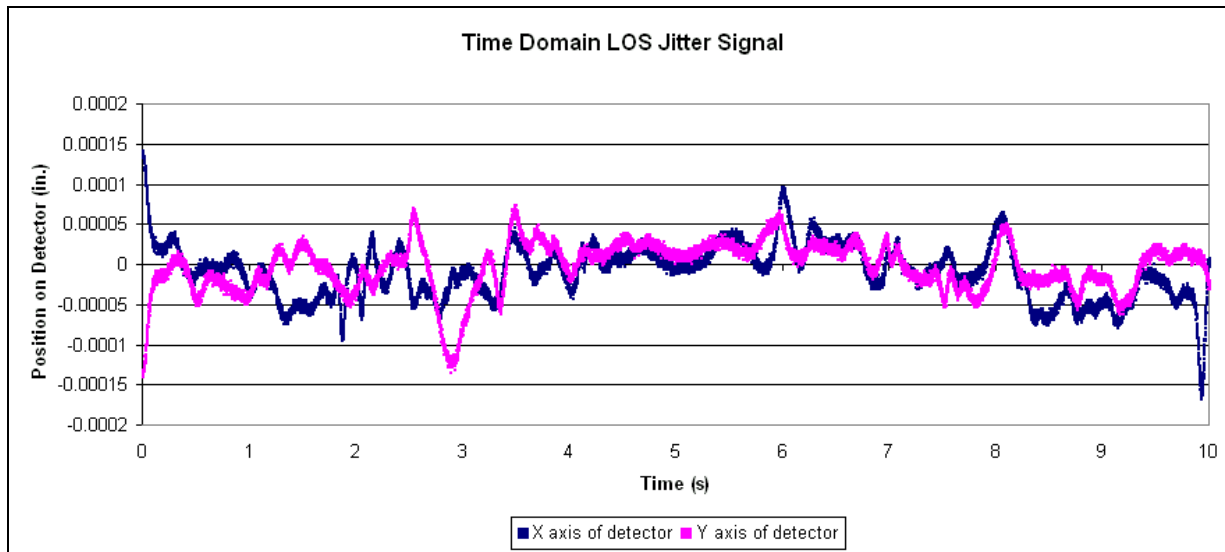


Figure 4.5. Time domain line of sight jitter signal.

Figure 4.5 shows random image motion recorded by the position sensing detector for both the x and the y axis. Table 4.1 tabulates the mean and standard deviation calculations that were calculated from the time domain data. The mean and standard deviation are reported in both inches and μrad .

Table 4.1. Mean and Standard Deviation of Image Jitter

	X Axis of Detector	Y Axis of Detector
Mean Value [inches]	-1.0 E-5	3.0 E-6
Mean Value [μrad]	-0.364	-0.125
Standard Deviation [inches]	3.367 E-5	3.084 E-5
Standard Deviation [μrad]	1.213	1.112

The software that was developed took the time domain position information from the detector and converted it into the frequency domain with methods described in the previous two sections. The results are shown in Figure 4.6.

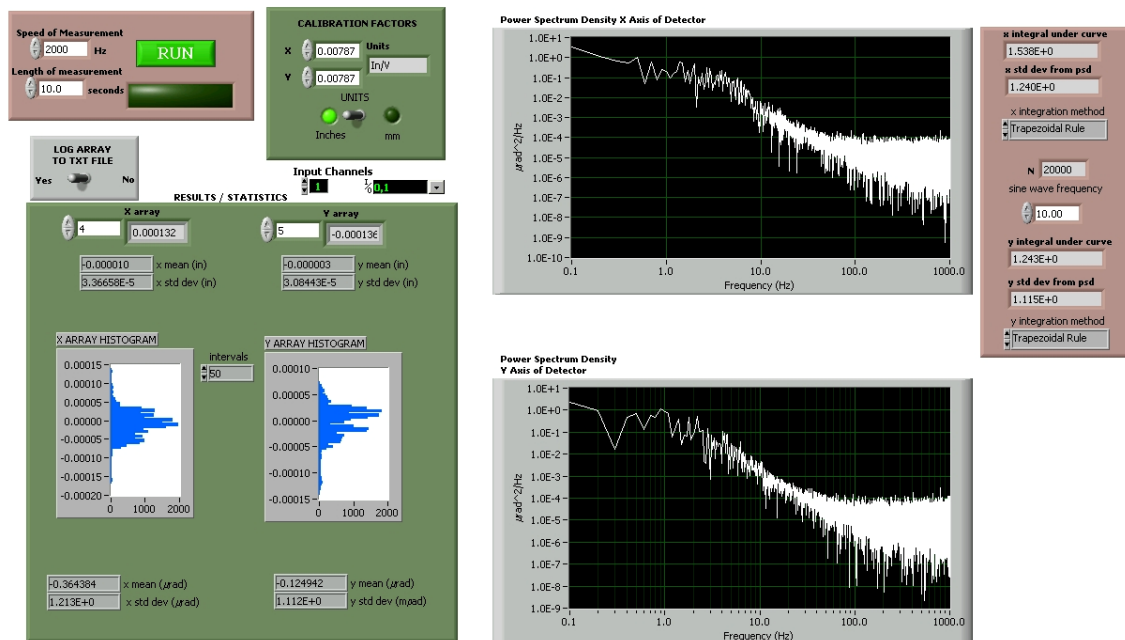


Figure 4.6. LOS Jitter Report for simple pointing system.

The output screen from the LabVIEW® software is shown in Figure 4.6. On the right hand side of the figure the power spectral density plots for each axis are displayed. To further check the validity of the plots, the curves are integrated and the square root of the integration is compared to the standard deviation of the time domain signal. Because of the many spikes and irregularities in the PSD curves, the value of the square root of the integration is not expected to exactly equal the standard deviation of the time domain signal. The results of the standard deviation calculated from the PSD curve compared to the standard deviation calculated from the time domain signal are presented in Table 4.2.

Table 4.2. Comparison of Standard Deviation Calculations

	Time Domain	Frequency Domain	% Difference
X Axis Standard Deviation [μrad]	1.213	1.240	2.2%
Y Axis Standard Deviation [μrad]	1.112	1.115	0.3%

Table 4.2 shows that the two different methods of calculating the standard deviations are in close agreement, providing more confidence that the Power Spectral Density plots are accurate.

The measurements presented in this section show that an extremely stiff system that is mounted on an isolated optical table will still experience image jitter. The sources of image jitter for this setup primarily come from vibrations in the floor that make their way through the isolated optical table and thermal gradients in the air. Although the values of line of sight jitter that were recorded were extremely small, some optical systems such as lithographic systems have image jitter requirements of less than 2 μrad .

This measurement system can be used to measure LOS jitter of more complicated optical systems. As long as a source can be imaged through the optical system of interest and focused onto a position sensing detector, line of sight jitter can be recorded and measured.

4.2. Adding Auxiliary Lenses to Alignment Telescopes

As described in the Optical Alignment section of the Background chapter of this thesis, the alignment telescope is an extremely useful tool to align optical systems. To align an optical system with an alignment telescope, a reference optical axis is established by aligning the reticles inside the telescope to a target. When optical elements are placed onto the reference axis, the alignment telescope must be refocused because the optical element will shift the image of the target closer or further away from the telescope. After the telescope is refocused, the element is aligned by adjusting the position of the element until the image of the target is realigned to the target. The position of the element needs to be adjusted to center the lens on the reference axis. If the lens is decentered then the lens will bend the reference axis and adjusting the lens position corrects this bending. The method described above is an effective way to precisely align a multiple element optical system. However, sometimes the image shift introduced by the optical elements pushes the image of the target to positions that are impossible for the alignment telescope to focus on. For example, if a system is to be aligned in a small laboratory, the image of the target can be shifted so far that the telescope can not focus on the images because the images have been shifted beyond the walls of the laboratory. During the formulation of the alignment plan for the system to be aligned, the geometry of the site where the alignment is to be performed must be analyzed to determine if the image shifts that will be introduced will need to be compensated for. To compensate for these unwanted image shifts a corrector lens can be installed in front of the telescope. This corrector lens can

compromise the alignment accuracy of the telescope if it is not properly installed and aligned.

4.2.1. First Order Optical Analysis

To analyze the impacts of image shifts during the alignment process a 1st order optical analysis is acceptable. To calculate the amount of image shift that is introduced by optical elements, the classic 1st order imaging equation will be used and is as follows:

$$\frac{1}{Z'} = \frac{1}{Z} + \frac{1}{f} \quad (4.6)$$

Where Z' is the image distance, Z is the object distance, and f is the focal length of the lens. An example of a simple alignment task will be investigated to demonstrate the technique of performing a 1st order analysis to analyze an alignment task. The task that will be investigated will be to align a lens system with an effective focal length of 650 mm to an axis that is defined by two reticles (R1 and R2) that are spaced at 1400 mm. This system is to be aligned with an alignment telescope mounted on an optical table that is 3 meters long. Figure 4.7 shows the schematic of the system to be aligned.

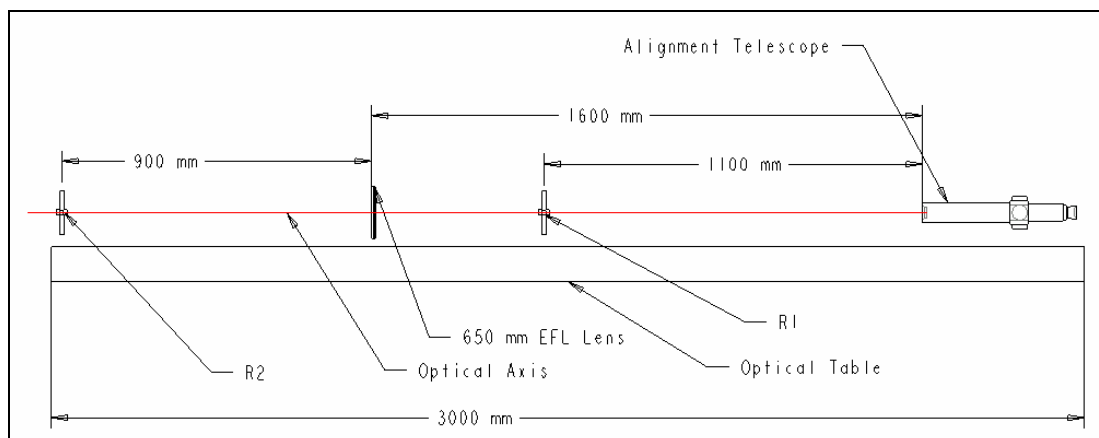


Figure 4.7. Simple optical system to be aligned on an optical table (side view).

The first step to align this system will be to place R1 and R2 on the table and adjust the position of the alignment telescope until the axis of the telescope passes through the center of both reticles. The next step of the alignment will be to place the lens with an EFL of 650 mm along the axis between the two reticles and 900 mm behind R2. The alignment telescope needs to focus on the image of R2 to align the lens but it can not focus on this image because the image location according to equation 4.6 will be 2340 mm to the right of the lens and this is behind the alignment telescope and off of the optical table. Using equation 4.6 and setting Z equal to -900 mm and f equal to 650 mm, Z' or the location of the image is found to be 2340 mm (see figure 4.8).

A negative lens can be placed in front of the alignment telescope to push the image of R2 in front of the telescope and this will eliminate the constraint of the optical table being too short. To size the power of the negative lens, the first order imaging equation is again used. The image of R2 is the object and is located 740 mm to the right of the location of

the compensating lens making Z is equal to $+740$. If a -200 mm lens is selected, then equation 4.6 reports that the new location of Z' is located at -274 mm or 274 mm in front of the alignment telescope (see Figure 4.8).

Because a negative lens has been used to push the image of R2 in front of the telescope, R1 is now imaged through a lens and the location of the R1 image must be investigated to ensure that it is in a desirable location. Using equation 4.6 and setting $Z = -1100$ mm and $f = -200$, the location of the image of R1 (Z') is equal to -169 mm or 169 mm in front of the telescope. Some alignment telescopes will not focus on an object this close causing further modification to the power of the negative lens to be necessary. In this example it is assumed that the alignment telescope is capable of focusing on this object, so there will not be any further modification to the power of the negative lens. Figure 4.8 shows the location of R1's image along with the locations of the image of R2 with and with out the compensating lens.

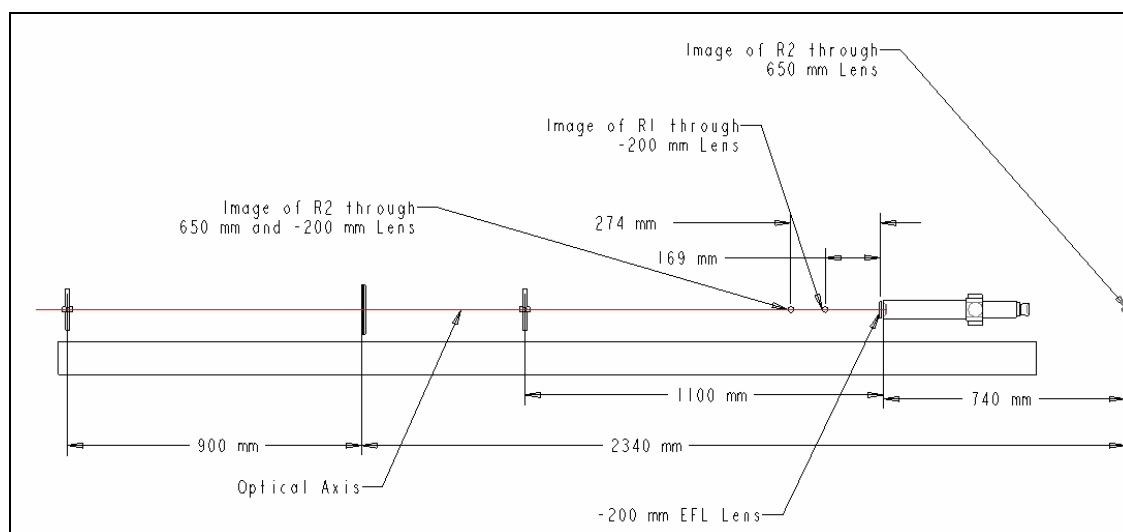


Figure 4.8. Image locations of reticles through an optical system.

4.2.2. Alignment of Compensating Lens to Telescope

The compensating lens that was used to push the images of the reticles in front of the telescope causes the optical axis of the telescope to no longer be aligned to the mechanical axis of the telescope. The optical axis and the mechanical axis of alignment telescopes are typically aligned to within 3 arc seconds. Many schemes can be used to align the compensating lens to the alignment telescope. The most straight forward method would be to make an adapter that holds the compensating lens and slips onto the end of the alignment telescope. An additional design constraint for this adapter would be its ability to be removed and replaced many times during use with out affecting the readings from the telescope. The adapter could be fabricated so that no alignment of the auxiliary lens was necessary by precisely machining the diameter of the adapter that slips on the end of the telescope, precisely machining the mount of the lens so that it is perfectly normal to barrel axis, and precisely machining the lens seat so that the lens could be perfectly centered in the seat with precision shims. The adapter mentioned above would be extremely expensive because the dimensions on the many critical surfaces of the adapter would need to be held to with in +/- 0.0001" to keep the error introduced by the adapter less than 10 arc seconds. In addition to an extremely well made adapter a custom lens with almost no wedge would be required, because any wedge in the lens will deviate the optical axis of the telescope. The relationship between the amount of beam deviation and the amount of wedge in a lens can be described by the following well known equation:

$$\delta = \alpha (n-1) \quad (4.7)$$

Where, δ is the amount of beam deviation, n is the index of refraction of the lens, and α is the amount of wedge in the lens. Most standard catalog lenses typically specify the wedge of the lens to be less than 3 arc minutes and would cause the beam to deviate by approximately 1.5 arc minutes if placed in front of the alignment telescope.

To minimize the cost of the adapter, the lens could be made so that the position of the lens is adjustable in the adapter. This design allows the adapter to be removed and replaced during use without the need for realignment. The cost and complexity of the adapter is reduced by only machining one precision surface and using catalog lenses with poor wedge tolerances. The design takes advantage of the precision surface that is located on the barrel of most alignment telescopes. The diameter barrel of an alignment telescope is typically held to within $\pm .0002''$ or 5 microns. If the diameter of the adapter is held tightly so that the adapter slips onto the end of the telescope with minimal clearance, the adapter can rotate smoothly on the telescope barrel once it is installed. The position of the lens is adjustable and is aligned by installing it on the end of the telescope and aligning the telescope onto a target. The adapter is then rotated on the barrel of the telescope and the position of the lens is decentered until no image movement is observed through the telescope. This design does not require a lens with 0 wedge because the wedge in the lens is compensated by decentering the compensating lens. By rotating the lens on the barrel of the telescope the exact position of the lens can be set so that the orientation of the lens is not critical allowing the adapter to be removed and replaced

during use of the telescope. This design is possible because decentering the lens causes beam deviation. When the right amount of decenter is introduced, this decenter can compensate for wedge that is inherent in a lens. Figure 4.9 shows how decentering a lens can compensate for wedge.

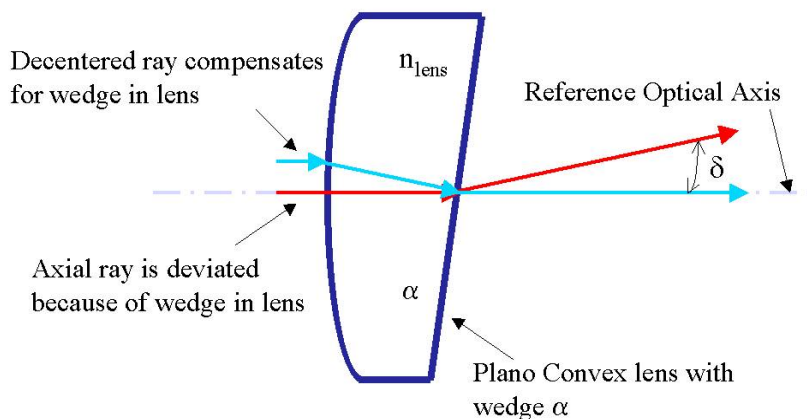


Figure 4.9. Decentering a lens compensates for wedge in a lens.

4.2.3. Hardware

The rotatable adapter previously described was built and tested. This adapter housed a -1000 mm lens that was placed in front of a Taylor Hobson alignment telescope. The adapter was machined out of 6061 Aluminum and only the surface that interfaced with the barrel of the telescope was given tight tolerances. See Appendix B to see the hardware drawing that was used to build the adapter. Figure 4.10 shows an exploded view of the adapter assembly that was built.

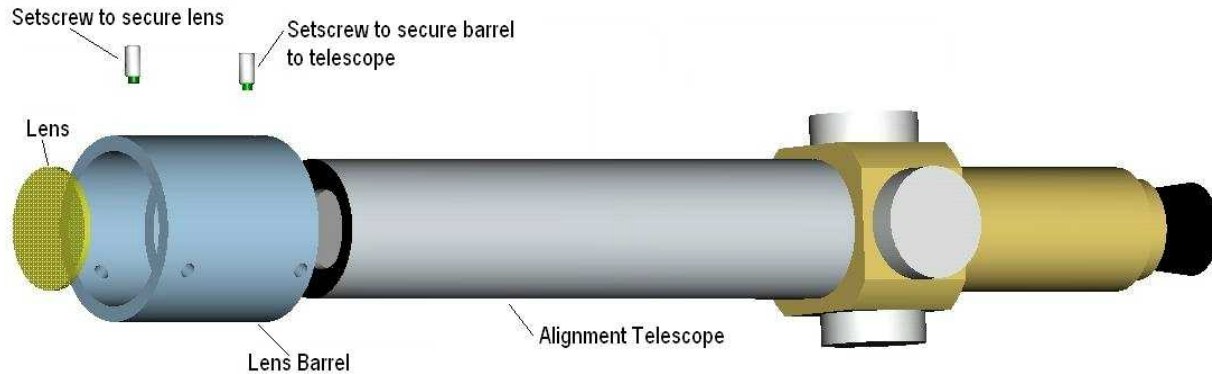


Figure 4.10. Exploded view of adapter assembly.

The barrel shown in Figure 4.10 rotates on the end of an alignment telescope and uses setscrews to adjust and secure the lens in the barrel. Nylon tipped setscrews were also added to secure the barrel to the telescope when the barrel did not need to be rotated. To test this design the lens barrel was installed on the telescope and the telescope was focused on a target 220 inches away. The position of the lens was adjusted by adjusting the setscrews until minimal image movement was observed as the barrel was rotated on the telescope. To measure the performance of this design, the lens barrel was removed and replaced and the amount of image movement was recorded. After less than 30 minutes of adjusting the position of the lens, the alignment of the telescope with the barrel and without the barrel was held to be less than 15 arc seconds.

This design could be improved by implementing a better way to adjust the lens position in the adapter. The nylon tipped setscrews are cumbersome to work with because the lens falls out when the screws are only slightly loosened. Also $\frac{1}{4}$ -20 adjustment screws

were chosen, and a finer pitched screw would allow for finer adjustment of the lens position. These improvements to this basic design would allow an auxiliary lens to be aligned to an alignment telescope with in 3 arc seconds and would cause minimal impact to the alignment between the mechanical and optical axis of the alignment telescope.

4.3. Expediting Alignments with an Adjustment Matrix

Before any complex optical system is to be aligned, an alignment plan must be generated so that the system is aligned in the proper sequence. Ideally the system should be aligned so that once an adjustment is made there is not a need to change that adjustment further in the alignment sequence. Sometimes this is not possible and the adjustment of one or more of optical the elements is an iterative process. Iterative alignments can be lengthy and frustrating. This section presents a method that can be employed to help expedite iterative alignments. The mechanics of the technique along with a detailed example of how this method can be used in practice will be presented. This technique is also useful if the actual adjustment is difficult. Sometimes optical elements are not adjusted with adjustment knobs but are adjusted with cumbersome shims or other methods. The shim is used because it extremely robust and will hold alignments for years but the initial alignment with shims can be extremely tedious.

4.3.1. *Technique to Expedite Complex Alignments*

Because optical systems can be approximated as linear shift invariant systems, the effects of perturbing the individual optical elements can be described with linear algebra. The technique to expedite complex alignments can be described in four basic steps as follows:

1. Identify what degrees of freedom will be adjusted during the alignment.
2. Make small adjustments to each degree of freedom and measure the corresponding impact the adjustment has to the overall system alignment.
3. Calculate the relationship between each degree of freedom and the corresponding change in alignment.
4. Use these relationships to predict how much adjustment is necessary to properly align the system.

The relationship between the degrees of freedom in the optical system and their affects on the system alignment can be described with the equation shown below.

$$\begin{bmatrix} \delta_1 \\ \delta_2 \\ \dots \\ \delta_n \end{bmatrix} = M \begin{bmatrix} k_1 \\ k_2 \\ \dots \\ k_n \end{bmatrix} \quad (4.8)$$

Where k is the amount of adjustment of each degree of freedom, δ is the effect that the degrees of freedom have on the alignment, and M is the adjustment matrix. Before this

matrix can be used the coefficients of the adjustment matrix must be found. Adjusting each of the degrees of freedom by known amounts and recording the corresponding impact to the overall system alignment is needed to find the coefficients of the adjustment matrix. Once the cause and effects have been recorded, the series of linear equations that results from the matrix can be written out and the individual coefficients of the adjustment matrix can be solved for.

After the adjustment matrix is found the optical system is fully defined and the matrix can be used to determine the amount of adjustment that is necessary to bring the entire system into alignment. The amount of adjustment is found by measuring the amount of misalignment in the system and generating a δ vector. This δ vector is then multiplied by the inverted adjustment matrix as shown in equation 4.9.

$$\begin{bmatrix} k_1 \\ k_2 \\ \dots \\ k_n \end{bmatrix} = M^{-1} \begin{bmatrix} \delta_1 \\ \delta_2 \\ \dots \\ \delta_n \end{bmatrix} \quad (4.9)$$

Because optical systems are not truly linear shift invariant system and because measurement error exists when measuring the δ values, this technique should not be expected to provide the exact solution the first time adjustments are made. But this solution should give the alignment engineer a systematic approach to making the difficult adjustments and allow him to converge on the optimum solution quickly.

4.3.2. Fold Mirror Alignment Using Adjustment Matrix

An iterative fold mirror alignment will be used as an example to demonstrate how this technique can be implemented. In this example a fold mirror needs to be aligned so that the bore sight ray through an optical system is aligned to two reticles. The alignment scenario is shown in figure 4.11.

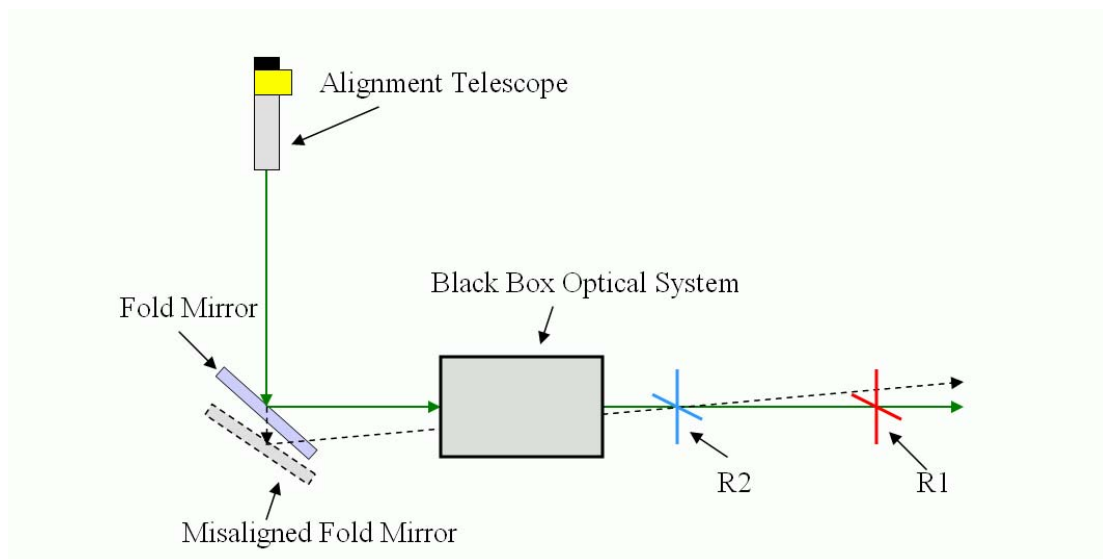


Figure 4.11. Fold mirror must be positioned to send bore sight through two reticles.

Figure 4.11 shows that an alignment telescope is to be used to accomplish this alignment and the telescope will be used to measure how much misalignment is in the system. Figure 4.11 shows that if the Fold Mirror is off in focus (dashed ray), the tip of the mirror can be adjusted so that the 1st Reticle is aligned but the 2nd is out of alignment making this an iterative alignment. The focus of the Fold mirror and the tip/tilt of the mirror must both be adjusted until both of the reticles are aligned according to the alignment telescope.

Not only is this alignment an iterative alignment, the fold mirror is to be adjusted with shims. The fold mirror will be mounted into a mirror cell and the shims will be placed behind three adjustment points on the cell and are labeled 1, 2, and 3 in figure 4.12. To make focus adjustments equal size shims will be placed at 1, 2, and 3. To make tilts about X equal sized shims will be added at 1 and 2 and an equal increment will be removed from 3. To make tilts about Y equal sized shims will be added at 2 and 3 and an equal increment will be removed from 1.

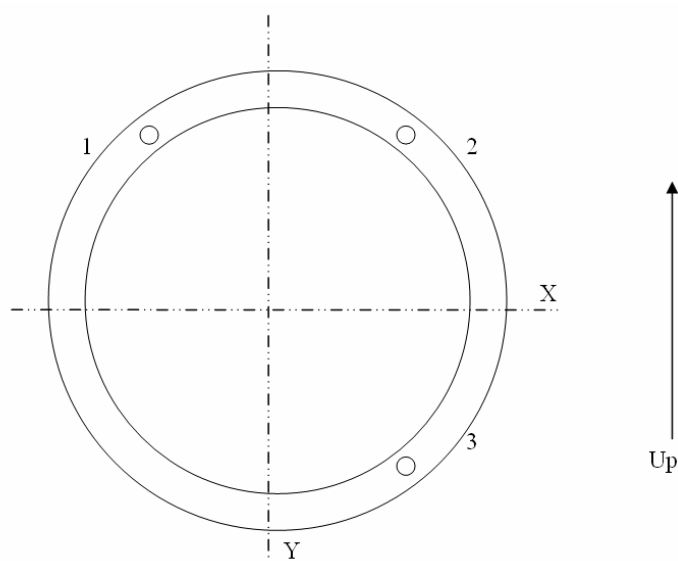


Figure 4.12. Fold Mirror Cell.

The first step in creating an adjustment matrix that can be used to align this fold mirror is to decide what adjustments are available and how they affect the system alignment. There are three obvious degrees of freedom and they are tilt about X, tilt about Y and focus on the Z axis. The tilt about the X and Y affects the ray angle in the x and y directions and the focus laterally shifts the exit ray in the X direction. The fold mirror

can not be adjusted to laterally shift the exit ray in the Y direction so R2 will be allowed to move in the Y direction to compensate for this lack of adjustment in the fold mirror.

Because an alignment telescope will be used to align the system, the telescope can also be used to measure the affects of the adjustments. Figure 4.13 shows the images of R1 and R2 in the alignment telescope and it shows the variables that can be measured.

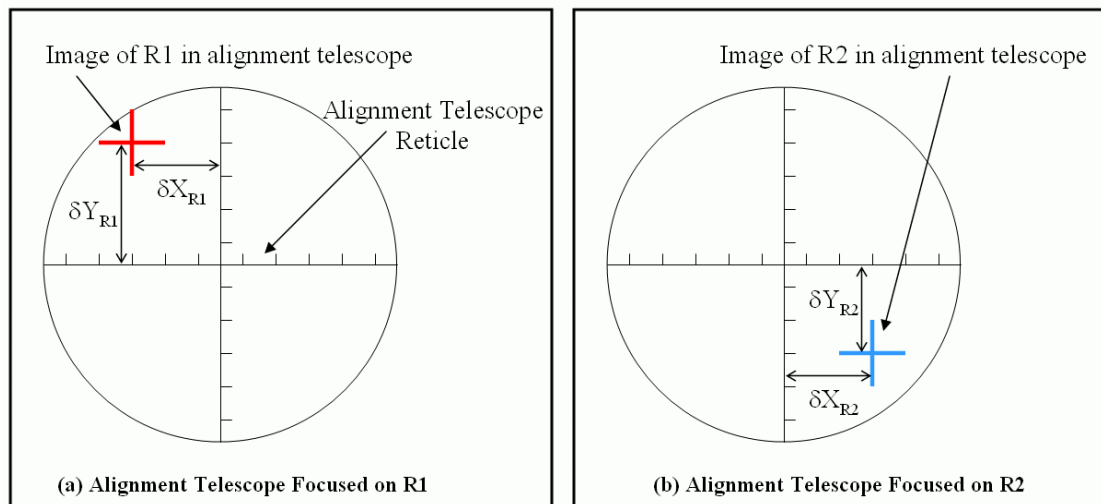


Figure 4.13. Images of R1 and R2 in alignment telescope

There have been 4 degrees of freedom identified and 4 measurements that can be made so now the adjustment matrix is ready to be built. The adjustment matrix will be 4 X 4 and is represented in the following formula:

$$\begin{bmatrix} \delta X_{R1} \\ \delta Y_{R1} \\ \delta X_{R2} \\ \delta Y_{R2} \end{bmatrix} = \begin{bmatrix} a11 & a12 & a13 & a14 \\ a21 & a22 & a23 & a24 \\ a31 & a32 & a33 & a34 \\ a41 & a42 & a43 & a44 \end{bmatrix} \begin{bmatrix} TiltX(rad) \\ TiltY(rad) \\ Focus(in) \\ R2_Y(in) \end{bmatrix} \quad (4.10)$$

To use equation 4.10, misalignments will be measured and then multiplied by the inverse of the adjustment matrix to find the desired adjustments necessary to align the system.

$$\begin{bmatrix} TiltX(rad) \\ TiltY(rad) \\ Focus(in) \\ R2_Y(in) \end{bmatrix} = \begin{bmatrix} a11 & a12 & a13 & a14 \\ a21 & a22 & a23 & a24 \\ a31 & a32 & a33 & a34 \\ a41 & a42 & a43 & a44 \end{bmatrix}^{-1} \begin{bmatrix} \delta X_{R1} \\ \delta Y_{R1} \\ \delta X_{R2} \\ \delta Y_{R2} \end{bmatrix} \quad (4.11)$$

Before equation 4.11 can be used to calculate the needed adjustments, the coefficients of the adjustment matrix must be found. These coefficients are found by perturbing the system by known amounts and recording the change of the positions of the reticles in the alignment telescope. For example if 0.00065” shims are used to tilt the fold mirror about the X axis then the shims affect on the system alignment is measured. δY_{R1} and δY_{R2} were measured to be -0.0296” and -0.0516” while δX_{R1} and δX_{R2} were measured to be 0.

Plugging the δ values into equation 4.10, the equation becomes:

$$\begin{bmatrix} 0 \\ -.0296 \\ 0 \\ -.0516 \end{bmatrix} = \begin{bmatrix} a11 & a12 & a13 & a14 \\ a21 & a22 & a23 & a24 \\ a31 & a32 & a33 & a34 \\ a41 & a42 & a43 & a44 \end{bmatrix} \begin{bmatrix} .00065 \\ 0 \\ 0 \\ 0 \end{bmatrix} \quad (4.12)$$

The coefficients a11, a21, a31, and a41 can be solved by using equation 4.12. They are found to be a11 = 0, a21 = -45.15, a31 = 0, and a41 = -78.87. The remaining coefficients of the adjustment matrix can be found by making known adjustments on the remaining degrees of freedom and measuring their impact. The completed adjustment matrix for

this example is shown in equation 4.13 and is written in the form so that it is useful to find how much adjustment is necessary to align the optical system.

$$\begin{bmatrix} TiltX(rad) \\ TiltY(rad) \\ Focus(in) \\ R2move \end{bmatrix} = \begin{bmatrix} 0 & 56.81 & 0 & 0 \\ -46.15 & 0 & -1.412 & 0 \\ 0 & 100 & 0 & 1 \\ -78.87 & 0 & -1.412 & 0 \end{bmatrix}^{-1} \begin{bmatrix} \delta X_{R1} \\ \delta Y_{R1} \\ \delta X_{R2} \\ \delta Y_{R2} \end{bmatrix} \quad (4.13)$$

Now that the adjustment matrix has been calculated, it is ready to predict how much each of the degrees of freedom will need to be adjusted in order to align the system. Simply measure the position of R1 and R2 in the alignment telescope to find the δ vector, then multiply the δ vector by the inverse of the adjustment matrix, and the result gives how much each degree of freedom must be adjusted to properly align the system.

This technique provides direction to an iterative alignment and computes the necessary adjustments that are needed to align an optical system. Many times an optical element that is to be aligned in a system is difficult to adjust, and minimizing the amount of adjustment iterations is critical in order to expedite the alignment process.

CHAPTER 5. CONCLUSION

5.1. Summary

The term “Laser Tracker” is a general term and could be used to describe many systems. The laser tracker that is the primary subject of this thesis is a metrology tool that incorporates optics, precision mechanics, servo systems, numerical computation, and computer control techniques to make precision 3D measurements.

In 1986, Kam Lau wrote a paper and filed US Patent number 4,714,339 that described what has been developed into the Laser Tracker system that is widely used today. Although many industries from Aerospace to Automotive have developed applications for this powerful tool, optical shop applications have not been extensively developed. A laser tracker combines data from a distance measuring interferometer with azimuth and elevation encoders to build a spherical coordinate. The tracker has a sophisticated servo system that allows the system to dynamically track a retroreflector through space. The data from the interferometer provides the radius portion of the spherical coordinate and the AZ and EL encoders provide the θ and ϕ portions of the coordinate. This system is housed in a portable unit allowing the system to be thought of a portable coordinate measuring machine that is capable of making both dynamic and static measurements. In

addition to being portable, the laser tracker system has an extremely long range of at least 35 meters. The laser tracker was initially developed to measure the dynamic performance of robots. Since 1985 many new applications have been developed for the tracker because of its extreme flexibility and high performance.

This thesis provides an extensive background section that investigates the theory of the laser tracker, error sources for the tracker, and current applications. An extensive list of references was built that describes the work that is currently being done with trackers and what improvements the different groups around the world are doing to improve its performance. This thesis builds upon the work presented in the background chapter by presenting an evaluation of the laser tracker for use in the optical shop. Many experiments were performed for the evaluation and these experiments are documented in this thesis. Finally, this thesis presents other optical testing and alignment techniques that have been developed but do not involve the laser tracker.

5.1.1. Evaluation of Laser Tracker as a tool for the Optical Shop

Many experiments were performed that evaluated the laser tracker's viability as a tool for the optical shop. The experiments that were performed evaluated the tracker's ability to measure the radius of curvature of a spherical surface, report the location of the center of curvature, track an image, and track the target through fold mirrors and diffraction gratings.

To test the tracker's ability to measure the radius of curvature of an optical element, the surface was profiled with the tracker and the results were compared to an interferometric autostigmatic test and the tracker was shown to perform remarkably well when measuring optics faster than R/2.0. Many variables were analyzed including the number of points required to define the surface, the location of the tracker with respect to the surface, and the R/# of the surface being measured. The only variable that had significant effects on the performance of the tracker was the R/# of the optic. As the speed of the optic is slowed down there is less sag in the surface and the tracker's performance is limited by its ability to measure sag. The sag error was found to be close to constant over all of the tests that were performed and this constant was used to develop a relationship between expected radius error and R/# of the optic being tested. For optics faster than R/2.0 the expected radius error was found to be better than 0.040 mm and for R/7.5 optics the expected error was found to be better than 0.50 mm.

The tracker was looked at as an alignment tool and to test the tracker's performance, the ability of the tracker to report a repeatable location of the center of curvature of an optic was measured. The same variables that were analyzed for the radius of curvature tests were analyzed for these tests and the results correlated well with the tracker's ability to measure radius of curvature. The same error vs. R/# relationships can be used to judge how well a tracker can report the location of the center of curvature. This series of tests highlighted the importance of a stiff mount when profiling a surface. When the tracker ball is placed on the surface, the surface can slightly move causing measurement error.

An Offner relay imaging system and the LSST telescope system were investigated as examples of systems that could potentially be aligned with the laser tracker. The performance of the tracker shows to be well within tolerance for most alignment tasks on these systems.

The tracker was also evaluated as a tool to track an image. An image is not a physical thing that the tracker ball can touch but the tracker ball can locate a camera or a detector that can detect the image. Image tracking is described and simulated in this thesis. To track an image a lateral effect position sensing detector (PSD) was employed to locate the image. The data from the PSD was combined with the data from the laser tracker by relating the two datasets to a common reference. The tracker's ability to change the coordinate system that it is measuring in is critical when combining the two data sets. The simulation of image tracking did not perform as well as expected only reporting the image location to within 0.030". There were many error sources and these sources were documented and image tracking should be expected to perform better with a more careful setup. Interface software for the PSD was built and the PSD was carefully characterized.

5.1.2. Other Testing and Alignment Techniques

This thesis also presents three optical testing and alignment techniques that are not related to the laser tracker. The resolution and sampling frequency capabilities of the PSD that was used in the image tracking section also enable this device to be used to measure line of sight image jitter. The interface software that was developed to track an

image was modified and configured to make both time and frequency domain image jitter measurements. The sampling frequency and the total time for the data set are set through the user interface panel and the software records a dataset from the PSD. Once the dataset is reported, the software outputs position information. The mean position and standard deviation for the datasets for each axis are reported. The software also does a frequency analysis and reports a power spectral density plot for each axis. Inputting known functions through the software and evaluating for expected results verified the software. Also, if the power spectral density curve is integrated, the answer should equal the standard deviation of the time domain data and these values are shown to match to within 2.2%.

This thesis also investigates a common problem when using an alignment telescope to align an optical system. When the reticles that are used to define an optical axis are imaged through the system to be aligned, the location of the images can be behind the alignment telescope and the telescope can not focus on these images. Placing a negative lens in front of the telescope can solve this problem, but the alignment of the optical axis of the telescope will no longer be aligned to the telescope. This thesis suggests a method of aligning this auxiliary lens to the telescope by using a simple adapter that rotates on the barrel of the alignment telescope. This adapter allows poor quality lenses with high wedge to be used as auxiliary lenses and their imperfections can be compensated for with decenter. Hardware was built and shown to only enter 15 seconds of alignment error when installed.

Finally, a technique of using an adjustment matrix is presented to expedite a difficult alignment. An example of using an alignment telescope to make an iterative alignment of a fold mirror is presented. This technique takes advantage of the linear nature of optical systems by measuring the effect of prescribed adjustments and using this information to build an adjustment matrix. This matrix can be used to predict the amount of adjustment necessary to put a system into alignment. This technique can be applied to other applications and is especially useful in difficult alignments that require an iterative alignment.

5.2. Future Work

The work that has been shown in this thesis shows that a laser tracker could be a potentially powerful tool in the optical shop. Only limited time was available on the tracker and more time and experience with this tool will open new doors for applications. Because of its versatility it is very common for shops that own these tools to find and develop new applications that they had not thought of when they first procured the system.

Spherical surfaces were concentrated on for the work in this thesis, more work needs to be done to investigate how the tracker performs with aspherical surfaces. Also, the relationships between R/# and expected error need to be investigated further by evaluating larger diameter optics to see if the relations scale. If so, the tracker could be

an invaluable tool that could measure the large-scale 8 meter mirrors that are currently being produced. Other studies could also be performed with the tracker that would investigate only using part of a surface to define the shape. This would enable the tracker to test annular mirrors or reduce risk of damaging an optical surface by allowing a surface to be profiled by staying outside of the clear aperture of the element.

The tracker's profiling features were investigated in this thesis but the information used to locate the center of curvature could be used to create a contour map of a surface. A contour map would be useful in the early stages of fabrication of a mirror where the surface quality is not good enough for interferometry.

The tracker has been shown to be a powerful alignment and image tracking tool. Well-defined techniques need to be developed for specific applications. For example the LSST system was given a top level analysis and the analysis shows that the tracker could meet most of the alignment requirements. A more detailed analysis on this system would be warranted.

Finally, some work was done that quantified how the tracker performed when tracking through optical elements such as diffraction gratings and fold mirrors. Using the tracker through optical systems has many potential applications such as testing total path length, field of view, or magnification.

APPENDIX A: PSD INTERFACE USER GUIDE AND SOFTWARE CODE

This appendix provides a users guide to the PSD interface software that was developed. The user's guide is intended to provide a reference to the many features that have been built into the PSD interface software. The PSD interface software was referenced in the PSD characterization section under Image Tracking in Chapter 3. This software is a general interface and could be used for applications other than image tracking as suggested in Chapter 3. This appendix also details the source code that was developed in LabVIEW.

A.1. PSD Software User's Guide

Figure A.1 shows a detailed view of the PSD interface that was developed in LabVIEW. The interface gives an X/Y position of the spot on the detector. The data on this plot can be zoomed in on to get a better view of how the spot is moving on the detector. The plot labeled measurement data shows the history of where the spot has been. In the example shown in Figure A.1, the X/Y positions had been recently adjusted; this is evident in the stair step plot that shows in the Measurement Data Plot. The interface includes many other features; each feature is given a separate brown box. Calibration Coefficients can be modified, 0.00787 in/V is the default value. Units can be changed from inches, mm, or Volts if only the Voltage from the PSD is desired. Whichever unit that is active will light up a green LED. Also, the average position can be recorded by clicking the "Get Average" button. A maximum of 10,000 data points will be read at approximately 1 kHz and the average X and Y position will be displayed. These average positions can be logged to a text file by clicking the "Log Average" button. Continuous data can also be logged to a text file by sliding the Continuous log switch. X and Y data will be sent to the text file at what ever increment the sampling rate is set at. The final feature of the Interface is the Calibration Offset switch. This switch allows the user to find the average

position of the spot on the detector, subtract these values from the actual position, and create a virtual zero point. This feature is useful for repeatability or frame of reference type measurements.

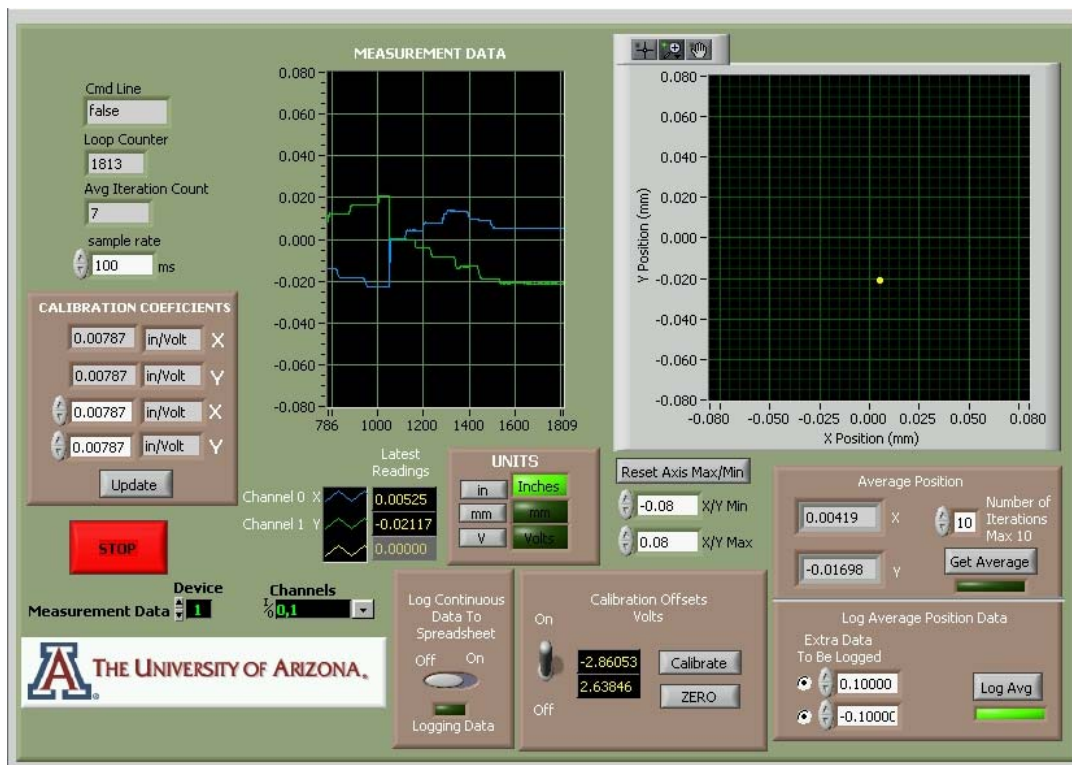


Figure A.1 PSD Software Interface Panel

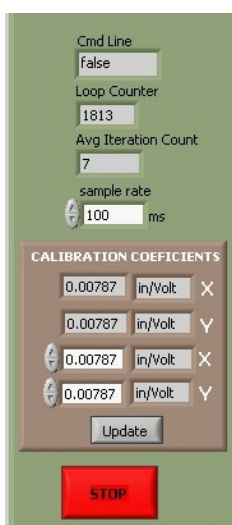


Figure A.2 Right Side Box

The right hand side of the interface will first be discussed and a close up view is shown in Figure A.2. To stop taking measurements from the PSD, simply click the red “STOP” button located near the bottom of the interface. The boxes that are grayed out are information boxes that can not be adjusted and only provide information. The Cmd Line box contains no useful information, it just displays the command that the software is currently running. The loop counter displays how many measurements have been taken from the PSD and the “Avg Iteration Count” says how many iterations have passed to create an average

position. Adjusting the sample rate gives the user the opportunity to adjust how much time is in between data points. The calibration coefficients box allows for the calibration coefficients to be updated depending on what area of the detector is being used. The gray boxes show what the coefficients currently are. To update them type the new value in the white box and click update. The gray boxes should update to the value that was entered.

The next part of the software interface that will be discussed will be the graphics windows. Two main graphics show up on the interface one provides real time information and the other provides historical information. The graphic on the far right of the screen provides a real time X-Y position of the spot on the detector and the yellow dot indicates where the spot is. Clicking the crosshair above the graph can allow the spot to be zoomed in on. To reset the axes, simply click the “Reset Axis Max/Min” button located below the graph. The measurement data graphic shows a historical plot of the position, the Y axis is the position and the X axis is the loop number.

One of the most useful features of the software is the Average Position box and this box is shown in Figure A.3. A maximum of 10,000 datapoints can be used to calculate the average and these datapoints are retrieved at approximately 1 kHz. Each time the get average button is clicked then the X and Y axis are measured and the green LED is lit when the data is being taken. The average data can also be logged to a spreadsheet. Click the “Log Avg” button and an average will be calculated and then pop up a dialog box asking you to name the file the average will be logged to will pop up. Each time the “Log Avg” button is clicked after

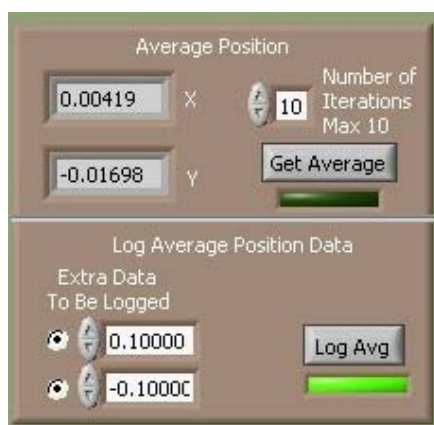


Figure A.3. Average Position Box

this, the data is logged on the next line of the file and the file name is not reentered. To create a new file, the “STOP” button should be clicked and then the software restarted. After restart, the next time the “Log Avg” button is clicked a new file will be created. Extra data can also be logged along with the X Y data. Just click the radio button and enter any number data that needs to be logged and this information will be logged along with the Average data.

The next box that will be discussed is the “Calibration Offsets” box and this box is shown in Figure A.4. This box allows the PSD to be zeroed at points other than the origin. This feature is useful when making relative measurements. To reset the origin click the



“Calibrate” button and the software will find the average position and calculate the offsets. When the On/Off switch is flipped to on, then the offsets are subtracted from the actual position causing all data to be reported with respect to the new location. The “Zero” button resets the offsets to zero.


Figure A.4. Calibration Offsets Box

Other features of the software include Latest Readings, Units, and Log Continuous Data. The Latest Readings reports the voltages from the PSD with the offsets subtracted in the offsets are turned on. The Units allow for the reported units to be inches, mm, or V. When “Volts” is selected, the calibration coefficients are set to 1 and data is taken directly from the PSD. When units are changed, the scales on the graphics should change. The last feature is the Log Continuous Data. This feature allows the X Y position data to continuously be logged to a text file. The data will be logged at whatever the sample rate is set to. When logging the green LED will light up indicating that the data is being logged.


A.2. PSD Interface Source Code

The following pages show the source code that was generated in LabVIEW that interfaced with the PSD.

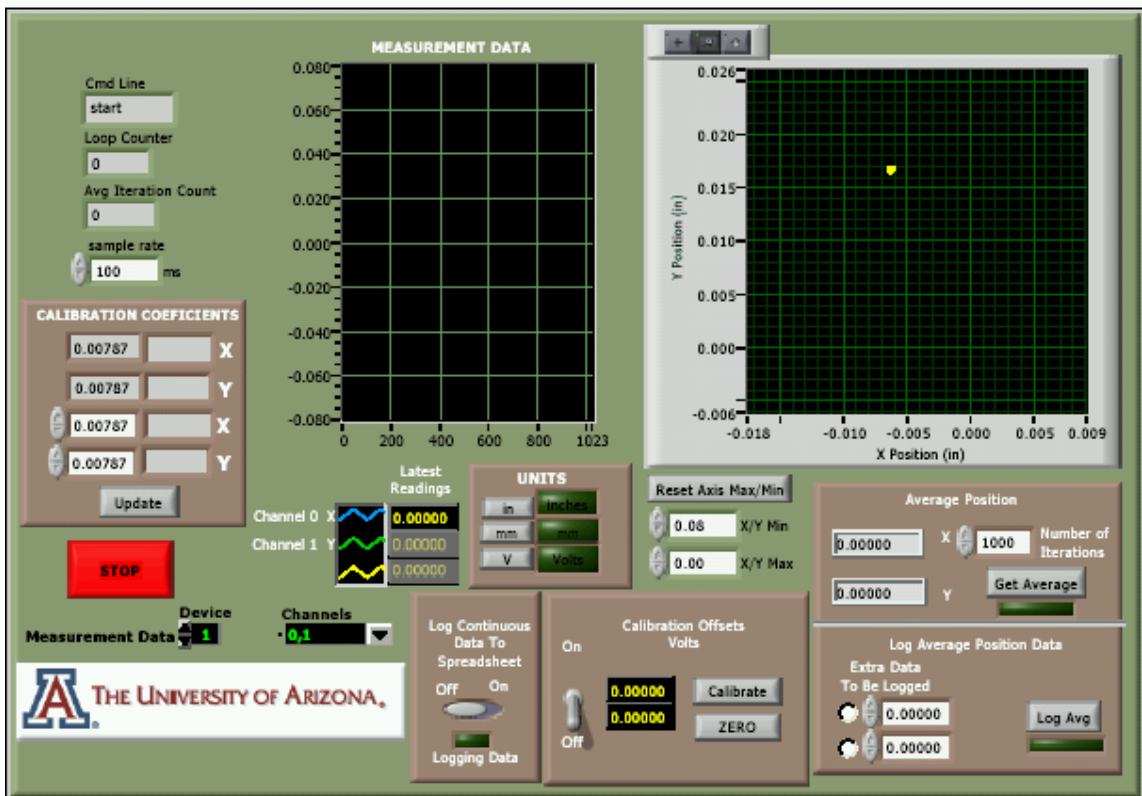
PSD_general1.vi
 C:\Program Files\National Instruments\LabVIEW 6.1\my stuff\PSD_general1.vi
 Last modified on 7/3/2003 at 10:14 AM
 Printed on 11/14/2003 at 4:35 PM

Page 1 

Connector Pane


 PSD_general1.vi

Front Panel



Cmd Line
 start

Loop Counter
 0

Avg Iteration Count
 0

sample rate
 100 ms

CALIBRATION COEFFICIENTS

0.00787 X
 0.00787 Y
 0.00787 X
 0.00787 Y

Update

STOP

Device
 1

Channels
 0,1

Measurement Data

MEASUREMENT DATA

Y Position (in)
 X Position (in)

Latest Readings
 Channel 0 X: 0.00000
 Channel 1 Y: 0.00000

UNITS
 in Inches
 mm mm
 V Volts

Reset Axis Max/Min
 0.08 X/Y Min
 0.00 X/Y Max

Average Position
 0.00000 X
 1000 Number of Iterations
 0.00000 Y
 Get Average

Log Average Position Data
 Extra Data To Be Logged
 0.00000
 0.00000
 Log Avg

Log Continuous Data To Spreadsheet
 Off On

Calibration Offsets Volts
 On
 0.00000
 0.00000
 Calibrate
 ZERO
 Off

Logging Data
 On

THE UNIVERSITY OF ARIZONA

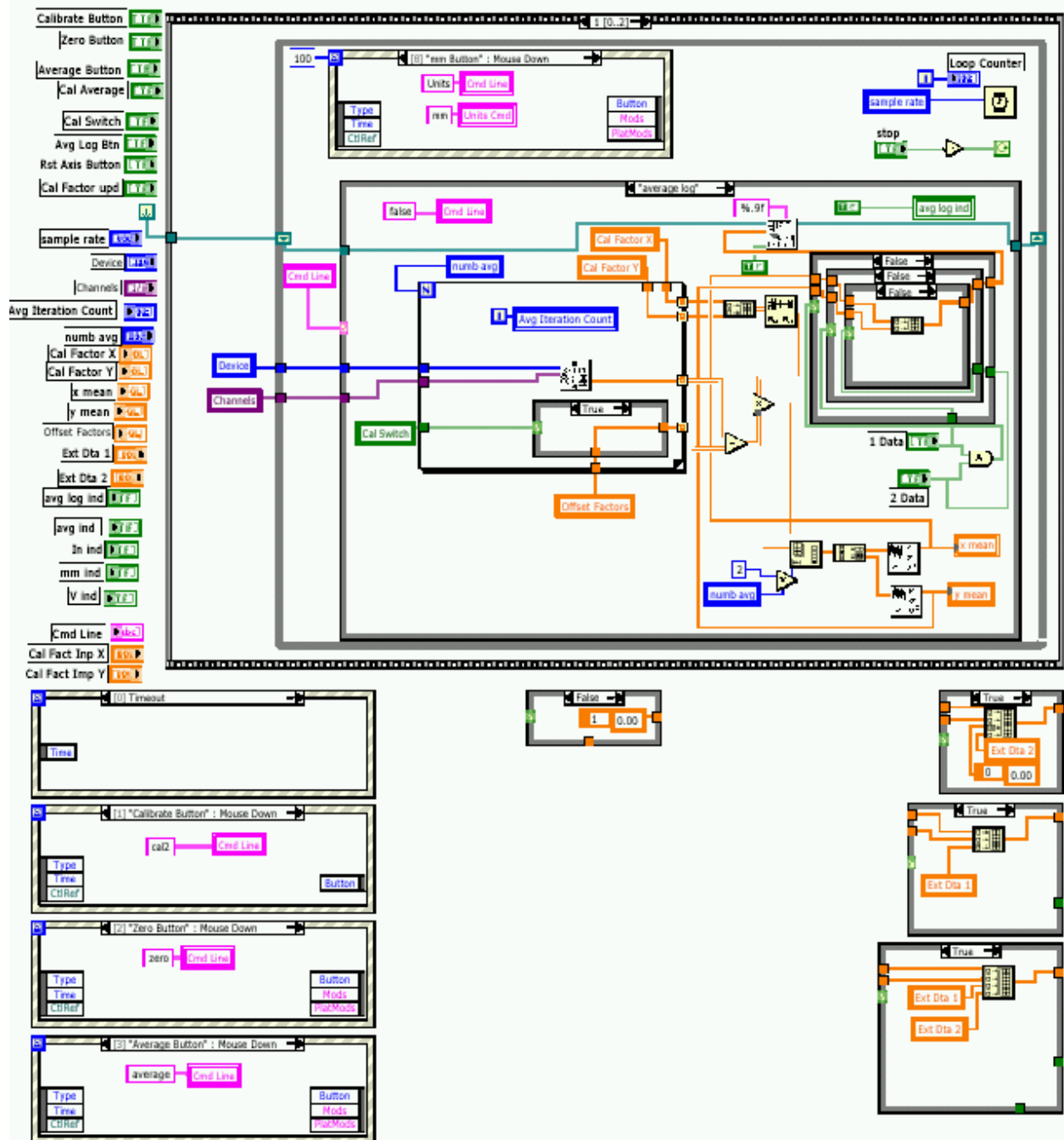
PSD_general1.vi

C:\Program Files\National Instruments\LabVIEW 6.1\my stuff\PSD general1.vi

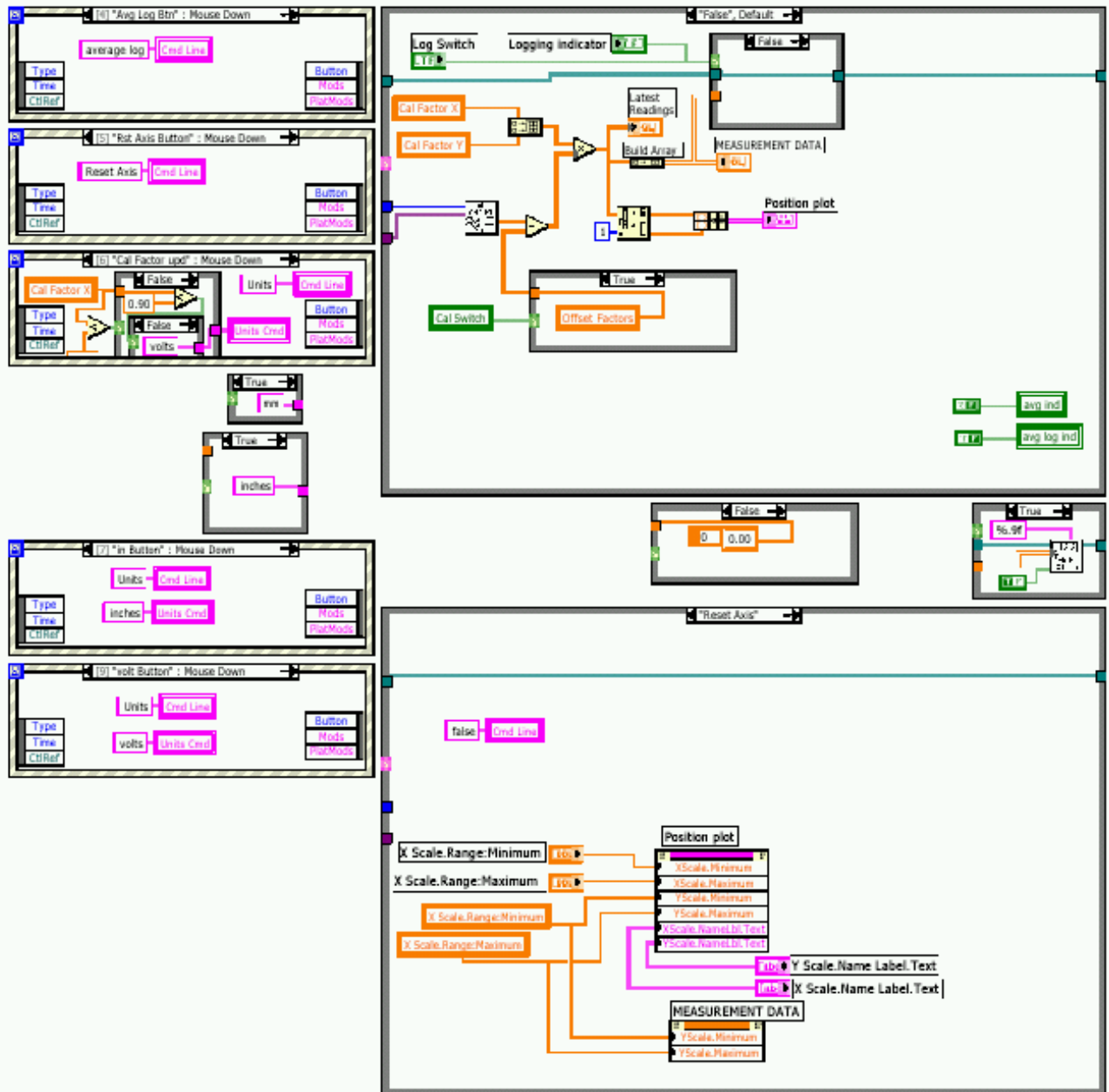
Last modified on 7/3/2003 at 10:14 AM

Printed on 11/14/2003 at 4:35 PM

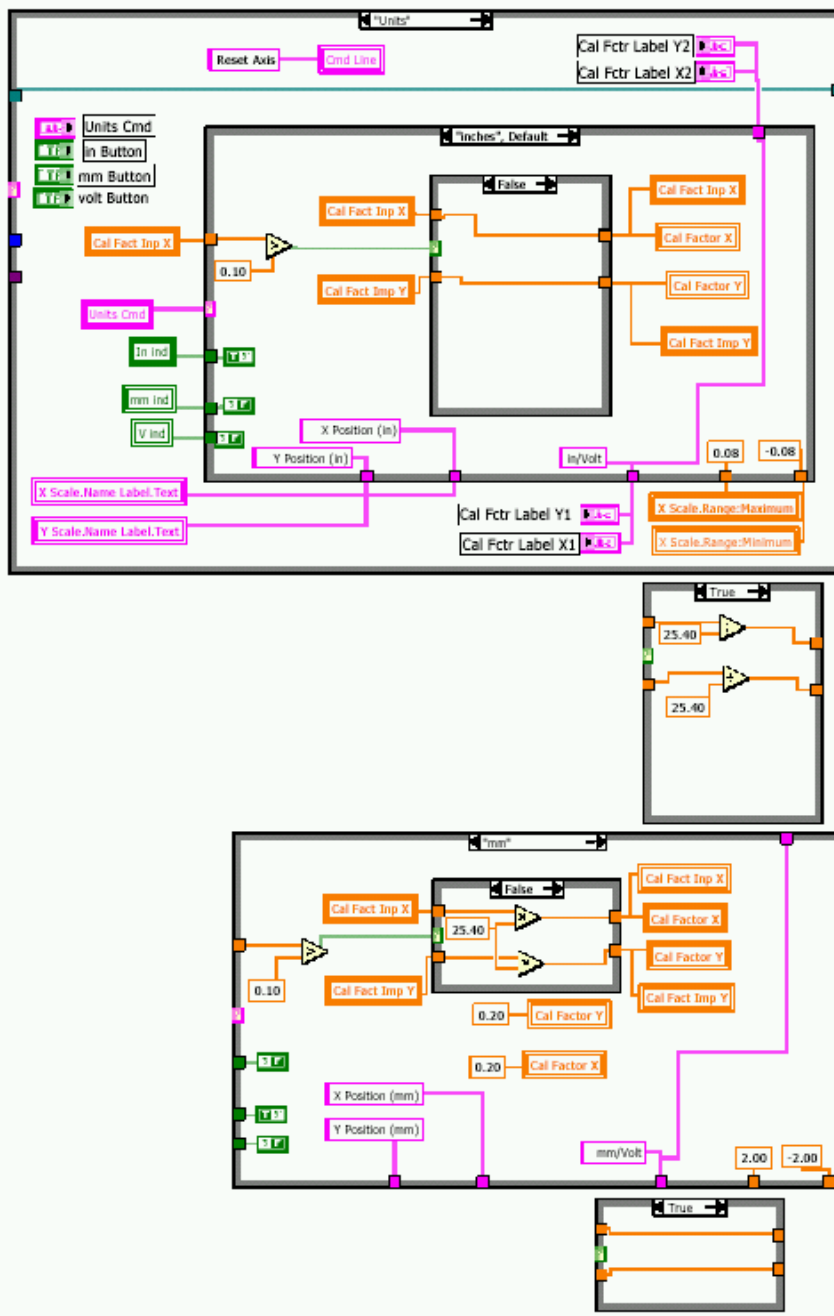
Block Diagram



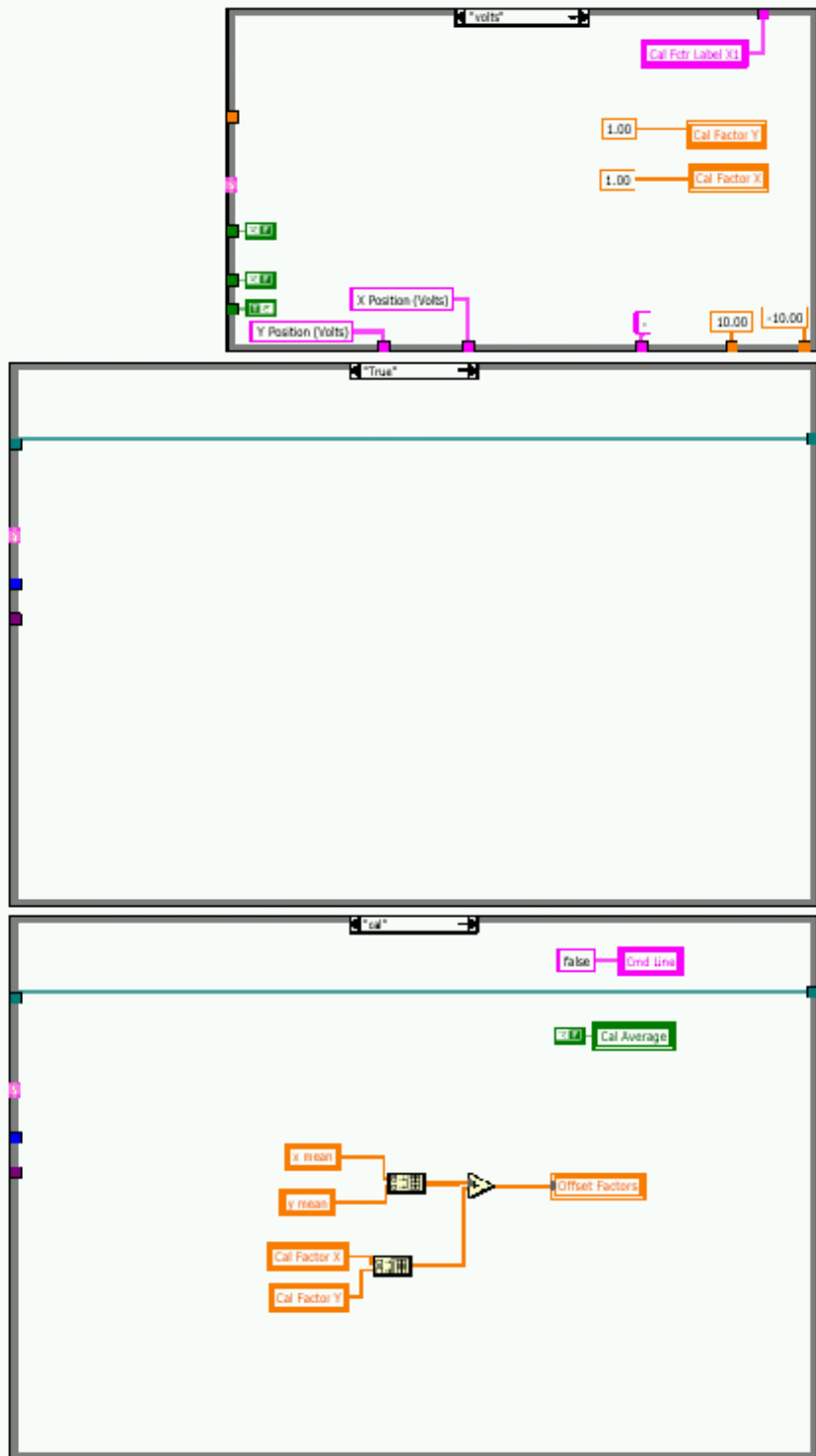
PSD_general1.vi
C:\Program Files\National Instruments\LabVIEW 6.1\my stuff\PSD general1.vi
Last modified on 7/3/2003 at 10:14 AM
Printed on 11/14/2003 at 4:35 PM



PSD_general1.vi
 C:\Program Files\National Instruments\LabVIEW 6.1\my stuff\PSD_general1.vi
 Last modified on 7/3/2003 at 10:14 AM
 Printed on 11/14/2003 at 4:35 PM



PSD_general1.vi
C:\Program Files\National Instruments\LabVIEW 6.1\my stuff\PSD general1.vi
Last modified on 7/3/2003 at 10:14 AM
Printed on 11/14/2003 at 4:35 PM



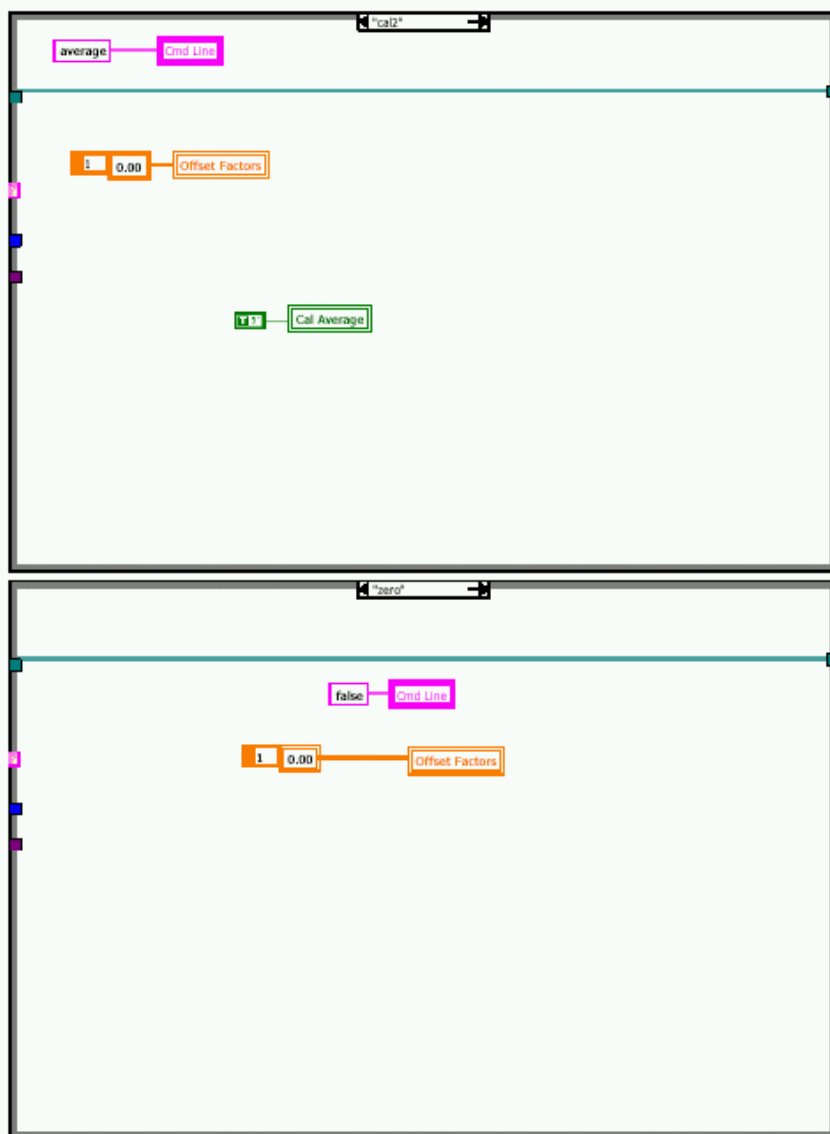
PSD_general1.vi

C:\Program Files\National Instruments\LabVIEW 6.1\my stuff\PSD_general1.vi

Last modified on 7/3/2003 at 10:14 AM

Printed on 11/14/2003 at 4:35 PM

Page 6

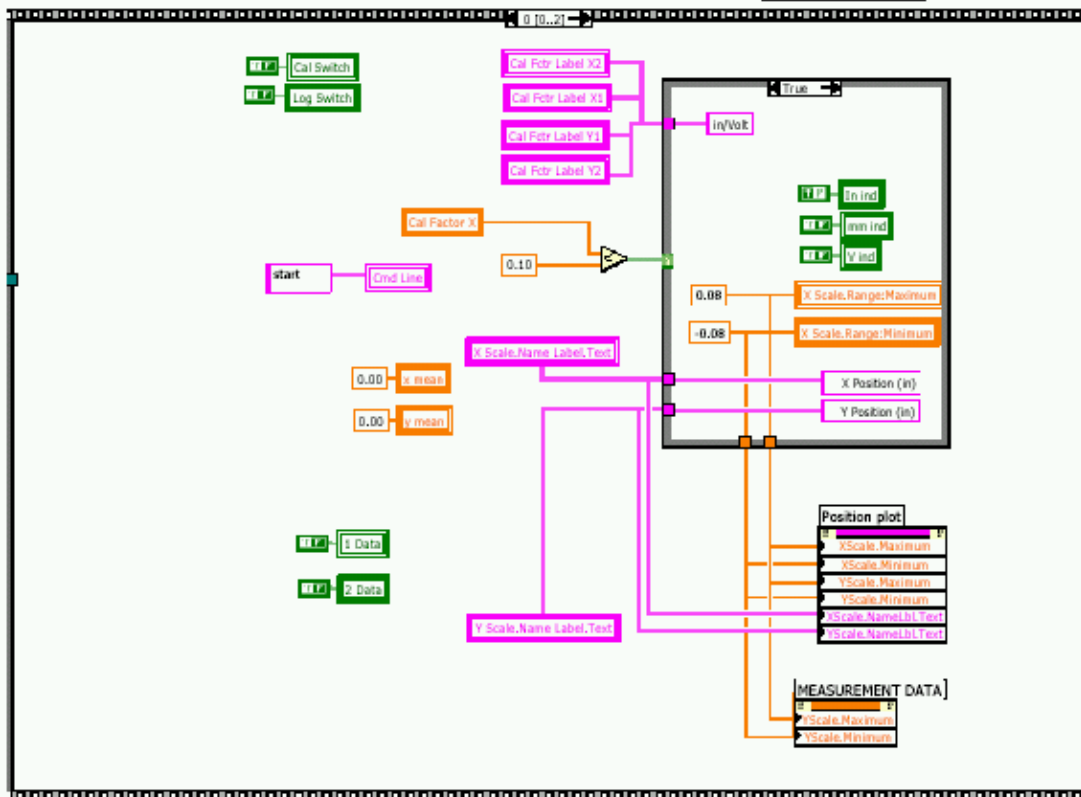
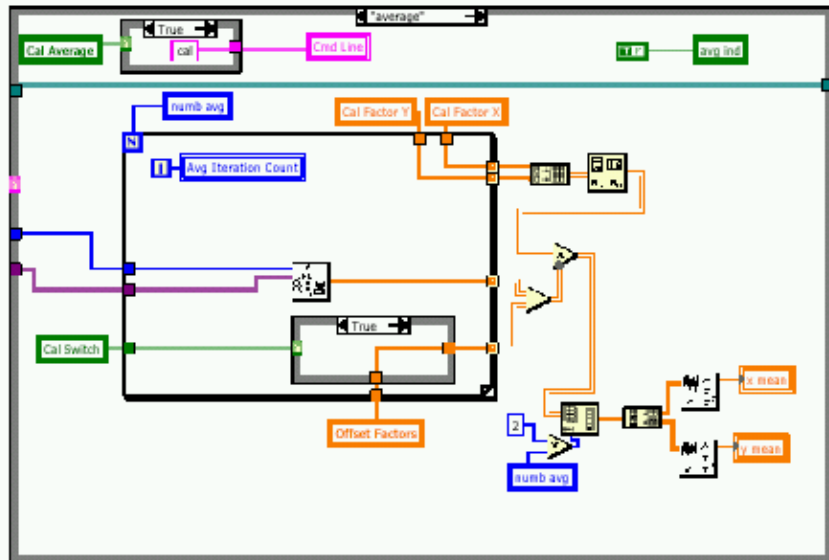


PSD_general1.vi

C:\Program Files\National Instruments\LabVIEW 6.1\my stuff\PSD_general1.vi

Last modified on 7/3/2003 at 10:14 AM

Printed on 11/14/2003 at 4:35 PM



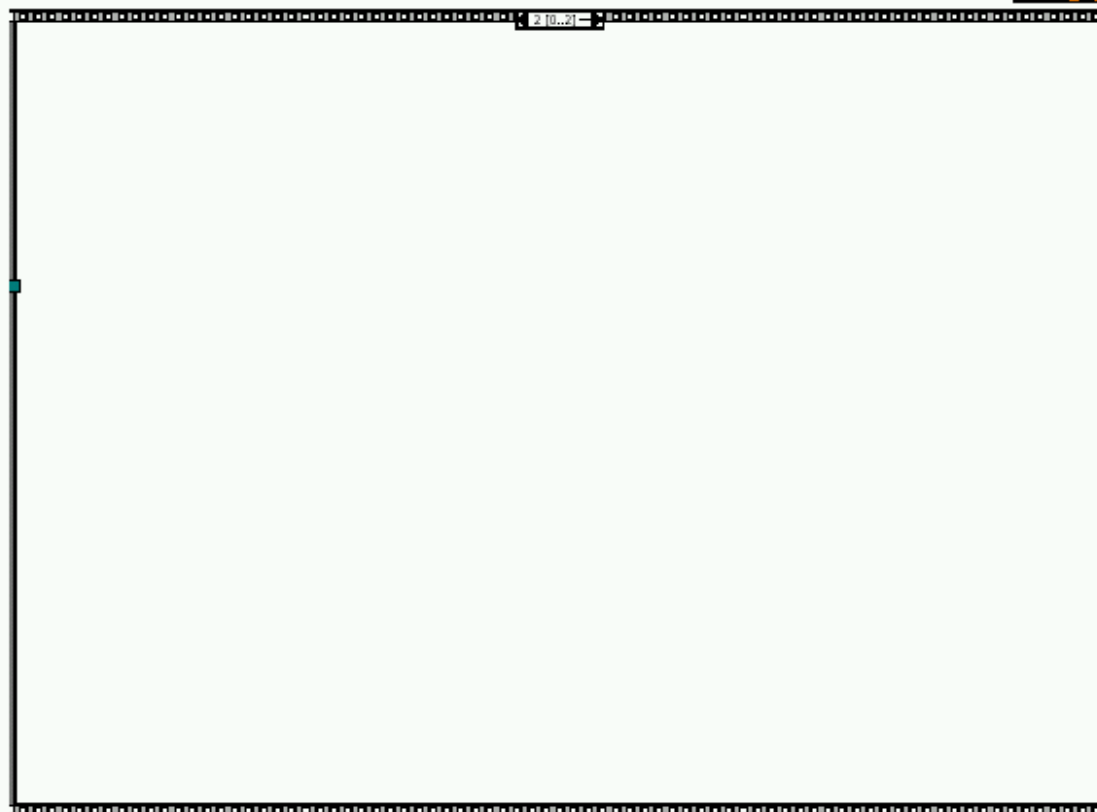
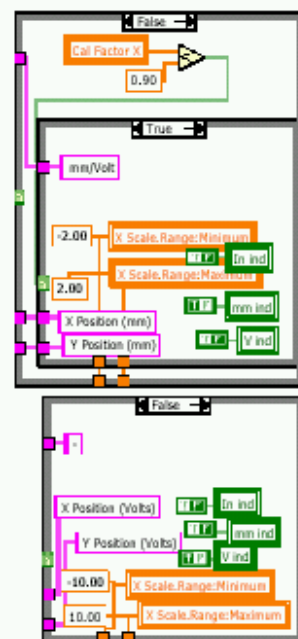


PSD_general1.vi

C:\Program Files\National Instruments\LabVIEW 6.1\my stuff\PSD general1.vi

Last modified on 7/3/2003 at 10:14 AM

Printed on 11/14/2003 at 4:35 PM



APPENDIX B: Hardware Drawings

This Appendix contains the actual hardware drawings that were generated to make the brackets referenced in Chapter 3 and Chapter 4.

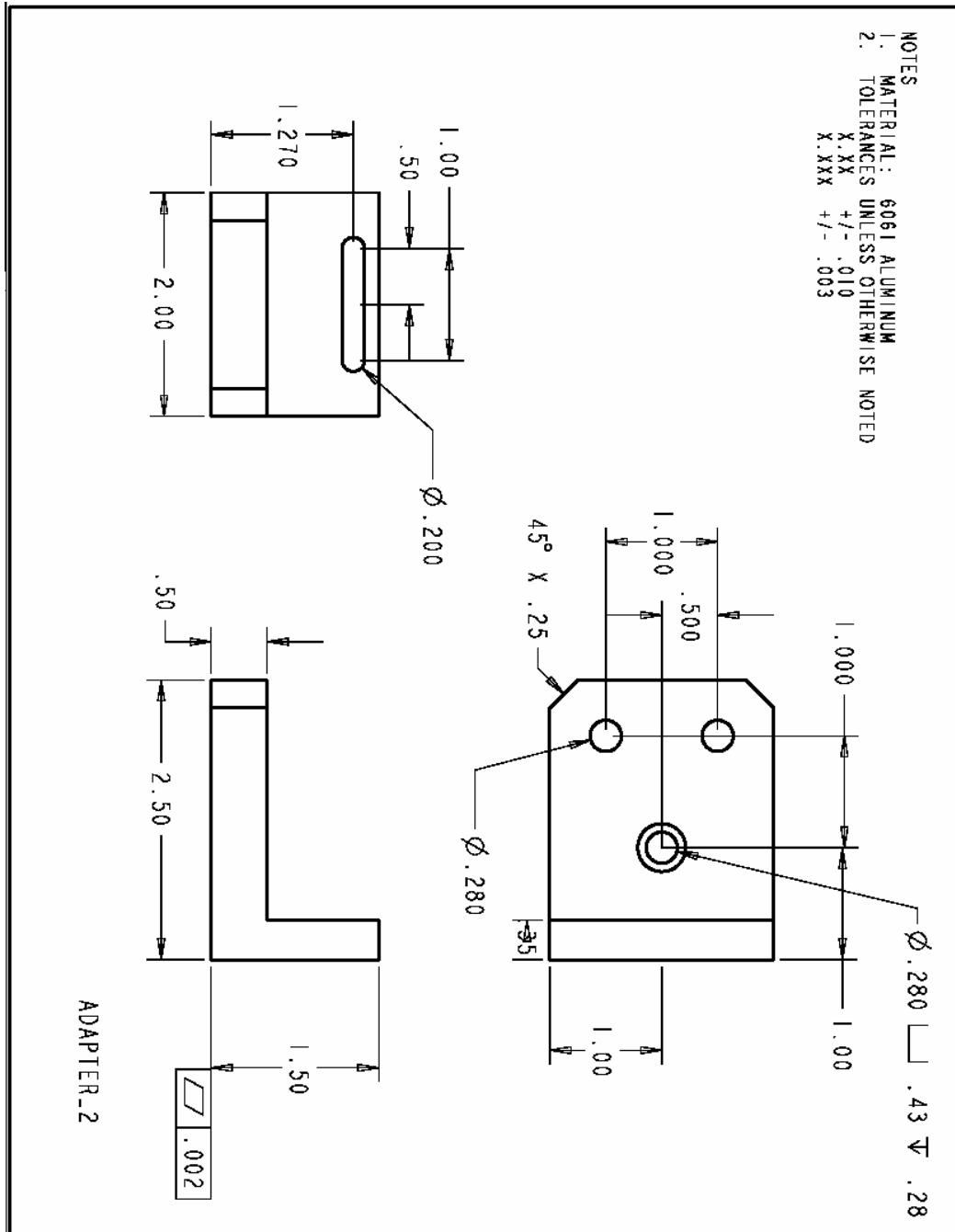


Figure B.1. L-Bracket to Hold PSD (Referenced 3.4.2.1)

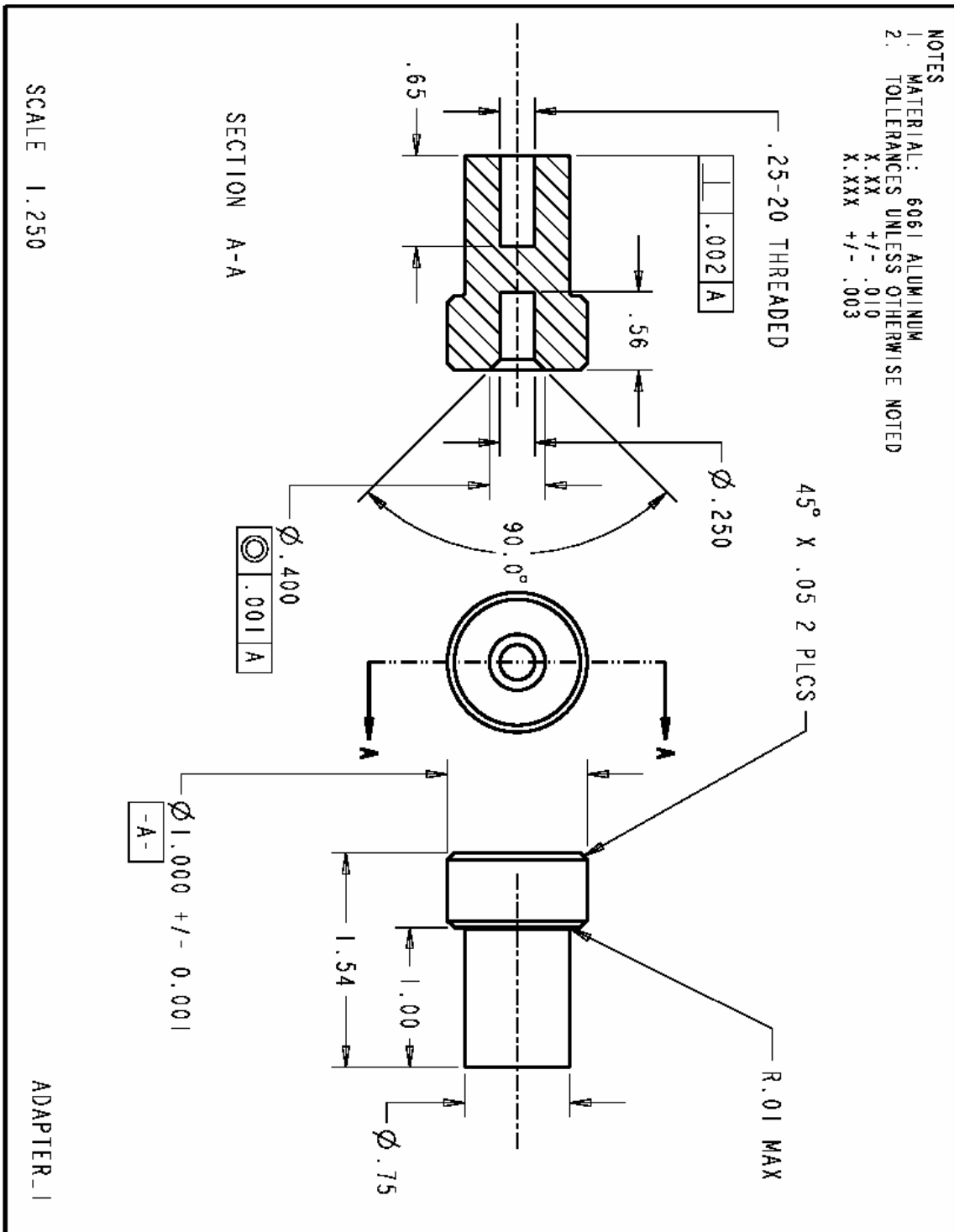


Figure B.2. Post to Hold Tracker Ball (Referenced 3.4.2.1)

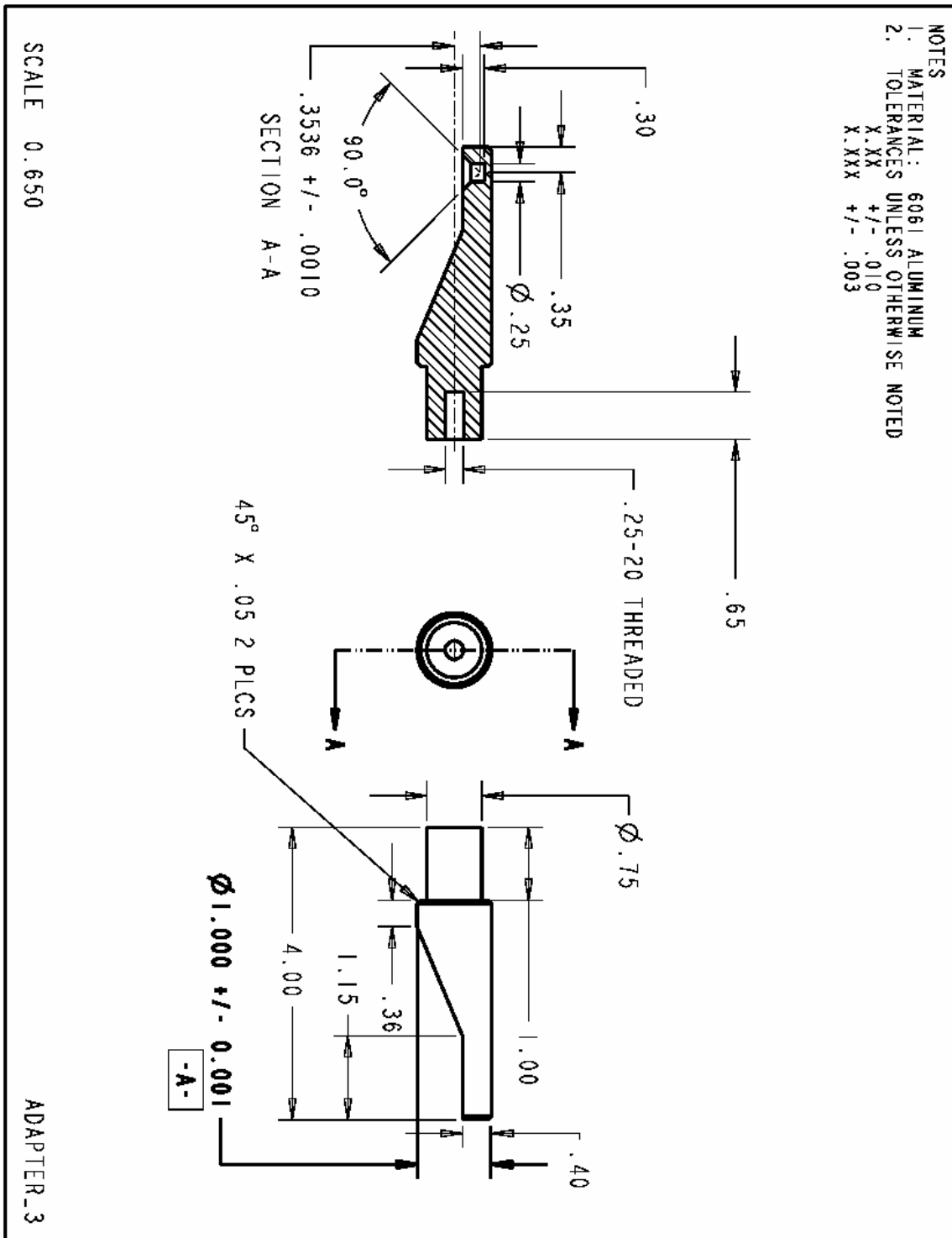


Figure B.3. Alternate Post to Hold Tracker Ball(Referenced 3.4.2.1)

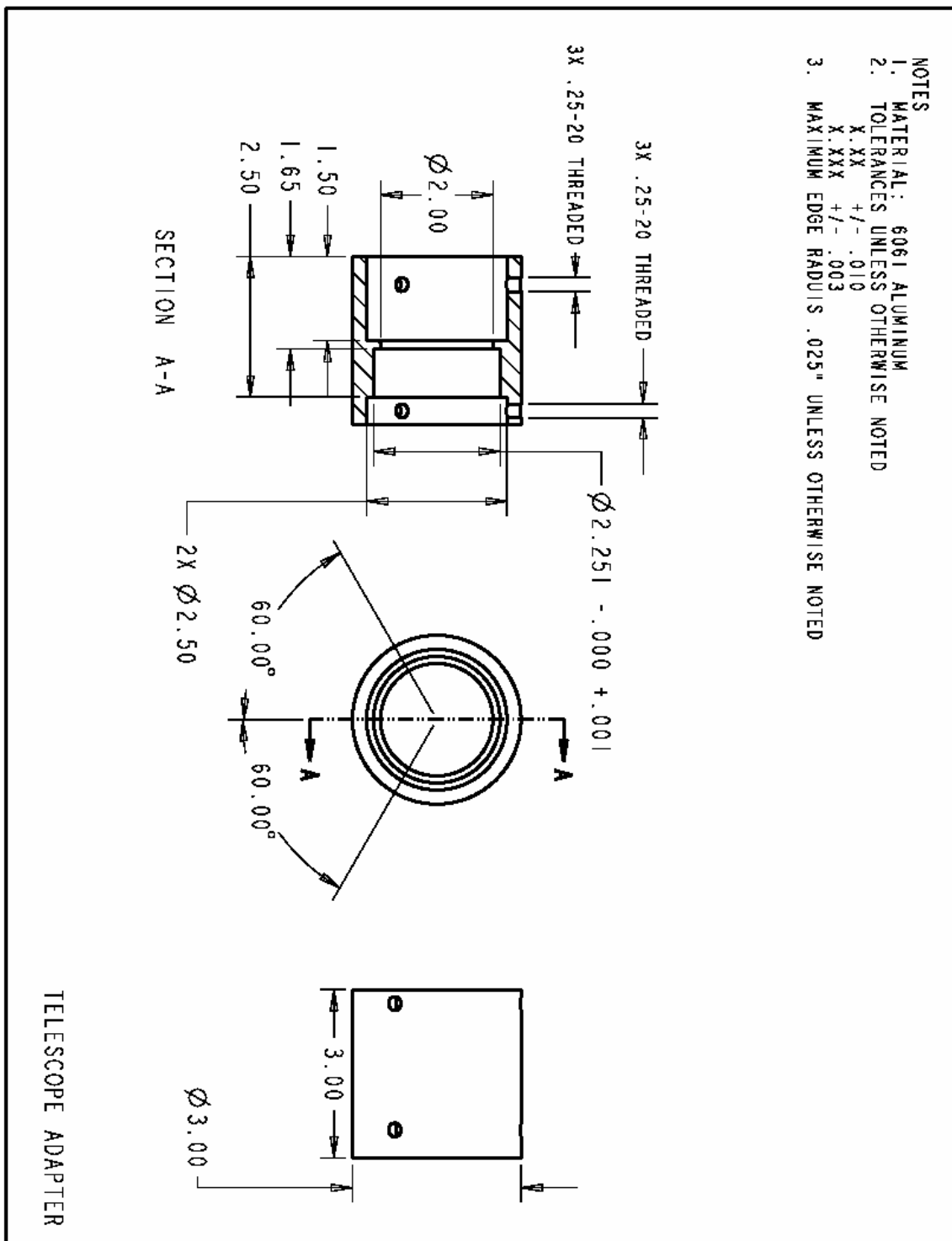


Figure B.4. Adapter to Mount Auxiliary Lens to Alignment Telescope (Referenced 4.2.3)

REFERENCES

1. K. Harding, "Application issues when using optical 3D systems in place of CMMs," in *Machine Vision and Three-Dimensional Imaging Systems for Inspection and Metrology II*, Kevin Harding, Ed., 2002, vol. 4567 of *Proceedings of SPIE*, pp. 1-10.
2. F. Chan, G. M. Brown, and M. Song, "Overview of three-dimensional shape measurement using optical methods," *Optical Engineering*, Vol. 39, no. 1, pp. 10-22, 2000.
3. F. Blais, "Review of 20 years of range sensor development," in *Videometrics VII*, S. F. El-Hakim, A. Gruen, and J. S. Walton, Eds., Vol. 5013 of *Proceedings of SPIE*, 2003, pp. 62-76.
4. D. L. Patrick, "Sandia National Labs' precision laser tracking systems," in *22nd International Congress on High-Speed Photography and Photonics*, Dennis L. Paisley, Ed., Vol. 2869 of *Proceedings of SPIE*, 1997, pp. 822-826.
5. D. L. Patrick, "Laser Tracker II: Sandia National Laboratories second-generation laser tracking system," in *Acquisition, Tracking, and Pointing V*, M. K. Masten and L. A. Stockum, Eds., Vol. 1482 of *Proceedings of SPIE*, 1991, pp. 61-68.
6. A. H. Greenleaf, "Self-calibrating surface measuring machine," *Optical Engineering*, vol. 22, no. 2, 1983, pp. 276-280
7. A. H. Greenleaf, "Computer-controlled optical surfacing," in *Active Optical Devices and Applications*, W. J. Cuneo, Jr., ed., Vol. 228 of *Proceedings of the Society of Photo-Optical Instrumentation Engineers*, 1980, pp. 41-54.
8. V. L. Krabbendam, G. P. Ruthven, V. P. Bennett, J. P. Blackburn, C. D. Cox, C. S. Keung, T. A. Facey, M. E. Furber, C. Neufeld, R. A. Rockwell, A. M. Sarnik, J. T. Stein, "Active optical system design for the 4.2-m SOAR telescope," in *Optical Design, Materials, Fabrication, and Maintenance*, P. Dierickx, ed., Vol. 4003 of *Proceedings of SPIE*, 2000, pp. 122-135.
9. K. Lau, R.J Hocken, and W.C. Haight, "Automatic laser tracking interferometer system for robot metrology," *Precision Engineering*, Vol. 8, no. 1, pp. 3-8, 1986.
10. K. C. Lau and R. J. Hocken, *Three and Five Axis Laser Tracking Systems*, United States Patent 4,714,339, granted December 22, 1987.
11. J. P. Prenninger, K. M. Filz, M. Incze, and H. Gander, "Real-time contactless measurement of robot pose in six degrees of freedom," *Measurement*, Vol. 14, pp. 255-264, 1995
12. J.H. Gilby, "Laser Tracker to Measure Robot," *Sensor Review*, Vol. 10, 1982, pp. 180-184.
13. T. Takatsuji, M. Goto, T. Kurosawa, Y. Tanimura, and Y. Koseki, "The first measurement of a three dimensional coordinate by use of a laser tracking interferometer system based on trilateration," *Meas. Sci. Technol.* 9, pp. 38-41, 1998.

-
14. E. B. Hughes, A. Wilson, and G. N. Peggs, "Design of a high-accuracy CMM based on multi-lateration techniques," *Annals of CIRP*, 2000, pp. 391-396.
 15. S. Osawa, T. Takatsuji, J. Hong, H. Noguchi, and T. Kurosawa, "Evaluation of the performance of a novel laser tracker used for coordinate measurements," in *Recent Developments in Traceable Dimensional Measurements*, J. Decker and N. Brown Eds., 2001, Vol. 4401 *Proceedings of SPIE*, pp. 127-135
 16. J. Wang, Z. Hu, Y. Liu, and J. Liang, "Experimental research on laser tracking system with galvanometer scanner for measuring spatial coordinates of moving target," in *Optical Measurement and Nondestructive Testing*, F. Song, Ed., 2000, Vol. 4221 of *Proceedings of SPIE*, pp. 10-14.
 17. Y. Liu, J. Wang, and J. Liang, "Length-measured method for virtual coordinate measurement by laser tracking system," in *Optical Manufacturing and Testing*, H. P. Stahl, Ed., Vol. 3782 of *Proceedings of SPIE*, pp. 567-575.
 18. Z. Hu, J. Wang, Y. Liu, and J. Liang, "Position and attitude measurement of moving target using laser tracking system with multiple measuring stations," in *Process Control and Inspection for Industry*, S. Zhang and W. Gao, Eds., 2000, Vol. 4222 of *Proceedings of SPIE*, pp. 66-70.
 19. S. A. Kyle, "Dimensional reference for robot calibration," in *Optical 3D Measurement Techniques II: Applications in Inspection, Quality Control, and Robotics*, A. Gruen and H. Kahmen, Eds., Vol. 2252 of *Proceedings of SPIE*, 1994, pp. 606-613.
 20. www.leica.com
 21. B. Elden, "The Refractive Index of Air," *Metrologia*, Vol. 2, No. 2, 1966, pp. 12-80.
 22. S. Sandwith, "Thermal Stability of Laser Tracking Interferometer Calibration," in *Three Dimensional Imaging, Optical Metrology, and Inspection V*, Vol. 3835 of *Proceedings of SPIE*, 1999, pp. 93-103.
 23. L. Fialovszky, "Surveying Instruments and their Operational Principles," Elsevier, Amsterdam, 1991.
 24. F. A. Redmond, "Tacheometry," The Technical Press Limited, London, 1951.
 25. H. Jiang, S. Osawa, T. Takatsuji, H. Noguchi, and T. Kurosawa, "High-performance laser tracker using an articulating mirror for the calibration of coordinate measuring machine," *Optical Engineering*, vol. 41, no. 3, pp. 632-637, 2002
 26. M. C. Berg, D. B. Rathburn, and K. W. Buffinton, "Precise control of the position of the end-effector of an industrial robot," *Proceedings of the ISCI/ASME Japan-USA Symposium on Flexible Automation*, 2002.
 27. M. C. Berg, D. B. Rathburn, and K. W. Buffinton, "Pulse width control of the position of the end-effector of an industrial robot," *Proceedings of the IFAC Conference on Mechatronic Systems*, 2002.

-
28. D. C. McCarthy, "Laser tracker stays on track," in *Photonics Spectra*, June 1999.
 29. W. Otto, A. Matthes, and H. Schiehle, "Measuring large aspherics using a commercially available 3D-coordinate measuring machine," in *Optical Design, Materials, Fabrication, and Maintenance*, P. Dierickx, Ed., Vol. 4003 of *Proceedings of SPIE*, 2000, pp. 91-97.
 30. www.zeiss.com/imt
 31. B. Jones, "JSF Designed with Joint Effort," *Quality Magazine*, June 2003.
 32. F. Blais, J. -A. Beraldin, S. F. El-Hakim, and L. Cournoyer, "Comparison of pose estimation methods of a 3D laser tracking system using triangulation and photogrammetry techniques," in *Videometrics and Optical Methods for 3D Shape Measurement*, Vol. 4309 of *Proceedings of SPIE*, 2000, pp. 185-194.
 33. J. -A. Beraldin, F. Blais, M. Rioux, L. Cournoyer, D. Laurin, and S. G. MacLean, "Eye-safe digital 3-D sensing for space applications," *Optical Engineering*, Vol. 39, no. 1, pp. 196-211, 2000.
 34. F. Blais, J. -A. Beraldin, S. F. El-Hakim, "Range Error Analysis of an Integrated Time of Flight, Triangulation, and Photogrammetric 3D Laser Scanning System", in *Laser Radar Technology and Applications V*, G. W. Kamerman, U. N. Singh, C. Werner, V. Molebny, Eds., Vol. 4035 of *Proceedings of SPIE*, 2000, pp. 236-247.
 35. www.axila.com
 36. R. Kneppers, "HP Laser Interferometers," *Vaisala News*, Vol. 151, pp. 34-37, 1999.
 37. D. Malacara, *Optical Shop Testing*, 1992
 38. G. Mandolfo and K. Wayne, "Laser Measurements in the Shop," *SPIE short course*, 1993, Boston.
 39. www.hp.com
 40. www.on-trak.com
 41. www.sitek.com
 42. L. Zhang, L. Fu, H. Shi, and Y. Lu, "Measurement of high-power laser resonator mirror's misalignment using PSD," in *Process Control and Inspection for Industry*, S. Zhang and W. Gau, Eds., Vol. 4222 of *Proceedings of SPIE*, 2000, pp. 366-371.
 43. R. V. Shack and K. Thompson, "Influence of alignment errors of a telescope system on its aberration field," *SPIE Vol. 251*, 1980, pp. 146-153.
 44. F. Y. Pan, "Measurement of Aspherical Surfaces Using a Test Plate and Computer Generated Holograms," PhD Dissertation, University of Arizona, 2002
 45. R. Bhatia, "Telescope alignment: is the zero-coma condition sufficient?," *SPIE*, 1985, proc 2479

-
46. B. A. McLeod, "Collimation of Fast Wide-Field Telescopes," Publications of the Astronomical Society of the Pacific, Vol. 108, 1996, pp. 217-219
 47. R. N. Wilson and B. Delabre, "Concerning the Alignment of Modern Telescopes: Theory, Practice, and Tolerances Illustrated by the ESO NTT," Publications of the Astronomical Society of the Pacific, Vol. 109, 1997, pp. 53-60.
 48. M. Rimmer, "Analysis of Perturbed Lens Systems," Applied Optics, Vol. 9, No. 3, 1970, pp. 533-537
 49. *Optical Alignment*, Taylor Hobson Limited, Centaprint Limited, England, 1998.
 50. J. E. Simmons, W. Schoening, D. Graham, and L. Ott, "Alignment of a four meter Ritchey-Chretien telescope," SPIE, Vol. 251, 1980, pp. 138-145
 51. J. H. Burge, P. Koudelka, "Optical test alignment using computer generated holograms," in *Optical Fabrication and Testing*, 105-107 (Optical Society of America, Washington DC, 2002).
 52. K. B. Doyle, V. L. Genberg, G. J. Michels, *Integrated Mechanical Analysis*, SPIE Press, 2002.